

The Gould's Belt Distances Survey (GOBELINS).
IV. Distance, Depth and Kinematics of the Taurus Star-Forming Region

PHILLIP A. B. GALLI,¹ LAURENT LOINARD,^{2,3} GISELA N. ORTIZ-LÉON,⁴ MARINA KOUNKEL,⁵ SERGIO A. DZIB,⁴
AMY J. MIODUSZEWSKI,⁶ LUIS F. RODRÍGUEZ,² LEE HARTMANN,⁷ RAMACHRISNA TEIXEIRA,¹ ROSA M. TORRES,⁸
JUANA L. RIVERA,² ANDREW F. BODEN,⁹ NEAL J. EVANS II,^{10,11,12} CESAR BRICEÑO,¹³ JOHN J. TOBIN,¹⁴ AND
MARK HEYER¹⁵

¹*Instituto de Astronomia, Geofísica e Ciências Atmosféricas, Universidade de São Paulo, Rua do Matão, 1226, Cidade Universitária, 05508-900, São Paulo - SP, Brazil*

²*Instituto de Radioastronomía y Astrofísica, Universidad Nacional Autónoma de México, Apartado Postal 3-72, Morelia 58089, México*

³*Instituto de Astronomía, Universidad Nacional Autónoma de México, Apartado Postal 70-264, 04510 Ciudad de México, México*

⁴*Max Planck Institut für Radioastronomie, Auf dem Hügel 69, D-53121, Bonn, Germany*

⁵*Department of Physics and Astronomy, Western Washington University, 516 High St, Bellingham, WA 98225, USA*

⁶*National Radio Astronomy Observatory, Domenici Science Operations Center, 1003 Lopezville Road, Socorro, NM 87801, USA*

⁷*Department of Astronomy, University of Michigan, 1085 S. University st., Ann Arbor, MI 48109, USA*

⁸*Centro Universitario de Tonalá, Universidad de Guadalajara, Avenida Nuevo Periférico No. 555, Ejido San José Tatepozco, C.P. 48525, Tonalá, Jalisco, México*

⁹*Division of Physics, Math and Astronomy, California Institute of Technology, 1200 East California Boulevard, Pasadena, CA 91125, USA*

¹⁰*Department of Astronomy, The University of Texas at Austin, 2515 Speedway, Stop C1400, Austin, TX 78712-1205, USA*

¹¹*Korea Astronomy and Space Science Institute, 776 Daedeokdaero, Daejeon 305-348, Korea*

¹²*Humanitas College, Global Campus, Kyung Hee University, Yongin-shi 17104, Korea*

¹³*Cerro Tololo Interamerican Observatory, Casilla 603, La Serena, Chile*

¹⁴*Homer L. Dodge Department of Physics and Astronomy, University of Oklahoma, 440 W. Brooks Street, Norman, OK 73019, USA*

¹⁵*Department of Astronomy, University of Massachusetts, Amherst, MA 01003, USA*

(Received January 1, 2018; Revised January 7, 2018; Accepted May 25, 2018)

Submitted to ApJ

ABSTRACT

We present new trigonometric parallaxes and proper motions of young stellar objects in the Taurus molecular cloud complex from observations collected with the Very Long Baseline Array as part of the Gould's Belt Distances Survey (GOBELINS). We detected 26 young stellar objects and derived trigonometric parallaxes for 18 stars with an accuracy of 0.3% to a few percent. We modeled the orbits of six binaries and determined the dynamical masses of the individual components in four of these systems (V1023 Tau, T Tau S, V807 Tau and V1000 Tau). Our results are consistent with the first trigonometric parallaxes delivered by the Gaia satellite and reveal the existence of significant depth effects. We find that the central portion of the dark cloud Lynds 1495 is located at $d = 129.5 \pm 0.3$ pc while the B 216 clump in the filamentary structure connected to it is at $d = 158.1 \pm 1.2$ pc. The closest and remotest stars in our sample are located at $d = 126.6 \pm 1.7$ pc and $d = 162.7 \pm 0.8$ pc yielding a distance difference of about 36 pc. We also provide a new distance estimate for HL Tau that was recently imaged. Finally, we compute the spatial velocity of the stars with published radial velocity and investigate the kinematic properties of the various clouds and gas structures in this region.

Keywords: astrometry - stars: distances - binaries: visual - techniques: interferometric - radiation mechanisms: non-thermal - stars: kinematics and dynamics

1. INTRODUCTION

Since the discovery of the first T Tauri star (Joy 1945) the nearby Taurus-Auriga molecular cloud complex (or simply “Taurus”) has become one of the most studied regions of low-mass star formation (see e.g. Kenyon et al. 2008, for the most recent review). Taurus hosts more than 300 known young stellar objects (YSO) including pre-main sequence stars and brown dwarfs which are spread over several star-forming clouds and clumps (Luhman et al. 2009; Joncour et al. 2017).

Taurus is composed of multiple filaments (Schneider & Elmegreen 1979; Hartmann 2002; Schmalzl et al. 2010; Panopoulou et al. 2014) and the spatial distribution of the YSOs in the plane of the sky shows that they are clustered in small groups in or around the different star-forming clouds (Gomez et al. 1993). The question then arises whether the various groups and substructures are bound and have a common origin. Although the morphology of the molecular clouds has been well characterized in previous studies based e.g. on CO surveys and extinction maps (Ungerechts & Thaddeus 1987; Cambrésy 1999; Dame et al. 2001; Dobashi et al. 2005), little progress has been made so far to constrain the three-dimensional structure of the complex. Distances to individual stars are urgently required to accurately determine the most fundamental properties of YSOs (luminosity, mass and age), and they could also provide important clues to unravel the history of star formation in this region.

The distance to Taurus is commonly accepted to be 140 pc (Elias 1978) based on several estimates using a wide variety of techniques. The first results obtained by Greenstein & Shapley (1937) and McCuskey (1939) using star counts returned a distance of 145 pc and 142 pc, respectively. Racine (1968) determined a shorter distance of 135 ± 10 pc from the photometry of bright stars associated with reflection nebulae. On the other hand, Gottlieb & Upson (1969) obtained a somewhat larger distance of 150 pc based on the reddening turn-on method. Later, Straizys & Meistas (1980) investigated the area around the dark clouds L 1538, L 1528, L 1521 and L 1495 from the Lynds catalog (Lynds 1962) using a similar approach, and concluded that they extend from 140 to 175 pc. In a companion study, Meistas & Straizys (1981) found that the front-edge of the southern clouds in the complex (L 1551, L 1546 and L 1543) seems to be located at about 140 pc. More recently, Kenyon et al. (1994) derived the canonical distance of 140 ± 10 pc for the northern portion of the Taurus clouds based on the method of spectroscopic parallaxes which is commonly used in the literature. The latter result

confirmed previous distance estimates to the Taurus region and supported the idea of a common distance to the various clouds of the complex.

It is important to note that the measurements listed here refer to the mean distance to Taurus based on indirect methods while the individual distances to most YSOs still remain poorly constrained. Trigonometric parallaxes in the *Hipparcos* catalog (ESA 1997) exist only for 17 stars with a median error of about 27%. Bertout et al. (1999) divided them into 3 groups (L1495 region, Auriga region and south Taurus) and calculated the mean distance. Using only single stars they concluded that the 3 subgroups are located, respectively, at 125_{-16}^{+21} , 140_{-13}^{+16} and 168_{-28}^{+42} pc. These values are statistically compatible between themselves, but they suggest important distance differences among the various clouds in the complex. The mean parallax of all (single) stars together yields a distance of 139_{-9}^{+10} pc which confirms previous measurements but at the same time blurs the existence of possible depth effects in this region.

In a different study, Bertout & Genova (2006) applied a variant of the convergent point method and derived the kinematic parallaxes for 67 cluster members using proper motions and radial velocities. The derived parallaxes have a typical error of 20%. They investigated the distances of the YSO subclasses in their sample, and concluded that the classical T Tauri stars are at distances between 126 and 173 pc while the weak emission-line T Tauri stars can be found on both sides of the molecular clouds between 106 and 259 pc. These results are indicative of real distance differences among Taurus stars which will be tested when more trigonometric parallaxes become available.

Very Long Baseline Interferometry (VLBI) has been used in recent years to deliver trigonometric parallaxes of nearby stars with an accuracy often better than 1% (see e.g. Melis et al. 2014; Forbrich et al. 2016). The first VLBI trigonometric parallax in Taurus was reported by Lestrade et al. (1999) who targeted the weak-line T Tauri star V773 Tau which was found to be at 148 ± 5 pc. Later, Torres et al. (2012) presented an improved solution for its distance which takes into account the orbital motion of the binary system placing it at 132.8 ± 2.3 pc. The second trigonometric parallax obtained from VLBI radio observations in Taurus was obtained by Loinard et al. (2007). They measured the distance of 147.6 ± 0.6 pc for T Tau Sb in the well-known T Tau triple system in the southern clouds of the complex. Subsequently, Torres et al. (2007) measured the trigonometric parallaxes of Hubble 4 and HDE 283572 in the central portion of the complex, and derived the distances of 132.8 ± 0.5 pc and 128.5 ± 0.6 pc, respectively.

In a companion study, [Torres et al. \(2009\)](#) measured a somewhat larger distance of 161.2 ± 0.9 pc for HP Tau G2 making it the most distant star with known trigonometric parallax in Taurus. In summary, V773 Tau, Hubble 4 and HDE 283572 which are associated with the most prominent dark cloud L 1495 are found to be at the same distance while T Tau Sb and HP Tau G2 are located at larger distances. There is growing evidence of significant dispersion along the line of sight, but the small number of cluster members with measured trigonometric parallaxes is still insufficient to construct a precise three-dimensional map of this region.

This paper is one in a series dedicated to measuring stellar distances based on VLBI observations as part of the Gould’s Belt Distances Survey (GOBELINS, [Loinard et al. 2011](#)). Previous papers of this project investigated the Ophiuchus ([Ortiz-León et al. 2017a](#)), Orion ([Kounkel et al. 2017](#)) and Serpens ([Ortiz-León et al. 2017b](#)) star-forming regions. Here, we present new trigonometric parallaxes and proper motions for YSOs in Taurus. It is organized as follows. In Section 2 we describe our sample and observations. The methodology used to fit the astrometry for both single stars and binaries is explained in Section 3. In Section 4 we present our results and comment on individual targets. In Section 5 we compare our results derived in this work with the trigonometric parallaxes delivered by the first data release of the Gaia space mission (Gaia-DR1, [Gaia Collaboration et al. 2016](#)) for the targets in common, and complement our sample with the Gaia stars not included in our observing program to construct the most complete, precise and accurate picture of three-dimensional structure of the Taurus region to date. In this section, we also discuss the kinematic properties of the stars and molecular clouds in this region (see Table 10). Finally, we summarize our results and conclusions in Section 6.

2. SAMPLE AND OBSERVATIONS

In a recent study, [Dzib et al. \(2015\)](#) reported on multi-epoch radio observations of the Taurus complex using the Karl G. Jansky Very Large Array (VLA). They detected 59 sources related to YSOs, 18 field stars and another 46 unidentified sources whose radio properties are consistent with YSOs. However, only 56% of the young stars identified in their study exhibit properties compatible with non-thermal radio emission that can be

detected with VLBI observations. These sources constitute the starting point of our sample for the GOBELINS project in the Taurus region.

The observations presented in this paper were obtained with the Very Long Baseline Array (VLBA) near the equinoxes of every year between August 2012 and October 2017. The data were recorded in dual polarization mode with a bandwidth of 256 MHz centered at $\nu = 5.0$ or 8.4 GHz (C- and X-bands, respectively). We observed with the X-band during the first 3 years of our observing program, and then switched to the C-band which reduced significantly the noise in our observations. The VLBA was pointed at the position of our targets that have been accommodated in 52 different fields. Table 1 lists the observed epochs, bands, pointing positions and calibrators for each field. In some of these fields two or more targets are observed simultaneously. We included additional phase centers within the primary beam to observe other sources reported by [Dzib et al. \(2015\)](#) independently of their nature (YSO candidates, field stars or extragalactic sources) as part of our observing strategy (see [Ortiz-León et al. 2017a](#), for more details). Doing so, we observed a total of 86 sources (or stellar systems) during our observing campaign of which 45 are known YSOs in the literature. As shown in Fig. 1 our targets are spread over the various molecular clouds in Taurus.

Our observations produced 164 different projects under the code BL175 (see Table 1). Each observing session consisted of cycles alternating between the target(s) and the main phase calibrator. The secondary calibrators were observed every ~ 50 minutes. In addition, we also observed blocks of geodetic calibrators over a wide range of elevations at the beginning and end of each session. The typical integration time in each cycle was ~ 2 minutes for science targets and ~ 1 minute for calibrators. The total integration time for projects that observed with the X-band and C-band were, respectively, 1.1 hours and 1.5 hours. The calibrators used in our observations are extragalactic sources and the positions of all sources in each project are referenced to the corresponding primary calibrator. The typical angular separation between the primary calibrator and the YSOs in our sample ranges from 0.9° to 3.7° .

Table 1. Observed fields in Taurus with the VLBA.

Project Code	Date	Band	α	δ	Calibrators
			(h:m:s)	($^{\circ}$ ' ")	
BL175C1	20-aug-2012	X	04 22 02.20	19 33 27.0	J0412+1856, J0428+1732, J0426+2327, J0412+2305
BL175C2	30-aug-2012	X	04 31 25.13	18 16 16.6	J0431+1731, J0428+1732, J0438+2153, J0440+1437
BL175C3	31-aug-2012	X	04 31 40.09	18 13 56.7	J0431+1731, J0428+1732, J0438+2153, J0440+1437
BL175C4	10-sep-2012	X	04 32 14.58	18 20 14.6	J0431+1731, J0428+1732, J0438+2153, J0440+1437
BL175C5	30-sep-2012	X	04 31 34.15	18 08 04.6	J0431+1731, J0428+1732, J0438+2153, J0440+1437
			04 32 29.47	18 14 00.3	
BL175C6	30-nov-2012	X	04 33 26.35	22 28 32.0	J0438+2153, J0450+2249, J0426+2350, J0431+1731
BL175C7	02-dec-2012	X	04 35 13.27	22 59 20.0	J0438+2153, J0426+2327, J0435+2532, J0450+2249
BL175C8	03-dec-2012	X	04 35 20.91	22 54 24.0	J0438+2153, J0426+2327, J0435+2532, J0450+2249
BL175C9	04-dec-2012	X	04 35 48.11	22 53 29.1	J0438+2153, J0426+2327, J0435+2532, J0450+2249
BL175CA	07-dec-2012	X	04 35 58.97	22 38 35.2	J0438+2153, J0426+2327, J0435+2532, J0450+2249
BL175CG	23-mar-2013	X	04 22 02.20	19 33 27.0	J0412+1856, J0428+1732, J0426+2327, J0412+2305
BL175CH	25-mar-2013	X	04 31 25.13	18 16 16.6	J0431+1731, J0428+1732, J0438+2153, J0440+1437
BL175CI	11-apr-2013	X	04 31 40.09	18 13 56.7	J0431+1731, J0428+1732, J0438+2153, J0440+1437
BL175CJ	22-apr-2013	X	04 32 14.58	18 20 14.6	J0431+1731, J0428+1732, J0438+2153, J0440+1437
BL175CK	28-apr-2013	X	04 31 34.15	18 08 04.6	J0431+1731, J0428+1732, J0438+2153, J0440+1437
			04 32 29.47	18 14 00.3	
BL175CL	30-apr-2013	X	04 33 26.35	22 28 32.0	J0438+2153, J0450+2249, J0426+2350, J0431+1731
BL175CM	21-may-2013	X	04 35 13.27	22 59 20.0	J0438+2153, J0426+2327, J0435+2532, J0450+2249
BL175CN	23-may-2013	X	04 35 20.91	22 54 24.0	J0438+2153, J0426+2327, J0435+2532, J0450+2249
BL175CO	24-may-2013	X	04 35 48.11	22 53 29.1	J0438+2153, J0426+2327, J0435+2532, J0450+2249
BL175CP	27-may-2013	X	04 35 58.97	22 38 35.2	J0438+2153, J0426+2327, J0435+2532, J0450+2249
BL175D0	30-may-2013	X	04 41 23.47	24 55 28.1	J0438+2153, J0435+2532, J0440+2728, J0450+2249
BL175CV	10-jun-2013	X	04 32 37.91	24 20 54.4	J0426+2327, J0435+2532, J0429+2724, J0438+2153
BL175D1	11-jun-2013	X	04 41 44.92	25 58 15.3	J0438+2153, J0435+2532, J0440+2728, J0450+2249
BL175CW	15-jun-2013	X	04 33 06.63	24 09 54.9	J0426+2327, J0435+2532, J0429+2724, J0438+2153
BL175CX	16-jun-2013	X	04 33 10.04	24 33 43.1	J0426+2327, J0435+2532, J0429+2724, J0438+2153
BL175CY	01-jul-2013	X	04 36 57.44	24 18 35.2	J0426+2327, J0435+2532, J0429+2724, J0438+2153
BL175CZ	04-jul-2013	X	04 34 39.24	25 01 00.8	J0435+2532, J0429+2724, J0438+2153, J0426+2327
BL175D2	14-jul-2013	X	04 42 06.41	25 22 59.5	J0429+2724, J0435+2532, J0440+2728, J0450+2249
BL175Z0	01-aug-2013	X	04 42 10.59	25 25 05.5	J0429+2724, J0435+2532, J0440+2728, J0450+2249
BL175D4	19-aug-2013	X	04 42 46.20	25 18 06.2	J0429+2724, J0435+2532, J0440+2728, J0450+2249
BL175D5	03-sep-2013	X	04 43 08.05	25 22 10.3	J0429+2724, J0435+2532, J0440+2728, J0450+2249
BL175D6	16-sep-2013	X	04 24 48.59	26 43 13.0	J0429+2724, J0435+2532, J0433+2905, J0426+2350
BL175D7	25-sep-2013	X	04 25 17.48	26 17 48.3	J0429+2724, J0435+2532, J0433+2905, J0426+2350
BL175D8	22-oct-2013	X	04 29 20.74	26 33 53.4	J0429+2724, J0435+2532, J0433+2905, J0426+2350
BL175D9	23-oct-2013	X	04 29 22.26	26 37 28.6	J0429+2724, J0435+2532, J0433+2905, J0426+2350
BL175DA	26-oct-2013	X	04 29 29.49	26 31 52.8	J0429+2724, J0435+2532, J0433+2905, J0426+2350
BL175DB	27-oct-2013	X	04 29 42.48	26 32 48.9	J0429+2724, J0435+2532, J0433+2905, J0426+2350
BL175DC	28-oct-2013	X	04 30 02.25	26 08 43.5	J0429+2724, J0435+2532, J0433+2905, J0426+2350

Table 1 continued

Table 1 (*continued*)

Project Code	Date	Band	α (h:m:s)	δ ($^{\circ}$ ' ")	Calibrators
BL175DD	29-oct-2013	X	04 31 14.45	27 10 17.6	J0429+2724, J0435+2532, J0433+2905, J0426+2350
BL175DE	30-oct-2013	X	04 31 48.73	25 40 21.8	J0429+2724, J0435+2532, J0433+2905, J0426+2350
BL175DF	06-nov-2013	X	04 15 15.92	29 12 44.6	J0408+3032, J0429+2724, J0359+2758, J0422+3058
BL175DG	08-nov-2013	X	04 18 30.10	28 26 47.3	J0429+2724, J0422+3058, J0408+3032, J0403+2600
BL175DH	10-nov-2013	X	04 18 33.37	28 37 32.2	J0429+2724, J0422+3058, J0408+3032, J0403+2600
BL175DI	17-nov-2013	X	04 18 40.62	28 19 15.3	J0429+2724, J0422+3058, J0408+3032, J0403+2600
BL175DK	30-nov-2013	X	04 19 16.12	27 50 48.2	J0429+2724, J0422+3058, J0408+3032, J0403+2600
BL175DJ	01-dec-2013	X	04 18 47.03	28 20 07.2	J0429+2724, J0422+3058, J0408+3032, J0403+2600
BL175DL	04-dec-2013	X	04 19 26.27	28 26 14.0	J0429+2724, J0422+3058, J0408+3032, J0403+2600
BL175DM	07-dec-2013	X	04 19 41.28	27 49 47.9	J0429+2724, J0422+3058, J0408+3032, J0403+2600
BL175DN	08-dec-2013	X	04 22 02.20	26 57 30.3	J0429+2724, J0422+3058, J0408+3032, J0403+2600
BL175DO	10-dec-2013	X	04 13 27.23	28 16 24.4	J0408+3032, J0359+2758, J0403+2600, J0422+3058
BL175DP	13-dec-2013	X	04 13 43.75	28 20 55.9	J0408+3032, J0359+2758, J0403+2600, J0422+3058
BL175DQ	06-jan-2014	X	04 14 12.93	28 12 11.9	J0408+3032, J0359+2758, J0403+2600, J0422+3058
BL175DR	07-jan-2014	X	04 14 48.00	27 52 34.4	J0408+3032, J0359+2758, J0403+2600, J0422+3058
BL175DS	27-jan-2014	X	04 16 28.11	28 07 35.4	J0429+2724, J0408+3032, J0422+3058, J0403+2600
BL175DT	28-jan-2014	X	04 18 25.42	25 21 56.4	J0412+2305, J0426+2327, J0429+2724, J0403+2600
BL175DU	30-jan-2014	X	04 55 34.45	30 28 08.4	J0459+3106, J0503+3403, J0512+2927, J0439+3045
BL175DV	31-jan-2014	X	04 55 36.97	30 17 54.8	J0459+3106, J0503+3403, J0512+2927, J0439+3045
BL175DW	08-feb-2014	X	04 56 07.08	30 27 26.7	J0459+3106, J0503+3403, J0512+2927, J0439+3045
BL175H0	02-apr-2014	X	04 29 22.26	26 37 28.6	J0429+2724, J0435+2532, J0433+2905, J0426+2350
			04 29 29.49	26 31 52.8	
			04 29 42.48	26 32 48.9	
BL175H1	04-apr-2014	X	04 30 02.25	26 08 43.5	J0429+2724, J0435+2532, J0433+2905, J0426+2350
			04 31 14.45	27 10 17.6	
			04 31 48.73	25 40 21.8	
BL175H2	06-apr-2014	X	04 18 30.10	28 26 47.3	J0429+2724, J0422+3058, J0408+3032, J0403+2600
			04 18 33.37	28 37 32.2	
			04 18 40.62	28 19 15.3	
BL175H3	07-apr-2014	X	04 18 47.03	28 20 07.2	J0429+2724, J0422+3058, J0408+3032, J0403+2600
			04 19 16.12	27 50 48.2	
			04 19 26.27	28 26 14.0	
BL175H4	08-apr-2014	X	04 19 41.28	27 49 47.9	J0429+2724, J0422+3058, J0408+3032, J0403+2600
			04 22 02.20	26 57 30.3	
			04 16 28.11	28 07 35.4	
BL175H5	10-apr-2014	X	04 13 27.23	28 16 24.4	J0408+3032, J0359+2758, J0403+2600, J0422+3058
			04 13 43.75	28 20 55.9	
			04 14 12.93	28 12 11.9	
BL175H6	11-apr-2014	X	04 55 34.45	30 28 08.4	J0459+3106, J0503+3403, J0512+2927, J0439+3045
			04 55 36.97	30 17 54.8	

Table 1 *continued*

Table 1 (continued)

Project Code	Date	Band	α (h:m:s)	δ ($^{\circ}$ ' ")	Calibrators
			04 56 07.08	30 27 26.7	
BL175H7	12-apr-2014	X	04 22 02.20	19 33 27.0	J0412+1856, J0428+1732, J0426+2327, J0412+2305
BL175H8	13-apr-2014	X	04 15 15.92	29 12 44.6	J0408+3032, J0429+2724, J0359+2758, J0422+3058
BL175H9	17-apr-2014	X	04 31 34.15	18 08 04.6	J0431+1731, J0428+1732, J0438+2153, J0440+1437
			04 32 29.47	18 14 00.3	
BL175HA	18-apr-2014	X	04 14 48.00	27 52 34.4	J0408+3032, J0359+2758, J0403+2600, J0422+3058
			04 18 25.42	25 21 56.4	J0412+2305, J0426+2327, J0429+2724
BL175AD	31-aug-2014	X	04 32 37.91	24 20 54.4	J0426+2327, J0435+2532, J0429+2724, J0438+2153
			04 33 06.63	24 09 54.9	
			04 33 10.04	24 33 43.1	
BL175EU	07-sep-2014	X	04 22 02.20	19 33 27.0	J0412+1856, J0428+1732, J0426+2327, J0412+2305
BL175AB	08-sep-2014	X	04 31 25.13	18 16 16.6	J0431+1731, J0428+1732, J0438+2153, J0440+1437
			04 31 40.09	18 13 56.7	
			04 32 14.58	18 20 14.6	
BL175AC	09-sep-2014	X	04 35 13.27	22 59 20.0	J0438+2153, J0426+2327, J0435+2532, J0450+2249
			04 35 20.91	22 54 24.0	
			04 35 48.11	22 53 29.1	
BL175CQ	13-sep-2014	X	04 15 15.92	29 12 44.6	J0408+3032, J0429+2724, J0359+2758, J0422+3058
BL175AE	14-sep-2014	X	04 41 23.47	24 55 28.1	J0438+2153, J0426+2327, J0435+2532, J0450+2249
			04 41 44.92	25 58 15.3	
			04 42 06.41	25 22 59.5	
BL175AF	15-sep-2014	X	04 42 10.59	25 25 05.5	J0429+2724, J0435+2532, J0440+2728, J0450+2249
			04 42 46.20	25 18 06.2	
			04 43 08.05	25 22 10.3	
BL175AG	19-sep-2014	X	04 24 48.59	26 43 13.0	J0429+2724, J0435+2532, J0433+2905, J0426+2350
			04 25 17.48	26 17 48.3	
			04 29 20.74	26 33 53.4	
BL175AH	20-sep-2014	X	04 29 22.26	26 37 28.6	J0429+2724, J0435+2532, J0433+2905, J0426+2350
			04 29 29.49	26 31 52.8	
			04 29 42.48	26 32 48.9	
BL175AJ	22-oct-2014	X	04 18 30.10	28 26 47.3	J0429+2724, J0422+3058, J0408+3032, J0403+2600
			04 18 33.37	28 37 32.2	
			04 18 40.62	28 19 15.3	
BL175AI	24-oct-2014	X	04 30 02.25	26 08 43.5	J0429+2724, J0435+2532, J0433+2905, J0426+2350
			04 31 14.45	27 10 17.6	
			04 31 48.73	25 40 21.8	
BL175AK	25-oct-2014	X	04 18 47.03	28 20 07.2	J0429+2724, J0422+3058, J0408+3032, J0403+2600
			04 19 16.12	27 50 48.2	
			04 19 26.27	28 26 14.0	
BL175AL	20-mar-2015	X	04 31 25.13	18 16 16.6	J0431+1731, J0428+1732, J0438+2153, J0440+1437

Table 1 continued

Table 1 (*continued*)

Project Code	Date	Band	α (h:m:s)	δ ($^{\circ}$ ' ")	Calibrators
			04 31 40.09	18 13 56.7	
			04 32 14.58	18 20 14.6	
BL175AM	21-mar-2015	X	04 35 13.27	22 59 20.0	J0438+2153, J0426+2327, J0435+2532, J0450+2249
			04 35 20.91	22 54 24.0	
			04 35 48.11	22 53 29.1	
BL175AN	23-mar-2015	X	04 32 37.91	24 20 54.4	J0426+2327, J0435+2532, J0429+2724, J0438+2153
			04 33 06.63	24 09 54.9	
			04 33 10.04	24 33 43.1	
BL175AO	28-mar-2015	X	04 41 23.47	24 55 28.1	J0438+2153, J0435+2532, J0440+2728, J0450+2249
			04 41 44.92	25 58 15.3	
			04 42 06.41	25 22 59.5	
BL175AP	29-mar-2015	X	04 42 10.59	25 25 05.5	J0429+2724, J0435+2532, J0440+2728, J0450+2249
			04 42 46.20	25 18 06.2	
			04 43 08.05	25 22 10.3	
BL175AY	30-mar-2015	X	04 24 48.59	26 43 13.0	J0429+2724, J0435+2532, J0433+2905, J0426+2350
			04 25 17.48	26 17 48.3	
			04 29 20.74	26 33 53.4	
BL175AZ	02-apr-2015	X	04 29 22.26	26 37 28.6	J0429+2724, J0435+2532, J0433+2905, J0426+2350
			04 29 29.49	26 31 52.8	
			04 29 42.48	26 32 48.9	
BL175DZ	07-apr-2015	X	04 18 47.03	28 20 07.2	J0429+2724, J0422+3058, J0408+3032, J0403+2600
			04 19 16.12	27 50 48.2	
			04 19 26.27	28 26 14.0	
BL175E6	09-apr-2015	X	04 19 41.28	27 49 47.9	J0429+2724, J0422+3058, J0408+3032, J0403+2600
			04 22 02.20	26 57 30.3	
			04 16 28.11	28 07 35.4	
BL175E8	10-apr-2015	X	04 13 27.23	28 16 24.4	J0408+3032, J0359+2758, J0403+2600, J0422+3058
			04 13 43.75	28 20 55.9	
			04 14 12.93	28 12 11.9	
BL175E9	13-apr-2015	X	04 55 34.45	30 28 08.4	J0459+3106, J0503+3403, J0512+2927, J0439+3045
			04 55 36.97	30 17 54.8	
			04 56 07.08	30 27 26.7	
BL175EA	14-apr-2015	X	04 31 34.15	18 08 04.6	J0431+1731, J0428+1732, J0438+2153, J0440+1437
			04 32 29.47	18 14 00.3	
BL175FN	17-apr-2015	X	04 18 30.10	28 26 47.3	J0429+2724, J0422+3058, J0408+3032, J0403+2600
			04 18 33.37	28 37 32.2	
			04 18 40.62	28 19 15.3	
BL175EC	19-apr-2015	X	04 14 48.00	27 52 34.4	J0408+3032, J0359+2758, J0403+2600, J0422+3058
			04 18 25.42	25 21 56.4	J0412+2305, J0426+2327, J0429+2724
BL175ED	20-apr-2015	X	04 36 57.44	24 18 35.2	J0426+2327, J0435+2532, J0429+2724, J0438+2153

Table 1 continued

Table 1 (continued)

Project Code	Date	Band	α (h:m:s)	δ ($^{\circ}$ ' ")	Calibrators
			04 35 58.97	22 38 35.2	
			04 50 51.95	22 49 05.9	
BL175FO	24-apr-2015	X	04 33 26.35	22 28 32.0	J0438+2153, J0450+2249, J0426+2350, J0431+1731
			04 34 39.24	25 01 00.8	J0435+2532, J0429+2724, J0426+2327
BL175EV	25-apr-2015	X	04 22 02.20	19 33 27.0	J0412+1856, J0428+1732, J0426+2327, J0412+2305
BL175EW	26-apr-2015	X	04 15 15.92	29 12 44.6	J0408+3032, J0429+2724, J0359+2758, J0422+3058
BL175GZ	04-sep-2015	X	04 31 25.13	18 16 16.6	J0431+1731, J0428+1732, J0438+2153, J0440+1437
			04 31 40.09	18 13 56.7	
			04 32 14.58	18 20 14.6	
BL175HC	11-sep-2015	X	04 32 37.91	24 20 54.4	J0426+2327, J0435+2532, J0429+2724, J0438+2153
			04 33 06.63	24 09 54.9	
			04 33 10.04	24 33 43.1	
BL175HD	12-sep-2015	X	04 41 23.47	24 55 28.1	J0438+2153, J0435+2532, J0440+2728, J0450+2249
			04 41 44.92	25 58 15.3	
			04 42 06.41	25 22 59.5	
BL175HE	18-sep-2015	X	04 42 10.59	25 25 05.5	J0429+2724, J0435+2532, J0440+2728, J0450+2249
			04 42 46.20	25 18 06.2	
			04 43 08.05	25 22 10.3	
BL175HF	20-sep-2015	X	04 24 48.59	26 43 13.0	J0429+2724, J0435+2532, J0433+2905, J0426+2350
			04 25 17.48	26 17 48.3	
			04 29 20.74	26 33 53.4	
BL175HB	16-oct-2015	X	04 35 13.27	22 59 20.0	J0438+2153, J0426+2327, J0435+2532, J0450+2249
			04 35 20.91	22 54 24.0	
			04 35 48.11	22 53 29.1	
BL175HG	27-sep-2015	X	04 29 22.26	26 37 28.6	J0429+2724, J0435+2532, J0433+2905, J0426+2350
			04 29 29.49	26 31 52.8	
			04 29 42.48	26 32 48.9	
BL175HH	29-sep-2015	X	04 30 02.25	26 08 43.5	J0429+2724, J0435+2532, J0433+2905, J0426+2350
			04 31 14.45	27 10 17.6	
			04 31 48.73	25 40 21.8	
BL175HJ	03-oct-2015	X	04 18 47.03	28 20 07.2	J0429+2724, J0422+3058, J0408+3032, J0403+2600
			04 19 16.12	27 50 48.2	
			04 19 26.27	28 26 14.0	
BL175HK	04-oct-2015	X	04 19 41.28	27 49 47.9	J0429+2724, J0422+3058, J0408+3032, J0403+2600
			04 22 02.20	26 57 30.3	
			04 16 28.11	28 07 35.4	
BL175HM	06-oct-2015	X	04 55 34.45	30 28 08.4	J0459+3106, J0503+3403, J0512+2927, J0439+3045
			04 55 36.97	30 17 54.8	
			04 56 07.08	30 27 26.7	
BL175HI	08-oct-2015	X	04 18 30.10	28 26 47.3	J0429+2724, J0422+3058, J0408+3032, J0403+2600

Table 1 continued

Table 1 (*continued*)

Project Code	Date	Band	α (h:m:s)	δ ($^{\circ}$ ' ")	Calibrators
			04 18 33.37	28 37 32.2	
			04 18 40.62	28 19 15.3	
BL175HL	09-oct-2015	X	04 13 27.23	28 16 24.4	J0408+3032, J0359+2758, J0403+2600, J0422+3058
			04 13 43.75	28 20 55.9	
			04 14 12.93	28 12 11.9	
BL175HN	11-oct-2015	X	04 31 34.15	18 08 04.6	J0431+1731, J0428+1732, J0438+2153, J0440+1437
			04 32 29.47	18 14 00.3	
BL175HO	12-oct-2015	X	04 14 48.00	27 52 34.4	J0408+3032, J0359+2758, J0403+2600, J0422+3058
			04 18 25.42	25 21 56.4	J0412+2305, J0426+2327, J0429+2724
BL175HP	13-oct-2015	X	04 36 57.44	24 18 35.2	J0426+2327, J0435+2532, J0429+2724, J0438+2153
			04 35 58.97	22 38 35.2	
			04 50 51.95	22 49 05.9	
BL175HQ	15-oct-2015	X	04 33 26.35	22 28 32.0	J0438+2153, J0450+2249, J0426+2350, J0431+1731
			04 34 39.24	25 01 00.8	J0435+2532, J0429+2724, J0426+2327
BL175HR	17-oct-2015	X	04 22 02.20	19 33 27.0	J0412+1856, J0428+1732, J0426+2327, J0412+2305
BL175HS	20-oct-2015	X	04 15 15.92	29 12 44.6	J0408+3032, J0429+2724, J0359+2758, J0422+3058
BL175I1	28-feb-2016	C	04 24 48.59	26 43 13.0	J0429+2724, J0435+2532, J0433+2905, J0426+2350
			04 25 17.48	26 17 48.3	
BL175I2	18-mar-2016	C	04 35 13.27	22 59 20.0	J0438+2153, J0426+2327, J0435+2532, J0450+2249
			04 35 20.91	22 54 24.0	
			04 35 48.11	22 53 29.1	
BL175I3	24-mar-2016	C	04 18 30.10	28 26 47.3	J0429+2724, J0422+3058, J0408+3032, J0403+2600
			04 18 33.37	28 37 32.2	
			04 18 40.62	28 19 15.3	
BL175I4	25-mar-2016	C	04 32 37.91	24 20 54.4	J0426+2327, J0435+2532, J0429+2724, J0438+2153
			04 33 06.63	24 09 54.9	
			04 33 10.04	24 33 43.1	
BL175I5	26-mar-2016	C	04 14 48.00	27 52 34.4	J0408+3032, J0359+2758, J0403+2600, J0422+3058
			04 18 25.42	25 21 56.4	J0412+2305, J0426+2327, J0429+2724
BL175I6	31-mar-2016	C	04 19 41.28	27 49 47.9	J0429+2724, J0422+3058, J0408+3032, J0403+2600
			04 22 02.20	26 57 30.3	
			04 16 28.11	28 07 35.4	
BL175I7	03-apr-2016	C	04 29 26.75	26 30 47.8	J0429+2724, J0435+2532, J0433+2905, J0426+2350
			04 42 10.59	25 25 05.5	
BL175I8	04-apr-2016	C	04 22 02.20	19 33 27.0	J0412+1856, J0428+1732, J0426+2327, J0412+2305
BL175I9	07-apr-2016	C	04 15 15.92	29 12 44.6	J0408+3032, J0429+2724, J0359+2758, J0422+3058
BL175IC	14-apr-2016	C	04 41 44.92	25 58 15.3	J0438+2153, J0435+2532, J0440+2728, J0450+2249
			04 42 06.41	25 22 59.5	
BL175IE	29-apr-2016	C	04 13 27.23	28 16 24.4	J0408+3032, J0359+2758, J0403+2600, J0422+3058
			04 14 12.93	28 12 11.9	

Table 1 continued

Table 1 (*continued*)

Project Code	Date	Band	α (h:m:s)	δ ($^{\circ}$ ' ")	Calibrators
BL175IF	01-may-2016	C	04 34 39.24	25 01 00.8	J0435+2532, J0429+2724, J0438+2153, J0426+2327
			04 31 40.09	18 13 56.7	J0431+1731, J0428+1732, J0440+1437
BL175IU	03-sep-2016	C	04 13 27.23	28 16 24.4	J0408+3032, J0359+2758, J0403+2600, J0422+3058
			04 14 12.93	28 12 11.9	
BL175IX	08-sep-2016	C	04 35 13.27	22 59 20.0	J0438+2153, J0426+2327, J0435+2532, J0450+2249
			04 35 20.91	22 54 24.0	
			04 35 48.11	22 53 29.1	
BL175IV	14-sep-2016	C	04 34 39.24	25 01 00.8	J0435+2532, J0429+2724, J0438+2153, J0426+2327
			04 31 40.09	18 13 56.7	J0431+1731, J0428+1732, J0440+1437
BL175IY	22-sep-2016	C	04 19 41.28	27 49 47.9	J0429+2724, J0422+3058, J0408+3032, J0403+2600
			04 22 02.20	26 57 30.3	
			04 16 28.11	28 07 35.4	
BL175J2	23-sep-2016	C	04 18 30.10	28 26 47.3	J0429+2724, J0422+3058, J0408+3032, J0403+2600
			04 18 40.62	28 19 15.3	
BL175J3	25-sep-2016	C	04 24 48.59	26 43 13.0	J0429+2724, J0435+2532, J0433+2905, J0426+2350
			04 29 22.26	26 37 28.6	
BL175J4	29-sep-2016	C	04 33 06.63	24 09 54.9	J0426+2327, J0435+2532, J0429+2724, J0438+2153
			04 33 10.04	24 33 43.1	
BL175IW	08-oct-2016	C	04 41 44.92	25 58 15.3	J0438+2153, J0435+2532, J0440+2728, J0450+2249
			04 42 06.41	25 22 59.5	
BL175J0	10-oct-2016	C	04 22 02.20	19 33 27.0	J0412+1856, J0428+1732, J0426+2327, J0412+2305
BL175J1	11-oct-2016	C	04 15 15.92	29 12 44.6	J0408+3032, J0429+2724, J0359+2758, J0422+3058
BL175IZ	13-oct-2016	C	04 29 26.75	26 30 47.8	J0429+2724, J0435+2532, J0433+2905, J0426+2350
			04 42 10.59	25 25 05.5	
BL175J5	14-oct-2016	C	04 14 48.00	27 52 34.4	J0408+3032, J0359+2758, J0403+2600, J0422+3058
			04 55 36.97	30 17 54.8	J0459+3106, J0503+3403, J0512+2927, J0439+3045
BL175JU	05-mar-2017	C	04 33 06.63	24 09 54.9	J0426+2327, J0435+2532, J0429+2724, J0438+2153
			04 33 10.04	24 33 43.1	
BL175JO	10-mar-2017	C	04 13 27.23	28 16 24.4	J0408+3032, J0359+2758, J0403+2600, J0422+3058
			04 14 12.93	28 12 11.9	
BL175JW	14-mar-2017	C	04 35 20.91	22 54 24.0	J0438+2153, J0435+2532, J0440+2728, J0450+2249
			04 42 06.41	25 22 59.5	
BL175JQ	15-mar-2017	C	04 16 28.11	28 07 35.4	J0429+2724, J0422+3058, J0408+3032, J0403+2600
			04 19 41.28	27 49 47.9	
BL175JS	18-mar-2017	C	04 18 30.10	28 26 47.3	J0429+2724, J0422+3058, J0408+3032, J0403+2600
			04 18 40.62	28 19 15.3	
BL175JP	26-mar-2017	C	04 34 39.24	25 01 00.8	J0435+2532, J0429+2724, J0438+2153, J0426+2327
			04 31 40.09	18 13 56.7	J0431+1731, J0428+1732, J0440+1437
BL175JV	11-apr-2017	C	04 14 48.00	27 52 34.4	J0408+3032, J0359+2758, J0403+2600, J0422+3058
			04 55 36.97	30 17 54.8	J0459+3106, J0503+3403, J0512+2927, J0439+3045

Table 1 continued

Table 1 (*continued*)

Project Code	Date	Band	α (h:m:s)	δ ($^{\circ}$ ' ")	Calibrators
BL175JT	13-apr-2017	C	04 24 48.59 04 29 22.26	26 43 13.0 26 37 28.6	J0429+2724, J0435+2532, J0433+2905, J0426+2350
BL175JY	14-apr-2017	C	04 29 42.48 04 42 10.59	26 32 48.9 25 25 05.5	J0429+2724, J0435+2532, J0433+2905, J0426+2350
BL175JZ	21-apr-2017	C	04 24 49.03 04 31 13.00	26 43 10.1 27 08 34.9	J0429+2724, J0435+2532, J0433+2905, J0426+2350
BL175JX	24-apr-2017	C	04 35 48.11	22 53 29.1	J0438+2153, J0426+2327, J0435+2532, J0450+2249
BL175KM	02-sep-2017	C	04 34 39.2 04 31 40.1	25 01 00.8 18 13 56.7	J0435+2532, J0429+2724, J0438+2153, J0426+2327 J0431+1731, J0428+1732, J0440+1437
BL175KO	03-sep-2017	C	04 18 30.1 04 18 40.6	28 26 47.3 28 19 15.3	J0429+2724, J0422+3058, J0408+3032, J0403+2600
BL175KQ	08-sep-2017	C	04 14 48.0 04 55 37.0	27 52 34.4 30 17 54.8	J0408+3032, J0359+2758, J0403+2600, J0422+3058 J0459+3106, J0503+3403, J0512+2927, J0439+3045
BL175KP	15-sep-2017	C	04 33 06.6 04 33 10.0	24 09 54.9 24 33 43.1	J0426+2327, J0435+2532, J0429+2724, J0438+2153
BL175KJ	18-sep-2017	C	04 24 48.2 04 29 22.3	26 43 15.9 26 37 28.6	J0429+2724, J0435+2532, J0433+2905, J0426+2350
BL175KL	25-sep-2017	C	04 13 27.2	28 16 24.4	J0408+3032, J0359+2758, J0403+2600, J0422+3058
BL175KT	03-oct-2017	C	04 24 49.0 04 31 13.0	26 43 10.1 27 08 34.9	J0429+2724, J0435+2532, J0433+2905, J0426+2350
BL175KS	05-oct-2017	C	04 29 42.5 04 42 10.6	26 32 48.9 25 25 05.5	J0429+2724, J0435+2532, J0433+2905, J0426+2350
BL175KN	06-oct-2017	C	04 35 48.1	22 53 29.1	J0438+2153, J0426+2327, J0435+2532, J0450+2249
BL175KU	12-oct-2017	C	04 33 06.6 04 33 10.0	24 09 54.9 24 33 43.1	J0426+2327, J0435+2532, J0429+2724, J0438+2153
BL175KV	14-oct-2017	C	04 35 20.9 04 42 06.4	22 54 24.0 25 22 59.5	J0438+2153, J0435+2532, J0440+2728, J0450+2249

NOTE—We provide for each field the NRAO project code, epoch of observation, observed band, coordinates of the field center and the calibrators (the main calibrator is the first source in the list).

The VLBA observations were correlated with the DiFX software correlator (Deller et al. 2011). Then, the data were edited and calibrated using the Astronomical Image Processing System (AIPS, Greisen 2003) following the standard prescription for VLBA data as described in Ortiz-León et al. (2017a). We applied the same calibration to all sources in the field when multiple targets were observed in the same session. The calibrated visibilities were imaged with a pixel size of 50-100 μ as and resulted in a typical angular resolution of 3 mas \times 1 mas at $\nu = 5.0$ GHz and 2 mas \times 0.8 mas at $\nu = 8.4$ GHz. The mean noise level in the calibrated images were 26 μ Jy/beam and 42 μ Jy/beam, respec-

tively, at the C- and X-bands. Finally, the source position (and the corresponding errors) were obtained from a two-dimensional Gaussian fitting using the AIPS task JMFIT.

As mentioned before, we observed a total of 86 targets in Taurus for the GOBELINS project, but only 52 sources could be detected in our observations. Table 2 lists the sources that have been observed in our campaign with the VLBA. We provide the minimum and maximum flux density measured at both frequencies, the brightness temperature T_B , the number of detections and observations for each source. In some cases we provide an upper flux density limit of 3σ (based on the noise level of the image) when the source was ob-

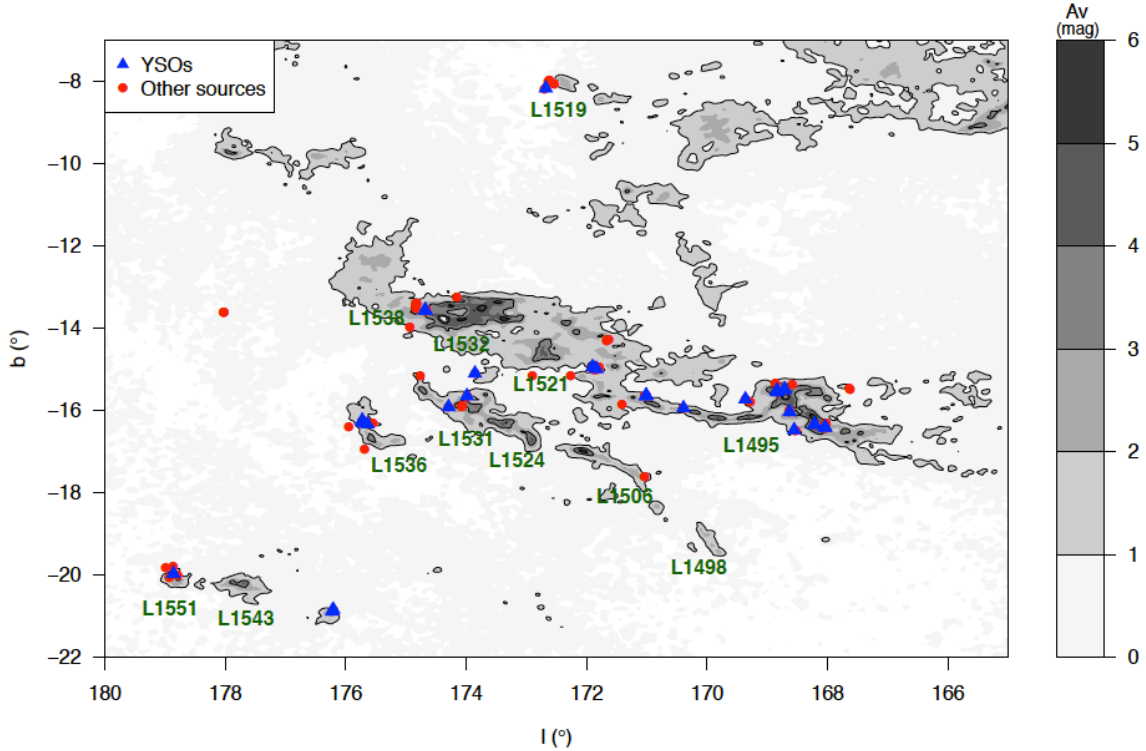


Figure 1. Location of our targets in the Taurus star-forming complex overlaid on the extinction map from Dobashi et al. (2005) in Galactic coordinates. The most prominent Lynds dark clouds (Lynds 1962) in this region are identified in this diagram.

served but could not be detected. In this context, it is important to mention that some of the YSOs targeted in this study are highly variable. For binaries and multiple systems that could be resolved in our observations we present the results for each component separately. We note that most sources in Table 2 exhibit a brightness temperature of $T_B > 10^6$ K which is consistent with non-thermal radio emission. Thirty-four sources in our initial target list were not detected, and we interpret the non detections with the VLBA as evidence that their radio emission is thermal. We consider a single detection to be valid when the flux density of the source is above a 5σ threshold where σ is the corresponding noise level of the image. Our effective sample of detected sources contains 26 stars that have been confirmed as YSOs in previous studies, and another 3 sources that require further monitoring to investigate their membership in the Taurus region. The remaining 23 sources that have been detected in our observations are likely to be background contaminants that are not related to the Taurus molecular clouds. As shown in Fig. 2 their proper motion, which are estimated at this stage from the position change rate of the source, are consistent with zero (within the astrometric errors) while the typi-

cal proper motion of YSOs in Taurus is about 22 mas/yr (see e.g. Bertout & Genova 2006).

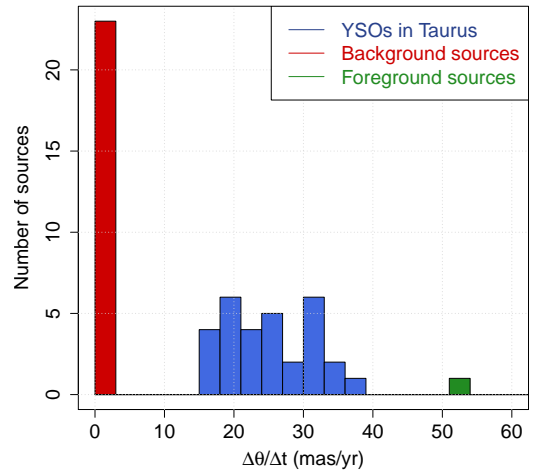


Figure 2. Histogram of the position change rate for all sources (including binaries) observed in our campaign with a minimum of two detections (see Table 2).

It is important to mention that some sources in our sample had been observed with the VLBA in the past.

Thus, we searched the National Radio Astronomy Observatory's (NRAO) data archive for additional information on our targets. We collected a total of 65 projects at different epochs that are listed in Table 3. These observations were performed between September 2003 and March 2009 which allows us to extend the time base of our analysis to more than 10 years of observations for some targets. This is particularly useful to investigate the orbital motion of binaries and multiple systems in our sample as discussed in the forthcoming sections of this paper. Although the source positions obtained from these observations have already been published in previous studies, we recalibrated these data using the same procedure that was adopted for the GOBELINS project to better combine the different data sets. The typical noise level and angular resolution that we obtain in the re-calibrated images from archival data are, respectively, 100 $\mu\text{Jy}/\text{beam}$ and $2 \text{ mas} \times 0.8 \text{ mas}$.

3. ASTROMETRY FITTING

3.1. *Single Stars*

The displacement of a single star in the plane of the sky is the combination of its proper motion (μ_α, μ_δ) and the trigonometric parallax (π) . In this case, the stellar coordinates as a function of time (t) are given by

$$\alpha(t) = \alpha_0 + \mu_\alpha t + \pi f_\alpha(t), \quad (1)$$

$$\delta(t) = \delta_0 + \mu_\delta t + \pi f_\delta(t), \quad (2)$$

where (α_0, δ_0) are the coordinates of the star at a given epoch (t_0) . The projections of the parallactic ellipse (f_α, f_δ) are given by (see e.g. Seidemann 1992)

$$f_\alpha = (X \sin \alpha - Y \cos \alpha) / \cos \delta, \quad (3)$$

$$f_\delta = X \cos \alpha \sin \delta + Y \sin \alpha \sin \delta - Z \cos \delta, \quad (4)$$

where (X, Y, Z) are the barycentric coordinates of the Earth (in units of A.U.) computed from the planetary ephemerides DE405 using the `novas` package in Python.

3.2. *Binaries*

Binaries and multiple systems are very common in the Taurus star-forming region (Duchêne 1999) and our sample contains many such systems that require a dedicated analysis. Since both stars in a binary system move around their common centre of gravity, their orbital motion projected onto the plane of the sky has to be taken into account to accurately determine the parallaxes and proper motions of the individual components.

At this stage it is important to distinguish between (i) binaries with orbital periods much longer than the monitoring time of our observing campaign, and (ii) binaries

with short or intermediate periods where our observations cover a significant fraction of the orbital period. In the first case, it is possible to assume a uniform acceleration (see e.g. Loinard et al. 2007) leading to

$$\alpha(t) = \alpha_0 + \mu_\alpha t + \frac{1}{2} a_\alpha t^2 + \pi f_\alpha(t), \quad (5)$$

$$\delta(t) = \delta_0 + \mu_\delta t + \frac{1}{2} a_\delta t^2 + \pi f_\delta(t), \quad (6)$$

where a_α and a_δ are the acceleration terms. In the second case, the effects of the binary motion and the existence of a non-uniform acceleration need to be taken into account. It is therefore necessary to fit for the full orbital motion and the astrometric parameters simultaneously. The orbital elements to be considered in this case are the semi-major axis a , the orbital period P , the eccentricity e , the epoch of periastron passage T_p , the argument of the ascending node Ω , the longitude of the periastron ω and the inclination i of the orbital plane. Thus, the equations for the primary component with semi-major axis a_1 can be written in the form

$$\alpha(t) = \alpha_0 + \mu_\alpha t + \pi f_\alpha(t) + a_1 Q_\alpha(t), \quad (7)$$

$$\delta(t) = \delta_0 + \mu_\delta t + \pi f_\delta(t) + a_1 Q_\delta(t), \quad (8)$$

where Q_α and Q_δ are the orbital factors. They are given by (see e.g. van de Kamp 1967)

$$Q_\alpha = B'x(t) + G'y(t), \quad (9)$$

$$Q_\delta = A'x(t) + F'y(t), \quad (10)$$

where the orientation factors B', A', G', F' are related to the Thiele-Innes constants as follows

$$B' = -\cos \omega \sin \Omega - \sin \omega \cos \Omega \cos i, \quad (11)$$

$$A' = -\cos \omega \cos \Omega + \sin \omega \sin \Omega \cos i, \quad (12)$$

$$G' = +\sin \omega \sin \Omega - \cos \omega \cos \Omega \cos i, \quad (13)$$

$$F' = +\sin \omega \cos \Omega + \cos \omega \sin \Omega \cos i. \quad (14)$$

The elliptical rectangular coordinates $x(t)$ and $y(t)$ are given by

$$x(t) = \cos E(t) - e, \quad (15)$$

$$y(t) = \sin E(t) \sqrt{1 - e^2}, \quad (16)$$

where $E(t)$ is the eccentric anomaly given by Kepler's transcendental equation. Similar equations hold for the secondary component. In this case, we replace a_1 by the semi-major axis a_2 of the secondary which is scaled by the mass ratio q of the two components.

To simplify the forthcoming discussion we denote the methodology described above to solve simultaneously for

the astrometric parameters and orbital elements of the binary system using absolute positions by the name “full model”. Some binaries in our sample also exhibit relative astrometry of the two components from optical and near-infrared observations (NIR) published in previous works which have been incorporated to our study. In this case, our analysis is limited to the right-hand term of Eqs. (7) and (8) to derive the orbital elements of the binary system. The resulting semi-major axis a refers to the relative orbit of the two components. We denote this solution using relative positions by the name “relative model”. Finally, we combine the absolute positions measured in this work and relative positions from the literature to perform a “joint fit” solution.

3.3. Solving the system of equations

The source positions obtained from the JMFIT task in AIPS were used to derive the astrometric and orbital parameters of the stars in our sample. Table 4 lists the measured positions for each source in our sample. However, it is important to mention that the positional uncertainties provided by JMFIT, which roughly represent the expected astrometric precision delivered by the VLBA, do not include various systematic errors that may significantly affect the accuracy of the computed astrometric parameters (see e.g. Pradel et al. 2006). To overcome this problem, additional errors were added quadratically to the positional errors given by JMFIT to adjust the reduced χ^2 value in the astrometric fit to unity (see also Menten et al. 2007; Ortiz-León et al. 2017a). These additional errors range in most cases from 0.05 to 0.30 mas for both single stars and binaries (the few exceptions are discussed in Sect. 4).

To solve for the astrometric and orbital elements of the star (or stellar system) we developed our own routine in the Python programming language based on the `emcee` package (Foreman-Mackey et al. 2013) which implements the Markov chain Monte Carlo (MCMC) method proposed by Goodman & Weare (2010). The algorithm was adapted to our purposes and applied to the general problem of computing the astrometric and orbital parameters from the astrometry fitting. Briefly, the method that we use in this work explores the parameter space using a number of walkers and iteration steps to solve the system of equations presented in Sects. 3.1 and 3.2 via Bayesian inference. The walkers move around the n -dimensional parameter space and take tentative steps towards the lowest value of χ^2 . This produces a distribution of the individual solutions given by the ensemble of walkers. We run the MCMC method typically with

200 walkers to sample the distribution of each parameter with a significant number of individual solutions. Then, we take the mean and standard deviation of the distribution of each parameter as our final result.

Our methodology based on the MCMC method was first applied to the sources previously investigated by our team in the Ophiuchus region (Ortiz-León et al. 2017a) for calibration purposes. We varied the number of iterations for each walker from 1 to 2000 steps, and verified that convergence of the Markov-chains of the ensemble of walkers is attained after ~ 100 iterations steps where the mean (and median) of the computed parameters are clearly bounded by the variance of the sample. Figure 3 illustrates the convergence of our results for the Ophiuchus source LFAM8 as an example. We find a trigonometric parallax of $\pi = 7.242 \pm 0.060$ mas based on the MCMC methodology described in this section which is in good agreement with the result of $\pi = 7.246 \pm 0.088$ mas reported by Ortiz-León et al. (2017a). Thus, the solutions based on the MCMC method presented in this paper are calculated using 500 iteration steps as a conservative threshold to ensure convergence of the Markov chains for both single stars and binaries in our sample.

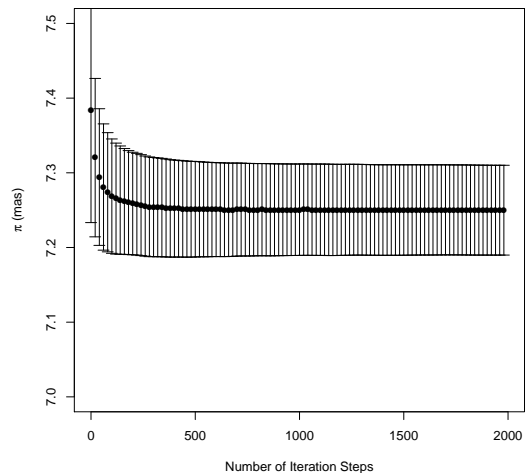


Figure 3. Convergence of the trigonometric parallax obtained for LFAM 8 based on the MCMC method implemented in this work. Each point is the average of the trigonometric parallax obtained by 200 walkers for each iteration step, and the error bars indicate the scatter of the solution given by the ensemble of walkers.

Table 2. VLBA detections and non-detections in Taurus.

GBS-VLA ^a	Other Identifier	Minimum Flux at 5.0 GHz (mJy)	Maximum Flux at 5.0 GHz (mJy)	Minimum Flux at 8.4 GHz (mJy)	Maximum Flux at 8.4 GHz (mJy)	$\log T_B$	Type ^b	Number
(1)	(2)	(3)	(4)	(5)	(6)	(7)	(8)	(9)
J041327.23+281624.4	V1096 Tau A	0.71 ± 0.05	9.2 ± 0.07	0.38 ± 0.08	0.55 ± 0.08	8.03	YSO	4/8
J041327.23+281624.4	V1096 Tau B	0.20 ± 0.04	0.36 ± 0.05	6.75	YSO	3/8
J041412.93+281211.9	V773 Tau Aa	2.77 ± 0.07	11.89 ± 0.07	0.36 ± 0.08	22.23 ± 0.20	8.66	YSO	7/7
J041412.93+281211.9	V773 Tau Ab	1.56 ± 0.07	1.56 ± 0.07	0.54 ± 0.11	1.57 ± 0.10	7.45	YSO	3/7
J041448.00+275234.4	V1098 Tau	0.22 ± 0.06	0.29 ± 0.06	1.41 ± 0.1	1.41 ± 0.1	7.48	YSO	3/8
J041628.11+280735.4	V1068 Tau	11.19 ± 0.09	11.19 ± 0.09	0.40 ± 0.13	0.40 ± 0.13	8.34	YSO	2/7
J041829.10+282618.8	2MASS J04182909+2826191	0.54 ± 0.05	1.79 ± 0.04	1.31 ± 0.1	1.31 ± 0.1	7.47	YSO	3/9
J041831.12+282715.9	HD 283518, V410 Tau	1.21 ± 0.04	3.59 ± 0.06	0.72 ± 0.09	13.62 ± 0.22	8.44	YSO	9/9
J041840.62+281915.3	V892 Tau	0.22 ± 0.06	0.22 ± 0.06	0.33 ± 0.10	0.38 ± 0.11	6.60	YSO	3/14
J041847.04+282007.2	Hubble 4a, V1023 Tau A	0.63 ± 0.06	1.44 ± 0.04	0.48 ± 0.09	14.94 ± 0.44	8.53	YSO	14/14
J041847.04+282007.2	Hubble 4b, V1023 Tau B	0.52 ± 0.04	0.52 ± 0.05	6.95	YSO	2/14
J041941.28+274947.9	V1070 Tau	0.29 ± 0.06	0.29 ± 0.06	0.58 ± 0.10	0.58 ± 0.10	7.02	YSO	2/7
J042159.43+193205.7	T Tau Sb	2.06 ± 0.06	2.62 ± 0.07	1.58 ± 0.09	4.58 ± 0.09	7.65	YSO	8/8
J042200.70+265732.2	2MASS J04220069+2657324	0.15 ± 0.05	0.15 ± 0.05	< 0.14	< 0.14	6.15	YSO	1/7
J042204.97+193448.3	2MASS J04220496+1934483	0.19 ± 0.05	0.19 ± 0.05	< 0.11	< 0.11	6.48	YSO	1/8
J042448.16+264315.9	V1201 Tau A	0.15 ± 0.05	2.40 ± 0.04	7.64	YSO	2/8
J042448.16+264315.9	V1201 Tau B	0.13 ± 0.04	0.46 ± 0.06	0.52 ± 0.07	0.53 ± 0.06	7.00	YSO	6/8
J042449.05+264310.2	HD 283641	0.36 ± 0.07	1.08 ± 0.06	0.45 ± 0.08	0.91 ± 0.09	7.26	YSO	5/6
J042920.70+263340.2	2MASS J04292071+2633406	0.22 ± 0.07	0.22 ± 0.07	6.65	YSO	1/4
J042942.47+263249.0	DI Tau	0.46 ± 0.05	0.46 ± 0.05	< 0.11	< 0.11	6.73	YSO	1/9
J043140.09+181356.7	XZ Tau	0.18 ± 0.05	0.70 ± 0.05	0.37 ± 0.1	0.37 ± 0.1	7.06	YSO	5/9
J043306.62+240954.8	V807 Tau Ba	0.28 ± 0.05	1.83 ± 0.05	0.36 ± 0.07	0.36 ± 0.07	7.51	YSO	5/9
J043310.04+243343.1	V830 Tau	1.02 ± 0.06	1.02 ± 0.06	0.5 ± 0.08	0.5 ± 0.08	7.18	YSO	2/9
J043439.24+250100.9	V1110 Tau	0.64 ± 0.06	0.64 ± 0.06	0.39 ± 0.08	0.57 ± 0.07	7.07	YSO	4/7
J043520.92+225424.0	FF Tau	0.22 ± 0.05	0.22 ± 0.05	< 0.10	< 0.10	6.53	YSO	1/9
J043542.05+225222.5	2MASS J04354203+2252226	0.24 ± 0.06	0.24 ± 0.06	0.94 ± 0.08	0.94 ± 0.08	7.20	YSO	2/9
J043554.17+225413.3	HP Tau G2	0.66 ± 0.05	4.55 ± 0.05	0.46 ± 0.08	3.07 ± 0.08	7.90	YSO	9/9

Table 2 continued

Table 2 (continued)

GBS-VLA ^a	Other Identifier	Minimum Flux at 5.0 GHz (mJy)	Maximum Flux at 5.0 GHz (mJy)	Minimum Flux at 8.4 GHz (mJy)	Maximum Flux at 8.4 GHz (mJy)	log T_B	Type ^b	Number
(1)	(2)	(3)	(4)	(5)	(6)	(7)	(8)	(9)
J044205.49+252256.0	V999 Tau	0.15 ± 0.04	0.83 ± 0.05	< 0.12	< 0.12	7.17	YSO	5/12
J044207.32+252303.0	V1000 Tau A	0.10 ± 0.04	0.96 ± 0.05	0.22 ± 0.08	0.29 ± 0.09	7.18	YSO	8/11
J044207.32+252303.0	V1000 Tau B	0.11 ± 0.04	0.22 ± 0.05	0.19 ± 0.07	0.22 ± 0.08	6.59	YSO	6/11
J045536.97+301754.8	HD 282630	0.28 ± 0.05	0.37 ± 0.04	0.34 ± 0.08	0.34 ± 0.08	6.85	YSO	3/7
J042922.26+263728.6	SDSS J042922.24+263728.7	0.12 ± 0.04	0.12 ± 0.04	0.19 ± 0.06	0.19 ± 0.06	6.62	Star?	2/8
J042926.77+263047.8		< 0.05	< 0.05	0.20 ± 0.07	0.20 ± 0.07	6.57	Star?	1/7
J043113.01+270834.8	WISE J043113.00+270834.9	< 0.07	< 0.07	0.20 ± 0.07	0.20 ± 0.07	6.59	Star?	1/6
J041443.21+275347.5		1.13 ± 0.05	1.14 ± 0.05	0.61 ± 0.08	0.76 ± 0.08	7.31	B	6/6
J041515.93+291244.5	WISE J041515.85+291244.3	0.23 ± 0.06	0.54 ± 0.09	7.06	B	5/5
J041825.42+252156.4	WISE J041825.43+252156.4	0.33 ± 0.05	0.33 ± 0.05	0.31 ± 0.07	0.37 ± 0.08	6.82	B	3/4
J042449.45+264304.1		0.19 ± 0.05	0.24 ± 0.04	0.32 ± 0.08	0.32 ± 0.08	6.80	B	3/6
J042452.48+264204.5	SDSS J042452.47+264204.5	3.87 ± 0.07	4.48 ± 0.09	7.95	B	4/4
J042920.74+263353.4	JH 507	0.19 ± 0.05	0.55 ± 0.07	7.04	B	4/4
J042929.49+263152.8	2MASS J04292949+2631528	13.33 ± 0.13	17.62 ± 0.10	8.62	B	5/5
J042939.59+263110.7		0.16 ± 0.05	0.29 ± 0.08	6.75	B	2/5
J043109.20+271045.3		0.23 ± 0.07	0.47 ± 0.11	6.81	B	4/4
J043229.46+181400.3	2MASS J04322946+1814002	7.84 ± 0.36	68.91 ± 0.64	9.09	B	5/5
J043235.22+242021.4	XEST 03-026	0.37 ± 0.05	0.37 ± 0.05	20.39 ± 0.13	27.71 ± 0.18	8.77	B	4/4
J043237.91+242054.5		0.16 ± 0.05	0.20 ± 0.05	0.34 ± 0.09	0.64 ± 0.09	7.17	B	5/5
J043306.02+243254.4	WISE J043305.95+243253.8	0.16 ± 0.05	0.20 ± 0.05	0.22 ± 0.07	0.22 ± 0.07	6.64	B	3/6
J043326.35+222832.0	SDSS J043326.34+222831.9	0.55 ± 0.06	1.08 ± 0.08	7.33	B	4/4
J044144.92+255815.3	WISE J044144.86+255815.0	0.17 ± 0.05	0.19 ± 0.06	0.16 ± 0.06	0.18 ± 0.06	6.51	B	4/6
J044210.59+252505.4	WISE J044210.55+252505.6	0.27 ± 0.07	0.43 ± 0.06	0.28 ± 0.06	0.30 ± 0.08	7.13	B	7/12
J044210.79+252420.2	WISE J044210.55+252505.6	0.94 ± 0.12	1.81 ± 0.10	7.58	B	8/8
J044246.20+251806.2		0.17 ± 0.05	0.27 ± 0.06	6.72	B	2/4
J044247.78+251825.7	WISE J044247.80+251825.3	0.67 ± 0.07	0.76 ± 0.09	7.17	B	4/4
J044252.01+251904.9	WISE J044251.97+251905.1	3.61 ± 0.14	4.26 ± 0.12	7.91	B	4/4
J044308.05+252210.2	2MASS J04430807+2522103	3.20 ± 0.09	4.15 ± 0.08	7.90	B	4/4
J045539.28+301627.2	WISE J045539.26+301627.1	0.72 ± 0.06	1.00 ± 0.08	7.23	B	4/4

Table 2 continued

Table 2 (continued)

GBS-VLA ^a Identifier	Other Identifier	Minimum Flux at 5.0 GHz (mJy)	Maximum Flux at 5.0 GHz (mJy)	Minimum Flux at 8.4 GHz (mJy)	Maximum Flux at 8.4 GHz (mJy)	$\log T_B$	Type ^b	Number Det./Obs.
(1)	(2)	(3)	(4)	(5)	(6)	(7)	(8)	(9)
J045607.08+302726.7		0.22 ± 0.06	0.47 ± 0.09	6.94	B	4/4
J041343.94+282054.8		< 0.12	< 0.12	...	—	0/4
J041343.94+282054.8		< 0.12	< 0.12	...	—	0/4
J041412.58+281155.7	2MASS J04141256+2811561	< 0.14	< 0.14	...	—	0/4
J041519.37+291247.9	WISE J041519.37+291247.7	< 0.06	...	< 0.10	< 0.10	...	—	0/7
J041635.09+280818.8		< 0.10	< 0.10	...	—	0/4
J041833.38+283732.2	2MASS J04183343+2837321	< 0.08	...	< 0.13	< 0.13	...	YSO	0/6
J041840.27+282036.0		< 0.07	...	< 0.11	< 0.11	...	—	0/14
J041851.49+282026.1	2MASS J04185147+2820264	< 0.07	...	< 0.13	< 0.13	...	YSO	0/9
J041916.12+275048.2	2MASS J04191612+2750481	< 0.13	< 0.13	...	—	0/5
J041926.27+282614.0	V819 Tau	< 0.13	< 0.13	...	YSO	0/5
J041940.54+274953.6	SDSS J041940.55+274953.5	< 0.14	< 0.14	...	—	0/4
J042202.20+265730.3	FS Tau	< 0.09	...	< 0.13	< 0.13	...	YSO	0/6
J042202.63+265709.1		< 0.14	< 0.14	...	—	0/4
J042517.49+261748.4	SDSS J042517.49+261748.5	< 0.06	...	< 0.11	< 0.11	...	—	0/5
J042939.80+263222.9		< 0.11	< 0.11	...	—	0/5
J043002.25+260843.4	SDSS J043002.24+260843.4	< 0.12	< 0.12	...	—	0/4
J043114.45+271017.6	V1320 Tau	< 0.11	< 0.11	...	YSO	0/4
J043116.56+271006.9		< 0.11	< 0.11	...	—	0/4
J043125.13+181616.6	V1073 Tau, HD 285845	< 0.10	< 0.10	...	—	0/5
J043134.15+180804.6	LDN 1551 IRS 5B	< 0.11	< 0.11	...	YSO	0/5
J043148.73+254021.8	SDSS J043148.70+254021.6	< 0.11	< 0.11	...	—	0/4
J043214.58+182014.6	V827 Tau	< 0.09	< 0.09	...	YSO	0/5
J043235.57+242008.5		< 0.12	< 0.12	...	—	0/4
J043513.27+225920.2	EZ Tau	< 0.07	...	< 0.10	< 0.10	...	—	0/7
J043550.97+225339.3		< 0.07	...	< 0.09	< 0.09	...	—	0/7
J043553.52+225408.9	HP Tau G3	< 0.09	< 0.09	...	YSO	0/5
J043558.97+223835.2	2MASS J04355892+2238353	< 0.10	< 0.10	...	YSO	0/4
J043657.44+241835.1		< 0.10	< 0.10	...	—	0/3

Table 2 continued

Table 2 (continued)

GBS-VLA ^a Identifier (1)	Other Identifier (2)	Minimum Flux at 5.0 GHz (mJy) (3)	Maximum Flux at 5.0 GHz (mJy) (4)	Minimum Flux at 8.4 GHz (mJy) (5)	Maximum Flux at 8.4 GHz (mJy) (6)	$\log T_B$ (7)	Type ^b (8)	Number Det./Obs. (9)
J044123.47+245528.1		< 0.11	< 0.11	...	—	0/4
J044209.56+252427.7		< 0.11	< 0.11	...	—	0/7
J044307.69+252348.2	WISE J044307.66+252347.5	< 0.11	< 0.11	...	—	0/4
J045534.44+302808.3	XEST 26-028	< 0.11	< 0.11	...	—	0/4
J045605.30+302541.7		< 0.10	< 0.10	...	—	0/4
J045607.27+302728.2		< 0.10	< 0.10	...	—	0/4

^a The GBS-VLA (Gould's Belt Very Large Array Survey) identifier is defined by Dzib et al. (2015).

^b Type of source: "YSO" = Young Stellar Object, "Star?" = field star and "B" = background source (Galactic or extragalactic).

Table 3. VLBA data in Taurus from the NRAO archive.

Project Code	Date	Source	Calibrators ^a
BM198A	11-mar-2004	V773 Tau A	J0403+2600, J0408+3032
BM198B	12-mar-2004	V773 Tau A	J0403+2600, J0408+3032
BM198C	13-mar-2004	V773 Tau A	J0403+2600, J0408+3032
BM198D	14-mar-2004	V773 Tau A	J0403+2600, J0408+3032
BM198E	15-mar-2004	V773 Tau A	J0403+2600, J0408+3032
BM198F	16-mar-2004	V773 Tau A	J0403+2600, J0408+3032
BM198G	17-mar-2004	V773 Tau A	J0403+2600, J0408+3032
BL128AA	08-sep-2005	V773 Tau A	J0408+3032, J0403+2600, J0429+2724, J0356+2903
BL128AB	15-nov-2005	V773 Tau A	J0408+3032, J0403+2600, J0429+2724, J0356+2903
BL128AC	21-jan-2006	V773 Tau A	J0408+3032, J0403+2600, J0429+2724, J0356+2903
BL128AD	01-apr-2006	V773 Tau A	J0408+3032, J0403+2600, J0429+2724, J0356+2903
BL128AE	12-jun-2006	V773 Tau A	J0408+3032, J0403+2600, J0429+2724, J0356+2903
BL128AF	05-sep-2006	V773 Tau A	J0408+3032, J0403+2600, J0429+2724, J0356+2903
BL146B	23-aug-2007	V773 Tau A	J0408+3032, J0403+2600, J0429+2724, J0356+2903
BL146C	29-aug-2007	V773 Tau A	J0408+3032, J0403+2600, J0429+2724, J0356+2903
BL146D	05-sep-2007	V773 Tau A	J0408+3032, J0403+2600, J0429+2724, J0356+2903
BL146E	11-sep-2007	V773 Tau A	J0408+3032, J0403+2600, J0429+2724, J0356+2903
BL146F	16-sep-2007	V773 Tau A	J0408+3032, J0403+2600, J0429+2724, J0356+2903
BL146G	21-sep-2007	V773 Tau A	J0408+3032, J0403+2600, J0429+2724, J0356+2903
BL146H	27-sep-2007	V773 Tau A	J0408+3032, J0403+2600, J0429+2724, J0356+2903
BL146I	03-oct-2007	V773 Tau A	J0408+3032, J0403+2600, J0429+2724, J0356+2903
BL146J	09-oct-2007	V773 Tau A	J0408+3032, J0403+2600, J0429+2724, J0356+2903
BL146K	17-oct-2007	V773 Tau A	J0408+3032, J0403+2600, J0429+2724, J0356+2903
BL146L	23-oct-2007	V773 Tau A	J0408+3032, J0403+2600, J0429+2724, J0356+2903
BL146M	27-oct-2007	V773 Tau A	J0408+3032, J0403+2600, J0429+2724, J0356+2903
BL146N	17-nov-2007	V773 Tau A	J0408+3032, J0403+2600, J0429+2724, J0356+2903
BM306	27-sep-2009	V773 Tau A	J0408+3032, J0403+2600, J0429+2724, J0356+2903
BL124BA	19-sep-2004	V1023 Tau	J0429+2724, J0433+2905, J0408+3032, J0403+2600
BL124BB	04-jan-2005	V1023 Tau	J0429+2724, J0433+2905, J0408+3032, J0403+2600
BL124BC	25-mar-2005	V1023 Tau	J0429+2724, J0433+2905, J0408+3032, J0403+2600
BL124BD	04-jul-2005	V1023 Tau	J0429+2724, J0433+2905, J0408+3032, J0403+2600
BL136AA	18-sep-2005	V1023 Tau	J0429+2724, J0433+2905, J0408+3032, J0403+2600
BL136AB	28-dec-2005	V1023 Tau	J0429+2724, J0433+2905, J0408+3032, J0403+2600
BL124CA	22-sep-2004	HDE 283572	J0429+2724, J0433+2905, J0408+3032, J0403+2600
BL124CB	06-jan-2005	HDE 283572	J0429+2724, J0433+2905, J0408+3032, J0403+2600
BL124CC	30-mar-2005	HDE 283572	J0429+2724, J0433+2905, J0408+3032, J0403+2600
BL124CD	23-jun-2005	HDE 283572	J0429+2724, J0433+2905, J0408+3032, J0403+2600
BL136BA	23-sep-2005	HDE 283572	J0429+2724, J0433+2905, J0408+3032, J0403+2600
BL136BB	24-dec-2005	HDE 283572	J0429+2724, J0433+2905, J0408+3032, J0403+2600

Table 3 continued

Table 3 (*continued*)

Project Code	Date	Source	Calibrators ^a
BL128BA	07-sep-2005	HP Tau G2	J0426+2327, J0435+2532, J0449+1754
BL128BB	16-nov-2005	HP Tau G2	J0426+2327, J0435+2532, J0449+1754
BL128BC	23-jan-2006	HP Tau G2	J0426+2327, J0435+2532, J0449+1754
BL128BD	31-mar-2006	HP Tau G2	J0426+2327, J0435+2532, J0449+1754
BL128BE	10-jun-2006	HP Tau G2	J0426+2327, J0435+2532, J0449+1754
BL128BF	08-sep-2006	HP Tau G2	J0426+2327, J0435+2532, J0449+1754
BT093AB	03-sep-2007	HP Tau G2	J0426+2327, J0435+2532, J0449+1754
BT093AC	04-dec-2007	HP Tau G2	J0426+2327, J0435+2532, J0449+1754
BL118A	24-sep-2003	T Tau Sb	J0428+1732, J0431+1731
BL118B	18-nov-2003	T Tau Sb	J0428+1732, J0431+1731
BL118C	15-jan-2004	T Tau Sb	J0428+1732, J0431+1731
BL118D	26-mar-2004	T Tau Sb	J0428+1732, J0431+1731
BL118E	13-may-2004	T Tau Sb	J0428+1732, J0431+1731
BL118F	08-jul-2004	T Tau Sb	J0428+1732, J0431+1731
BL124AA	16-sep-2004	T Tau Sb	J0428+1732, J0426+2327, J0412+1856
BL124AB	09-nov-2004	T Tau Sb	J0428+1732, J0426+2327, J0412+1856
BL124AC	28-dec-2004	T Tau Sb	J0428+1732, J0426+2327, J0412+1856
BL124AD	23-feb-2005	T Tau Sb	J0428+1732, J0426+2327, J0412+1856
BL124AE	09-may-2005	T Tau Sb	J0428+1732, J0426+2327, J0412+1856
BL124AF	08-jul-2005	T Tau Sb	J0428+1732, J0426+2327, J0412+1856
BS171	10-mar-2007	V807 Tau B	J0426+2327, J0429+2724, J0450+2249
BS176A	19-mar-2008	V807 Tau B	J0426+2327, J0429+2724, J0450+2249
BS176B	04-jun-2008	V807 Tau B	J0426+2327, J0429+2724, J0450+2249
BS176C	28-aug-2008	V807 Tau B	J0426+2327, J0429+2724, J0450+2249
BS176D	10-dec-2008	V807 Tau B	J0426+2327, J0429+2724, J0450+2249
BS176E	06-mar-2009	V807 Tau B	J0426+2327, J0429+2724, J0450+2249

^a The main calibrator is the first source in the list.

Table 4. VLBA measured positions for the sources in our sample.

Project Code	Julian Day	α		δ		σ_α	σ_δ	
		(h:m:s)		(d:m:s)		(sec)	(arcsec)	
V1096 Tau								
First source:								
BL175E8	2457123.49009	04	13	27.23089125	28 16	24.2804961	0.00000214	0.0000826
BL175HL	2457304.99447	04	13	27.23164300	28 16	24.2750503	0.00000318	0.0001228
BL175IE	2457508.42722	04	13	27.23100894	28 16	24.2641215	0.00000214	0.0000568
BL175IU	2457635.08049	04	13	27.23210035	28 16	24.2605681	0.00000030	0.0000086

Table 4 continued

Table 4 (*continued*)

Project Code	Julian Day			α			δ	σ_α	σ_δ
				(h:m:s)			(d:m:s)	(sec)	(arcsec)
Second source:									
BL175IE	2457508.42722	04	13	27.23206682	28	16	24.2607435	0.00000470	0.0001528
BL175JO	2457823.56275	04	13	27.23212501	28	16	24.2389033	0.00000615	0.0001748
BL175KL	2458021.98861	04	13	27.23362587	28	16	24.2229736	0.00001134	0.0002244
V773 Tau A									
First source:									
BM198A	2453076.34166	04	14	12.91903483	28	12	12.2288905	0.00000933	0.0001195
BM198B	2453077.34166	04	14	12.91904738	28	12	12.2292264	0.00000283	0.0000582
BM198C	2453078.34166	04	14	12.91902199	28	12	12.2290431	0.00000486	0.0000776
BM198D	2453079.34164	04	14	12.91902426	28	12	12.2288853	0.00000824	0.0001612
BM198E	2453080.34132	04	14	12.91902779	28	12	12.2288400	0.00000379	0.0000583
BM198F	2453081.34132	04	14	12.91902332	28	12	12.2287441	0.00000934	0.0001767
BM198G	2453082.34132	04	14	12.91903108	28	12	12.2286920	0.00000289	0.0000539
BL128AA	2453622.00127	04	14	12.92153448	28	12	12.2019074	0.00000091	0.0000217
BL128AB	2453689.81561	04	14	12.92115364	28	12	12.1960137	0.00000259	0.0000654
BL128AC	2453756.63270	04	14	12.92074305	28	12	12.1908771	0.00000208	0.0000953
BL128AD	2453827.43855	04	14	12.92114398	28	12	12.1862610	0.00000060	0.0000176
BL128AE	2453899.24225	04	14	12.92180141	28	12	12.1810787	0.00000468	0.0001318
BL128AF	2453984.01014	04	14	12.92268480	28	12	12.1788681	0.00000392	0.0001313
BL146B	2454336.04604	04	14	12.92404754	28	12	12.1561299	0.00000073	0.0000194
BL146C	2454342.02950	04	14	12.92402354	28	12	12.1553075	0.00000065	0.0000172
BL146E	2454354.99426	04	14	12.92390743	28	12	12.1534522	0.00000384	0.0001042
BL146F	2454359.98061	04	14	12.92388964	28	12	12.1534475	0.00000223	0.0000483
BL146G	2454364.96686	04	14	12.92388780	28	12	12.1528596	0.00000476	0.0001557
BL146H	2454370.95035	04	14	12.92390505	28	12	12.1527755	0.00000213	0.0000440
BL146K	2454390.89597	04	14	12.92405162	28	12	12.1517545	0.00000246	0.0000567
BL146M	2454400.86840	04	14	12.92392191	28	12	12.1505119	0.00000157	0.0000387
BL146N	2454421.81133	04	14	12.92372311	28	12	12.1495137	0.00000100	0.0000373
BM306	2455101.83854	04	14	12.92729955	28	12	12.0998316	0.00000128	0.0000402
BL175DQ	2456663.68285	04	14	12.93233851	28	12	11.9687653	0.00000129	0.0000425
BL175E8	2457123.49009	04	14	12.93332846	28	12	11.9300992	0.00000297	0.0000906
BL175H5	2456758.48992	04	14	12.93259568	28	12	11.9593395	0.00000018	0.0000046
BL175HL	2457304.99447	04	14	12.93467238	28	12	11.9200012	0.00000079	0.0000252
BL175IE	2457508.42722	04	14	12.93422635	28	12	11.9018151	0.00000046	0.0000094
BL175IU	2457635.08049	04	14	12.93503898	28	12	11.8936105	0.00000110	0.0000279
BL175JO	2457823.56275	04	14	12.93422196	28	12	11.8772228	0.00000021	0.0000054
Second source:									
BM198B	2453077.34166	04	14	12.91920729	28	12	12.2308727	0.00000355	0.0000734
BM198C	2453078.34166	04	14	12.91922522	28	12	12.2311559	0.00000780	0.0001522
BM198D	2453079.34164	04	14	12.91923426	28	12	12.2307429	0.00000466	0.0000904

Table 4 *continued*

Table 4 (continued)

Project Code	Julian Day			α		δ		σ_α	σ_δ
				(h:m:s)	(d:m:s)	(sec)	(arcsec)		
BM198E	2453080.34132	04	14	12.91923663	28	12	12.2307739	0.00000365	0.0000492
BM198F	2453081.34132	04	14	12.91925907	28	12	12.2305721	0.00001196	0.0002318
BM198G	2453082.34132	04	14	12.91925013	28	12	12.2300748	0.00000581	0.0001293
BL128AA	2453622.00127	04	14	12.92143290	28	12	12.2012723	0.00000135	0.0000361
BL128AB	2453689.81561	04	14	12.92131239	28	12	12.1978325	0.00000245	0.0000676
BL128AC	2453756.63270	04	14	12.92095469	28	12	12.1920112	0.00000254	0.0001161
BL128AD	2453827.43855	04	14	12.92104811	28	12	12.1855132	0.00000061	0.0000217
BL128AF	2453984.01014	04	14	12.92258156	28	12	12.1785780	0.00000161	0.0000586
BL146B	2454336.04604	04	14	12.92388138	28	12	12.1548706	0.00000151	0.0000491
BL146C	2454342.02950	04	14	12.92393725	28	12	12.1553660	0.00000237	0.0000491
BL146E	2454354.99426	04	14	12.92410004	28	12	12.1555427	0.00000961	0.0002467
BL146F	2454359.98061	04	14	12.92410830	28	12	12.1551514	0.00000162	0.0000394
BL146H	2454370.95035	04	14	12.92407807	28	12	12.1533466	0.00001267	0.0001229
BL146K	2454390.89597	04	14	12.92395429	28	12	12.1515895	0.00000114	0.0000307
BL146M	2454400.86840	04	14	12.92396709	28	12	12.1513541	0.00000127	0.0000336
BL146N	2454421.81133	04	14	12.92392816	28	12	12.1499864	0.00000073	0.0000236
BM306	2455101.83854	04	14	12.92720320	28	12	12.0989609	0.00000129	0.0000398
BL175DQ	2456663.68285	04	14	12.93259528	28	12	11.9699816	0.00000369	0.0001192
BL175HL	2457304.99447	04	14	12.93458736	28	12	11.9199596	0.00000121	0.0000357
BL175IU	2457635.08049	04	14	12.93526018	28	12	11.8947988	0.00000201	0.0000514
V1098 Tau									
BL175DR	2456664.68012	04	14	47.97514216	27	52	34.2258129	0.00000159	0.0000435
BL175I5	2457474.52600	04	14	47.97687328	27	52	34.1642580	0.00000897	0.0002983
BL175J5	2457675.97685	04	14	47.97827686	27	52	34.1517890	0.00000947	0.0001841
V1068 Tau									
BL175H4	2456756.49552	04	16	28.11398675	28	07	35.3618865	0.00000608	0.0002952
BL175JQ	2457828.55994	04	16	28.11539503	28	07	35.2864392	0.00000027	0.0000072
2MASS J04182909+2826191									
BL175DG	2456604.84427	04	18	29.10498216	28	26	18.8043289	0.00000178	0.0000517
BL175I3	2457472.53492	04	18	29.10578314	28	26	18.7557610	0.00000237	0.0000641
BL175KO	2458000.11726	04	18	29.10778410	28	26	18.7292780	0.00000060	0.0000182
HD 283518									
BL175AJ	2456952.95707	04	18	31.11844013	28	27	15.7860071	0.00000195	0.0000455
BL175DG	2456604.84427	04	18	31.11764132	28	27	15.8094619	0.00000323	0.0000737
BL175FN	2457130.47151	04	18	31.11804683	28	27	15.7705111	0.00000183	0.0000504
BL175H2	2456754.50123	04	18	31.11728542	28	27	15.7962583	0.00000051	0.0000099
BL175HI	2457303.99705	04	18	31.11916746	28	27	15.7618634	0.00000139	0.0000306
BL175I3	2457472.53492	04	18	31.11850338	28	27	15.7472040	0.00000050	0.0000143
BL175J2	2457655.06198	04	18	31.11988476	28	27	15.7378804	0.00000104	0.0000289
BL175JS	2457831.57723	04	18	31.11913087	28	27	15.7227679	0.00000131	0.0000309

Table 4 continued

Table 4 (*continued*)

Project Code	Julian Day			α		δ		σ_α	σ_δ
				(h:m:s)		(d:m:s)		(sec)	(arcsec)
BL175KO	2458000.11726	04	18	31.12055382	28	27	15.7140159	0.00000113	0.0000316
V892 Tau									
BL175AJ	2456952.95707	04	18	40.61721095	28	19	15.1934728	0.00000709	0.0002577
BL175FN	2457130.47151	04	18	40.61705735	28	19	15.1887750	0.00001133	0.0002547
BL175I3	2457472.53492	04	18	40.61874667	28	19	15.1848175	0.00000779	0.0002702
V1023 Tau									
First source:									
BL124BA	2453267.99141	04	18	47.03273704	28	20	07.3989160	0.00000194	0.0000566
BL124BB	2453374.69925	04	18	47.03195145	28	20	07.3889580	0.00000338	0.0000943
BL124BC	2453455.47808	04	18	47.03188434	28	20	07.3815212	0.00000059	0.0000141
BL124BD	2453556.20230	04	18	47.03279950	28	20	07.3751238	0.00000264	0.0000701
BL136AA	2453631.99451	04	18	47.03307242	28	20	07.3702589	0.00000234	0.0000439
BL136AB	2453732.71901	04	18	47.03234046	28	20	07.3605755	0.00000139	0.0000306
BL175AJ	2456952.95707	04	18	47.03870271	28	20	07.1395482	0.00000599	0.0001472
BL175AK	2456955.94887	04	18	47.03868534	28	20	07.1391202	0.00000307	0.0000788
BL175DI	2456613.81969	04	18	47.03817905	28	20	07.1653746	0.00000344	0.0001125
BL175DJ	2456627.78105	04	18	47.03805348	28	20	07.1638188	0.00000366	0.0001482
BL175DZ	2457120.49916	04	18	47.03807794	28	20	07.1223505	0.00000246	0.0000903
BL175FN	2457130.47151	04	18	47.03817331	28	20	07.1217692	0.00000389	0.0001134
BL175H2	2456754.50123	04	18	47.03776076	28	20	07.1518265	0.00000380	0.0000584
BL175H3	2456755.49850	04	18	47.03772022	28	20	07.1519711	0.00000095	0.0000176
BL175HI	2457303.99705	04	18	47.03915070	28	20	07.1097996	0.00000111	0.0000223
BL175HJ	2457299.01069	04	18	47.03919348	28	20	07.1104589	0.00000165	0.0000628
BL175I3	2457472.53492	04	18	47.03842442	28	20	07.0918583	0.00000173	0.0000528
BL175J2	2457655.06198	04	18	47.03975579	28	20	07.0773651	0.00000273	0.0000806
BL175JS	2457831.57723	04	18	47.03909636	28	20	07.0564644	0.00000096	0.0000252
BL175KO	2458000.11726	04	18	47.04086088	28	20	07.0420352	0.00000117	0.0000352
Second source:									
BL175J2	2457655.06198	04	18	47.04210383	28	20	07.0556409	0.00000199	0.0000699
BL175JS	2457831.57723	04	18	47.04116027	28	20	07.0496104	0.00000264	0.0000686
V1070 Tau									
BL175E6	2457122.49270	04	19	41.27993968	27	49	47.7684510	0.00000368	0.0001280
BL175JQ	2457828.55994	04	19	41.28112838	27	49	47.7215125	0.00001017	0.0003221
T Tau Sb									
BL118A	2452906.98152	04	21	59.42530458	19	32	05.7177447	0.00000149	0.0000519
BL118B	2452961.83470	04	21	59.42498901	19	32	05.7167877	0.00000217	0.0000632
BL118C	2453019.67298	04	21	59.42460196	19	32	05.7154182	0.00000532	0.0001753
BL118D	2453091.47639	04	21	59.42455053	19	32	05.7156660	0.00000139	0.0000490
BL118E	2453139.34532	04	21	59.42489157	19	32	05.7162678	0.00000216	0.0000613
BL118F	2453195.19242	04	21	59.42535452	19	32	05.7168794	0.00000193	0.0000519

Table 4 continued

Table 4 (continued)

Project Code	Julian Day	α			δ			σ_α	σ_δ
		(h:m:s)			(d:m:s)			(sec)	(arcsec)
BL124AA	2453264.99958	04	21	59.42555422	19	32	05.7167745	0.00000226	0.0000565
BL124AB	2453318.85214	04	21	59.42530136	19	32	05.7159188	0.00000328	0.0000605
BL124AC	2453367.71835	04	21	59.42495572	19	32	05.7146562	0.00000494	0.0001236
BL124AD	2453425.55966	04	21	59.42477431	19	32	05.7141146	0.00000144	0.0000389
BL124AE	2453500.35521	04	21	59.42516093	19	32	05.7152997	0.00000587	0.0002035
BL124AF	2453560.19135	04	21	59.42567042	19	32	05.7158899	0.00000234	0.0000666
BL175C1	2456160.05829	04	21	59.43082603	19	32	05.6775494	0.00000071	0.0000208
BL175CG	2456375.47180	04	21	59.43051210	19	32	05.6700787	0.00000151	0.0000478
BL175EU	2456908.07274	04	21	59.43282803	19	32	05.6550849	0.00000221	0.0000444
BL175EV	2457138.40793	04	21	59.43276339	19	32	05.6452563	0.00000187	0.0000449
BL175H7	2456760.44308	04	21	59.43165649	19	32	05.6587215	0.00000212	0.0000412
BL175HR	2457312.92983	04	21	59.43389549	19	32	05.6393294	0.00000061	0.0000133
BL175I8	2457483.46302	04	21	59.43368910	19	32	05.6310770	0.00000160	0.0000386
BL175J0	2457671.94680	04	21	59.43499974	19	32	05.6242630	0.00000145	0.0000351
2MASS J04220069+2657324									
BL175I6	2457479.51756	04	22	00.70159409	26	57	32.2221699	0.00001916	0.0002906
2MASS J04220496+1934483									
BL175I8	2457483.46302	04	22	04.96967772	19	34	48.1921823	0.00001298	0.0003782
V1201 Tau									
First source:									
BL175I1	2457447.59306	04	24	48.16759759	26	43	15.8324452	0.00000040	0.0000123
BL175KJ	2458015.03904	04	24	48.16982186	26	43	15.7852040	0.00002083	0.0004156
Second source:									
BL175AY	2457112.52075	04	24	48.16587197	26	43	15.8380910	0.00000301	0.0000664
BL175D6	2456551.98899	04	24	48.16552716	26	43	15.8611304	0.00000155	0.0000621
BL175I1	2457447.59306	04	24	48.16651140	26	43	15.8259709	0.00000355	0.0001095
BL175J3	2457657.02050	04	24	48.16787903	26	43	15.8208406	0.00000310	0.0000789
BL175JT	2457857.47054	04	24	48.16758130	26	43	15.8113735	0.00000690	0.0002582
BL175KJ	2458015.03904	04	24	48.16873035	26	43	15.8077056	0.00000870	0.0001738
HD 283641									
BL175AY	2457112.52075	04	24	49.05721592	26	43	10.1389572	0.00000351	0.0000852
BL175D6	2456551.98899	04	24	49.05678964	26	43	10.1670888	0.00000305	0.0000804
BL175HF	2457286.04620	04	24	49.05842301	26	43	10.1333730	0.00000271	0.0000603
BL175JZ	2457865.44898	04	24	49.05898202	26	43	10.1042734	0.00001129	0.0001647
BL175KT	2458029.99808	04	24	49.06003925	26	43	10.0993622	0.00000342	0.0000672
2MASS J04292071+2633406									
BL175D8	2456587.89069	04	29	20.71195265	26	33	40.1840012	0.00000310	0.0001419
DI Tau									
BL175IZ	2457674.98070	04	29	42.48270733	26	32	48.7653960	0.00000576	0.0001264
XZ Tau A									

Table 4 continued

Table 4 (*continued*)

Project Code	Julian Day	α		δ		σ_α	σ_δ	
		(h:m:s)		(d:m:s)		(sec)	(arcsec)	
BL175AB	2456909.07819	04	31	40.09742757	18 13	56.6810369	0.00000662	0.0001751
BL175IF	2457510.29653	04	31	40.09798379	18 13	56.6529997	0.00000180	0.0000533
BL175IV	2457646.01944	04	31	40.09895214	18 13	56.6480055	0.00000571	0.0001823
BL175JP	2457839.48901	04	31	40.09847877	18 13	56.6379928	0.00000686	0.0003222
BL175KM	2457999.05288	04	31	40.09970131	18 13	56.6325338	0.00000508	0.0002023
V807 Tau B								
First source:								
BS171	2454170.52099	4	33	6.62478461	24 9	54.9897097	0.00000446	0.0001265
BS176A	2454545.49509	4	33	6.62554683	24 9	54.9531558	0.00000885	0.0001386
BS176C	2454707.05276	4	33	6.62701096	24 9	54.9399241	0.00000045	0.0000106
BL175HC	2457277.07074	4	33	6.63207855	24 9	54.7636720	0.00000284	0.0001037
BL175I4	2457473.53391	4	33	6.63109755	24 9	54.7448511	0.00000077	0.0000214
BL175J4	2457661.00951	4	33	6.63224890	24 9	54.7305718	0.00000663	0.0001580
BL175KP	2458012.04714	4	33	6.63265218	24 9	54.6991288	0.00001361	0.0002653
BL175KU	2458038.97343	4	33	6.63257459	24 9	54.6959478	0.00000156	0.0000459
Second source:								
BS176A	2454545.49509	4	33	6.62819963	24 9	54.9628596	0.00000145	0.0000410
V830 Tau								
BL175HC	2457277.07074	04	33	10.03886881	24 33	42.9238221	0.00000272	0.0000722
BL175KU	2458038.97343	04	33	10.03986954	24 33	42.8795713	0.00000186	0.0000567
V1110 Tau								
BL175CZ	2456478.19069	04	34	39.22801832	25 01	00.8647883	0.00000301	0.0001162
BL175FO	2457137.44688	04	34	39.22004215	25 01	00.8421765	0.00000513	0.0001080
BL175HQ	2457310.97263	04	34	39.21936943	25 01	00.8397658	0.00000247	0.0000609
BL175KM	2457999.05288	04	34	39.21227377	25 01	00.8189967	0.00000457	0.0000958
FF Tau								
BL175JW	2457827.53277	04	35	20.91839284	22 54	23.9377063	0.00000661	0.0002069
2MASS J04354203+2252226								
BL175HB	2457311.97510	04	35	42.04763707	22 52	22.3485495	0.00000173	0.0000445
BL175KN	2458032.98233	04	35	42.04906851	22 52	22.3151875	0.00001409	0.0003389
HP Tau G2								
BL128BA	2453621.02472	04	35	54.16132309	22 54	13.4115516	0.00000347	0.0001034
BL128BB	2453690.83367	04	35	54.16118880	22 54	13.4083727	0.00000193	0.0000897
BL128BC	2453758.64799	04	35	54.16089813	22 54	13.4047983	0.00000490	0.0001433
BL128BD	2453826.46235	04	35	54.16104658	22 54	13.4018946	0.00000358	0.0001227
BL128BE	2453897.26849	04	35	54.16170598	22 54	13.3998600	0.00000088	0.0000277
BL128BF	2453987.02276	04	35	54.16231412	22 54	13.3970976	0.00000337	0.0001126
BT093AB	2454347.03702	04	35	54.16331531	22 54	13.3813722	0.00000273	0.0001037
BT093AC	2454438.78553	04	35	54.16310090	22 54	13.3762746	0.00000592	0.0001339
BL175AC	2456910.07547	04	35	54.16852241	22 54	13.2569104	0.00000250	0.0001183

Table 4 continued

Table 4 (continued)

Project Code	Julian Day	α			δ			σ_α	σ_δ
		(h:m:s)			(d:m:s)			(sec)	(arcsec)
BL175AM	2457103.54430	04	35	54.16795846	22	54	13.2515753	0.00000052	0.0000133
BL175C9	2456265.77248	04	35	54.16757923	22	54	13.2845767	0.00000144	0.0000650
BL175CO	2456437.30285	04	35	54.16783252	22	54	13.2748966	0.00000458	0.0001230
BL175HB	2457311.97510	04	35	54.16916650	22	54	13.2475448	0.00000235	0.0000638
BL175I2	2457465.55463	04	35	54.16880998	22	54	13.2410299	0.00000223	0.0000499
BL175IX	2457640.07756	04	35	54.17009639	22	54	13.2370206	0.00000407	0.0000944
BL175JX	2457868.43324	04	35	54.17003288	22	54	13.2273711	0.00000031	0.0000079
BL175KN	2458032.98233	04	35	54.17110124	22	54	13.2223770	0.00000202	0.0000456
V999 Tau									
BL175I7	2457482.00805	04	42	05.48753562	25	22	55.9357291	0.00000212	0.0000563
BL175IC	2457493.44611	04	42	05.48760415	25	22	55.9339160	0.00000305	0.0000716
BL175JW	2457827.53277	04	42	05.48809798	25	22	55.9199587	0.00000407	0.0001110
BL175JY	2457858.46892	04	42	05.48834572	25	22	55.9193334	0.00000598	0.0002329
BL175KS	2458031.99263	04	42	5.48948427	25	22	55.9136201	0.00001037	0.0002728
V1000 Tau									
First source:									
BL175AO	2457110.52612	04	42	07.32853859	25	23	02.9501876	0.00000948	0.0001902
BL175HD	2457278.06793	04	42	07.32953978	25	23	02.9409586	0.00000766	0.0001373
BL175I7	2457482.00805	04	42	07.32844691	25	23	02.9293092	0.00001460	0.0003591
BL175IZ	2457674.98070	04	42	07.32930795	25	23	02.9225642	0.00001094	0.0002668
BL175JW	2457827.53277	04	42	07.32838665	25	23	02.9154859	0.00000182	0.0000474
BL175JY	2457858.46892	04	42	07.32859912	25	23	02.9162039	0.00000963	0.0003245
BL175KS	2458031.99263	04	42	07.32989614	25	23	02.9145752	0.00000816	0.0002228
BL175KV	2458040.94749	04	42	07.32983457	25	23	02.9139646	0.00001945	0.0003817
Second source:									
BL175AO	2457110.52612	04	42	07.32744510	25	23	02.9593624	0.00001172	0.0001604
BL175HD	2457278.06793	04	42	07.32885274	25	23	02.9567504	0.00000610	0.0001787
BL175I7	2457482.00805	04	42	07.32849501	25	23	02.9475677	0.00000848	0.0002105
BL175JW	2457827.53277	04	42	07.32940284	25	23	02.9244146	0.00000932	0.0002331
BL175JY	2457858.46892	04	42	07.32965249	25	23	02.9220492	0.00000858	0.0002828
BL175KS	2458031.99263	04	42	07.33041298	25	23	02.9096857	0.00001034	0.0002937
HD 282630									
BL175E9	2457126.48192	04	55	36.97446144	30	17	54.7296915	0.00000409	0.0001375
BL175J5	2457675.97685	04	55	36.97577642	30	17	54.6956389	0.00000261	0.0001012
BL175KQ	2458005.07476	04	55	36.97615616	30	17	54.6734360	0.00000679	0.0001833
HDE 283572									
BL124CA	2453270.98321	04	21	58.85214490	28	18	06.3894324	0.00000032	0.0000090
BL124CB	2453376.69377	04	21	58.85145730	28	18	06.3800150	0.00000480	0.0000910
BL124CC	2453460.46440	04	21	58.85146242	28	18	06.3727241	0.00000148	0.0000280
BL124CD	2453545.23233	04	21	58.85236582	28	18	06.3677244	0.00000049	0.0000102

Table 4 continued

Table 4 (continued)

Project Code	Julian Day	α			δ			σ_α	σ_δ
		(h:m:s)			(d:m:s)			(sec)	(arcsec)
BL136BA	2453636.98113	04	21	58.85280655	28	18	06.3625435	0.00000709	0.0001311
BL136BB	2453728.72991	04	21	58.85221180	28	18	06.3550925	0.00000322	0.0000867
GBS-VLA J042922.26+263728.6									
BL175D9	2456588.88760	04	29	22.26012841	26	37	28.6241460	0.00000388	0.0001570
BL175JT	2457857.47054	04	29	22.26012139	26	37	28.6246214	0.00000749	0.0002222
GBS-VLA J042926.77+263047.8									
BL175AH	2456921.04444	04	29	26.74382963	26	30	47.6835190	0.00000476	0.0001745
GBS-VLA J043113.01+270834.8									
BL175HH	2457295.02163	04	31	13.00318585	27	08	34.8559697	0.00000606	0.0001080
GBS-VLA J041443.21+275347.5									
BL175DR	2456664.68012	04	14	43.20661836	27	53	47.4647481	0.00000177	0.0000623
BL175EC	2457132.46101	04	14	43.20662329	27	53	47.4650295	0.00000183	0.0000387
BL175HA	2456766.46308	04	14	43.20663208	27	53	47.4648841	0.00000195	0.0000531
BL175HO	2457307.98108	04	14	43.20662968	27	53	47.4651523	0.00000210	0.0000508
BL175I5	2457474.52600	04	14	43.20658568	27	53	47.4654784	0.00000193	0.0000391
BL175J5	2457675.97685	04	14	43.20661533	27	53	47.4649411	0.00000129	0.0000386
GBS-VLA J041515.93+291244.5									
BL175CQ	2456914.02197	04	15	15.91675221	29	12	44.4602683	0.00000489	0.0001045
BL175DF	2456602.84987	04	15	15.91678035	29	12	44.4596381	0.00000347	0.0001149
BL175EW	2457139.40576	04	15	15.91675044	29	12	44.4602843	0.00000392	0.0000949
BL175H8	2456761.43970	04	15	15.91675430	29	12	44.4600766	0.00000351	0.0000922
BL175HS	2457315.92170	04	15	15.91676815	29	12	44.4601297	0.00000461	0.0001134
GBS-VLA J041825.42+252156.4									
BL175DT	2456685.62225	04	18	25.41989117	25	21	56.3755658	0.00000628	0.0001694
BL175HA	2456766.46308	04	18	25.41985400	25	21	56.3750369	0.00000429	0.0001047
BL175I5	2457474.52600	04	18	25.41986074	25	21	56.3754329	0.00000457	0.0001239
GBS-VLA J042449.45+264304.1									
BL175HF	2457286.04620	04	24	49.45310866	26	43	04.0779280	0.00000409	0.0001513
BL175I1	2457447.59306	04	24	49.45311131	26	43	04.0779505	0.00000452	0.0001133
BL175J3	2457657.02050	04	24	49.45310454	26	43	04.0781200	0.00001085	0.0002738
GBS-VLA J042452.48+264204.5									
BL175AG	2456920.04717	04	24	52.48270712	26	42	04.5588355	0.00000097	0.0000229
BL175AY	2457112.52075	04	24	52.48269249	26	42	04.5588123	0.00000045	0.0000105
BL175D6	2456551.98899	04	24	52.48269665	26	42	04.5587069	0.00000035	0.0000112
BL175HF	2457286.04620	04	24	52.48269054	26	42	04.5589510	0.00000044	0.0000116
GBS-VLA J042920.74+263353.4									
BL175AG	2456920.04717	04	29	20.73726361	26	33	53.3526771	0.00000558	0.0001731
BL175AY	2457112.52075	04	29	20.73727480	26	33	53.3528436	0.00000344	0.0000870
BL175D8	2456587.89069	04	29	20.73726838	26	33	53.3526378	0.00000427	0.0001139
BL175HF	2457286.04620	04	29	20.73726477	26	33	53.3527734	0.00000192	0.0000683

Table 4 continued

Table 4 (continued)

Project Code	Julian Day	α		δ		σ_α	σ_δ		
		(h:m:s)		(d:m:s)		(sec)	(arcsec)		
GBS-VLA J042929.49+263152.8									
BL175AH	2456921.04444	04	29	29.48495908	26	31	52.7830409	0.00000017	0.0000049
BL175AZ	2457115.51256	04	29	29.48495348	26	31	52.7830110	0.00000015	0.0000043
BL175DA	2456591.87976	04	29	29.48495794	26	31	52.7829877	0.00000008	0.0000032
BL175H0	2456750.51190	04	29	29.48495426	26	31	52.7830586	0.00000014	0.0000044
BL175HG	2457293.02708	04	29	29.48495776	26	31	52.7830734	0.00000010	0.0000027
GBS-VLA J042939.59+263110.7									
BL175AH	2456921.04444	04	29	39.58797477	26	31	10.6966120	0.00000451	0.0001348
BL175HG	2457293.02708	04	29	39.58797557	26	31	10.6969234	0.00000353	0.0001259
GBS-VLA J043109.20+271045.3									
BL175AI	2456954.95160	04	31	9.19522684	27	10	45.3060450	0.00000708	0.0001498
BL175DD	2456594.87157	04	31	9.19522501	27	10	45.3062145	0.00000404	0.0001872
BL175H1	2456752.50643	04	31	9.19521683	27	10	45.3063584	0.00000552	0.0002258
BL175HH	2457295.02163	04	31	9.19522632	27	10	45.3065017	0.00000283	0.0000824
GBS-VLA J043229.46+181400.3									
BL175C5	2456200.90919	04	32	29.46165667	18	14	00.2088511	0.00000036	0.0000088
BL175CK	2456411.37427	04	32	29.46166027	18	14	00.2089048	0.00000112	0.0000287
BL175EA	2457127.43944	04	32	29.46166382	18	14	00.2087503	0.00000033	0.0000075
BL175H9	2456765.43058	04	32	29.46166605	18	14	00.2087775	0.00000011	0.0000030
BL175HN	2457306.94859	04	32	29.46166212	18	14	00.2088103	0.00000008	0.0000021
GBS-VLA J043235.22+242021.4									
BL175AD	2456901.09943	04	32	35.21418303	24	20	21.3604563	0.00000011	0.0000032
BL175AN	2457105.53885	04	32	35.21417103	24	20	21.3605934	0.00000012	0.0000032
BL175CV	2456454.25640	04	32	35.21418261	24	20	21.3604174	0.00000010	0.0000039
BL175HC	2457277.07074	04	32	35.21418929	24	20	21.3605589	0.00000010	0.0000029
GBS-VLA J043237.91+242054.5									
BL175AD	2456901.09943	04	32	37.91220730	24	20	54.4123584	0.00000389	0.0001047
BL175AN	2457105.53885	04	32	37.91219663	24	20	54.4123998	0.00000300	0.0001185
BL175CV	2456454.25640	04	32	37.91221517	24	20	54.4124766	0.00000211	0.0000734
BL175HC	2457277.07074	04	32	37.91220049	24	20	54.4127160	0.00000587	0.0002006
BL175I4	2457473.53391	04	32	37.91219405	24	20	54.4122528	0.00000495	0.0001104
GBS-VLA J043306.02+243254.4									
BL175HC	2457277.07074	04	33	6.01696124	24	32	54.3384220	0.00000569	0.0001212
BL175I4	2457473.53391	04	33	6.01695303	24	32	54.3383599	0.00000921	0.0002163
BL175J4	2457661.00951	04	33	6.01696502	24	32	54.3384314	0.00000884	0.0001770
GBS-VLA J043326.35+222832.0									
BL175C6	2456261.78305	04	33	26.34815922	22	28	31.9855971	0.00000121	0.0000500
BL175CL	2456413.36805	04	33	26.34816078	22	28	31.9855960	0.00000220	0.0000673
BL175FO	2457137.44688	04	33	26.34815466	22	28	31.9857088	0.00000104	0.0000305
BL175HQ	2457310.97263	04	33	26.34815937	22	28	31.9855104	0.00000163	0.0000468

Table 4 continued

Table 4 (continued)

Project Code	Julian Day	α		δ		σ_α	σ_δ		
		(h:m:s)		(d:m:s)		(sec)	(arcsec)		
GBS-VLA J044144.92+255815.3									
BL175AO	2457110.52612	04	41	44.91503305	25	58	15.2703243	0.00000664	0.0001446
BL175HD	2457278.06793	04	41	44.91503962	25	58	15.2705269	0.00000508	0.0001631
BL175IC	2457493.44611	04	41	44.91498954	25	58	15.2711434	0.00000980	0.0002906
BL175IW	2457669.96284	04	41	44.91497022	25	58	15.2694326	0.00000999	0.0002463
GBS-VLA J044210.59+252505.4									
BL175AP	2457111.52348	04	42	10.58347904	25	25	05.4533338	0.00000222	0.0000840
BL175HE	2457284.05166	04	42	10.58347820	25	25	05.4536485	0.00000524	0.0001364
BL175I7	2457482.00805	04	42	10.58341214	25	25	05.4544059	0.00000654	0.0001127
BL175IC	2457493.53605	04	42	10.58341695	25	25	05.4527184	0.00001350	0.0002539
BL175IW	2457670.05329	04	42	10.58328462	25	25	05.4508966	0.00001366	0.0003367
BL175IZ	2457674.98070	04	42	10.58348921	25	25	05.4534785	0.00001001	0.0002447
BL175JY	2457858.46892	04	42	10.58349963	25	25	05.4536354	0.00000351	0.0000979
GBS-VLA J044210.79+252420.2									
BL175AE	2456915.06181	04	42	10.78518041	25	24	20.1630787	0.00000268	0.0000809
BL175AF	2456916.05808	04	42	10.78519071	25	24	20.1632043	0.00000194	0.0000503
BL175AO	2457110.52612	04	42	10.78515031	25	24	20.1629188	0.00000197	0.0000498
BL175AP	2457111.52348	04	42	10.78520278	25	24	20.1629396	0.00000107	0.0000333
BL175D2	2456488.16365	04	42	10.78519262	25	24	20.1631267	0.00000308	0.0001119
BL175HD	2457278.06793	04	42	10.78516181	25	24	20.1627940	0.00000100	0.0000371
BL175HE	2457284.05166	04	42	10.78520160	25	24	20.1630443	0.00000091	0.0000272
BL175Z0	2456506.11442	04	42	10.78520109	25	24	20.1631525	0.00000128	0.0000341
GBS-VLA J044246.20+251806.2									
BL175AP	2457111.52348	04	42	46.20007669	25	18	06.1944843	0.00000356	0.0001226
BL175D4	2456524.06543	04	42	46.20007963	25	18	06.1949407	0.00000242	0.0001050
GBS-VLA J044247.78+251825.7									
BL175AF	2456916.05808	04	42	47.76513414	25	18	25.6885967	0.00000612	0.0001095
BL175AP	2457111.52348	04	42	47.76514029	25	18	25.6885402	0.00000405	0.0001189
BL175D4	2456524.06543	04	42	47.76514860	25	18	25.6886535	0.00000166	0.0000611
BL175HE	2457284.05166	04	42	47.76513826	25	18	25.6885444	0.00000303	0.0000610
GBS-VLA J044252.01+251904.9									
BL175AF	2456916.05808	04	42	52.00857921	25	19	04.8769703	0.00000130	0.0000323
BL175AP	2457111.52348	04	42	52.00858895	25	19	04.8767277	0.00000088	0.0000244
BL175D4	2456524.06543	04	42	52.00859829	25	19	04.8768535	0.00000045	0.0000151
BL175HE	2457284.05166	04	42	52.00858864	25	19	04.8768072	0.00000074	0.0000202
GBS-VLA J044308.05+252210.2									
BL175AF	2456916.05808	04	43	08.04644357	25	22	10.2042598	0.00000053	0.0000167
BL175AP	2457111.52348	04	43	08.04646089	25	22	10.2038252	0.00000040	0.0000109
BL175D5	2456539.02447	04	43	08.04645650	25	22	10.2039933	0.00000034	0.0000122
BL175HE	2457284.05166	04	43	08.04646101	25	22	10.2039981	0.00000033	0.0000091

Table 4 continued

Table 4 (*continued*)

Project Code	Julian Day	α		δ		σ_α	σ_δ		
		(h:m:s)		(d:m:s)		(sec)	(arcsec)		
GBS-VLA J045539.28+301627.2									
BL175DV	2456688.61448	04	55	39.27935994	30	16	27.1776275	0.00000180	0.0000502
BL175E9	2457126.48192	04	55	39.27936026	30	16	27.1776498	0.00000115	0.0000331
BL175H6	2456759.48717	04	55	39.27936755	30	16	27.1776711	0.00000140	0.0000443
BL175HM	2457302.00237	04	55	39.27936122	30	16	27.1777823	0.00000147	0.0000375
GBS-VLA J045607.08+302726.7									
BL175DW	2456696.59278	04	56	7.07563919	30	27	26.6652676	0.00000273	0.0000935
BL175E9	2457126.48192	04	56	7.07563142	30	27	26.6650612	0.00000353	0.0000866
BL175H6	2456759.48717	04	56	7.07563550	30	27	26.6652553	0.00000437	0.0000809
BL175HM	2457302.00237	04	56	7.07561911	30	27	26.6654178	0.00000378	0.0000816

4. RESULTS

We present trigonometric parallaxes for 18 stars in our sample with a minimum of 3 detections during our observing campaign. The trigonometric parallaxes and proper motions derived in this study are listed in Table 5. In addition, we derived the orbital elements of six binary and multiple systems in our sample which are given in Table 6. The best fit solution of our results are collectively illustrated in Figures 4 and 5. In Table 7 we compare the astrometry derived from the full model and joint fit for the binaries with measured relative positions in the literature. The relative astrometry model for these sources is illustrated in Figure 6. In the following we comment on the properties of the individual stars (and stellar systems) that have been investigated. We present our discussion about individual sources in the order that they appear in Table 2.

4.1. V1096 Tau

V1096 Tau is a binary system that could be resolved in our observations. Both components were simultaneously detected in only one epoch (project BL175IE) where the primary component of the system V1096 Tau A exhibits a flux density of 0.71 ± 0.05 mJy that is almost twice that of the secondary component (V1096 Tau B) with 0.36 ± 0.05 mJy. We detected the primary and secondary, respectively, in a total of 4 and 3 epochs. However, our observations cover a small fraction of the orbit so that the fit including the orbital motion of the system does not converge. So, we fit the measured positions of the individual components solely for the proper motion and parallax. We included the acceleration term in the astrometry fit for the primary component which indeed represents a better description to the data, but

this was not possible for the secondary due to the limited number of detections available. Our result for the secondary component is only indicative and should be regarded with caution as it is likely to be biased by the non-corrected orbital motion of the system. The systematic errors that we add to the stellar positions of V1096 Tau A and V1096 Tau B (as described in Sect 3.3) reach up to 1 mas and 3 mas, respectively, and they are significantly larger as compared to the other stars. The weighted mean parallax of the results given in Table 5 for the two components is $\pi = 8.04 \pm 0.50$ mas. This is consistent with a distance estimate of $d = 124.4_{-7.2}^{+8.2}$ pc. Despite the admittedly large errors on our results, this is the first distance determination for this binary system to date. The weighted mean proper motions of the two components is $\mu_\alpha \cos \delta = 2.612 \pm 0.691$ mas/yr and $\mu_\delta = -17.372 \pm 0.676$ mas/yr. V1096 Tau continues to be monitored by our team, and the results presented in this paper will be refined when more observations become available.

4.2. V773 Tau

V773 Tau is a well-known quadruple system (see e.g. Duchêne et al. 2003; Woitas 2003) and the source detected in our observations is the primary component V773 Tau A which itself is a tight binary. V773 Tau A has been detected in a total of 7 epochs during our observing, but a simultaneous detection of both components occurred only in 3 epochs (see Table 4). Moreover, it has also been observed with the VLBA in 27 additional epochs between March 2004 and September 2009 for projects BM198, BL128, BL146 and BM306 (see Table 3). We note that project BM198 observed J0403+2600 as the main phase calibrator while the other projects (including GOBELINS) used J0408+3032 instead. We corrected the positions mea-

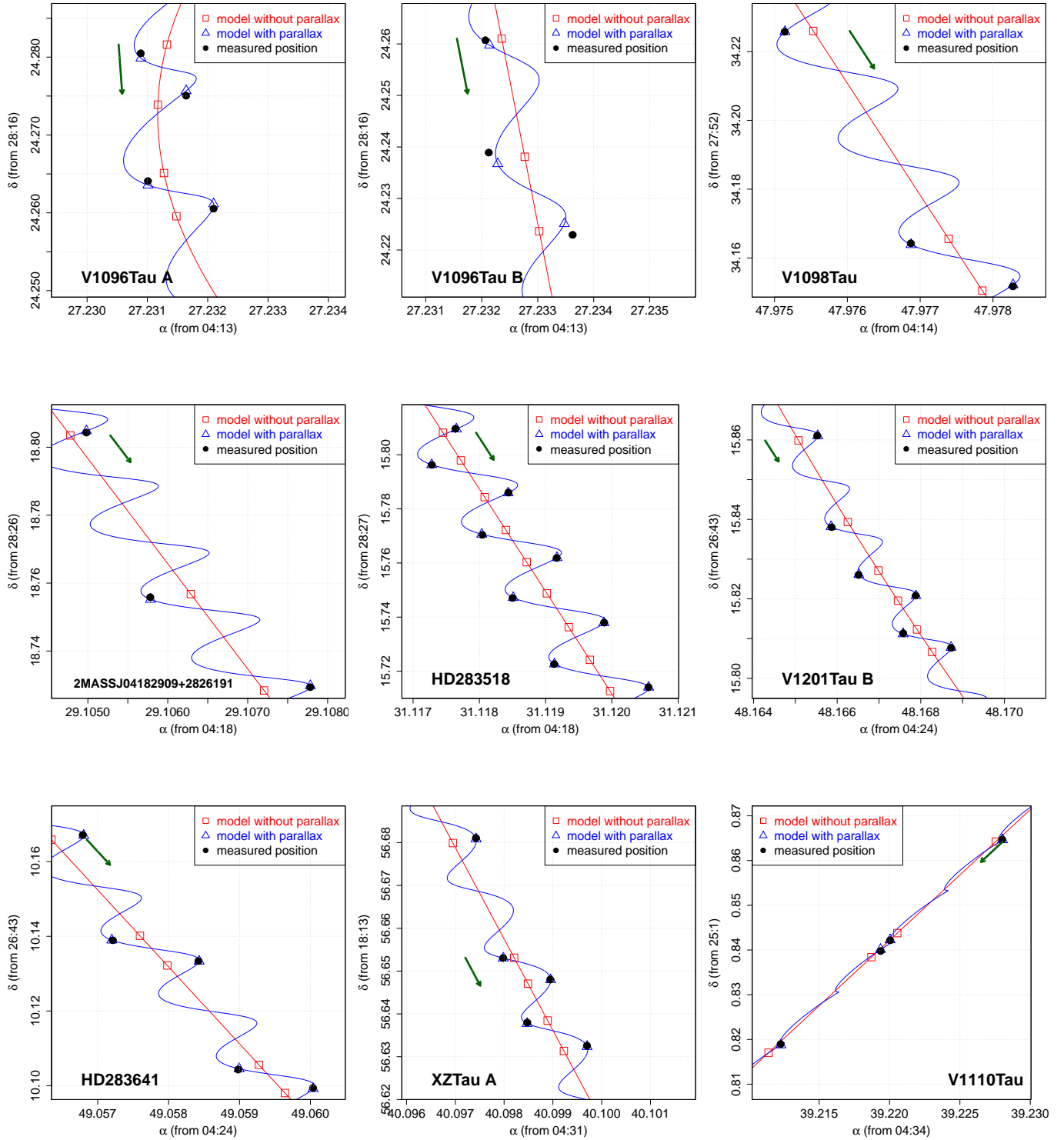


Figure 4. Astrometry fit for the single and long orbital period YSOs in our sample. Measured positions with the VLBA are shown as black circles and their corresponding error bars (including systematic errors) are mostly smaller than the symbols. The red line indicates the model with the parallax signature removed, and the blue line represents the model including the parallax. Red squares and blue triangles mark the expected positions for the corresponding models. The green arrow shows the direction of the stellar proper motions in the plane of the sky.

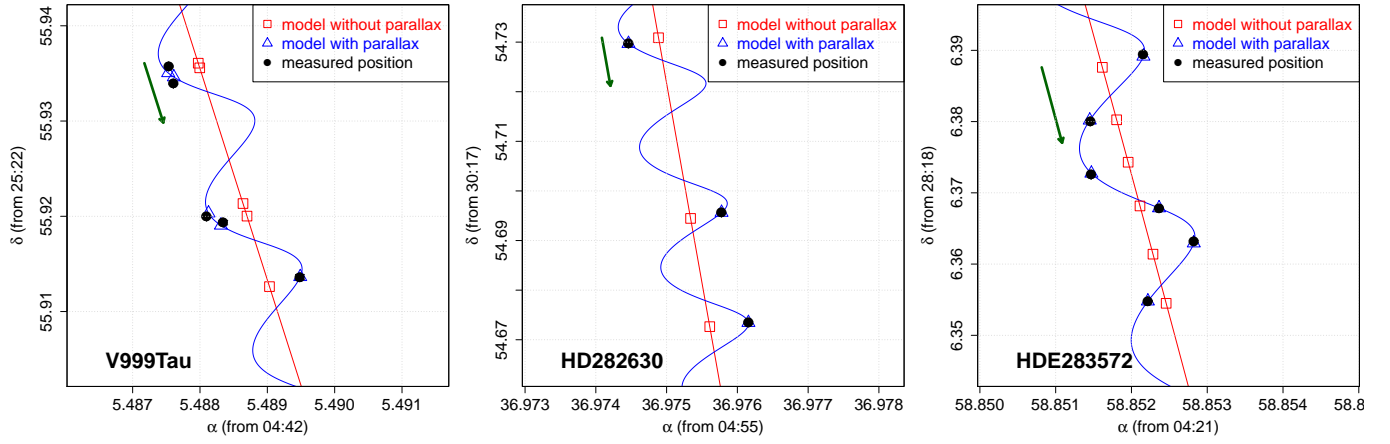


Figure 4. continued.

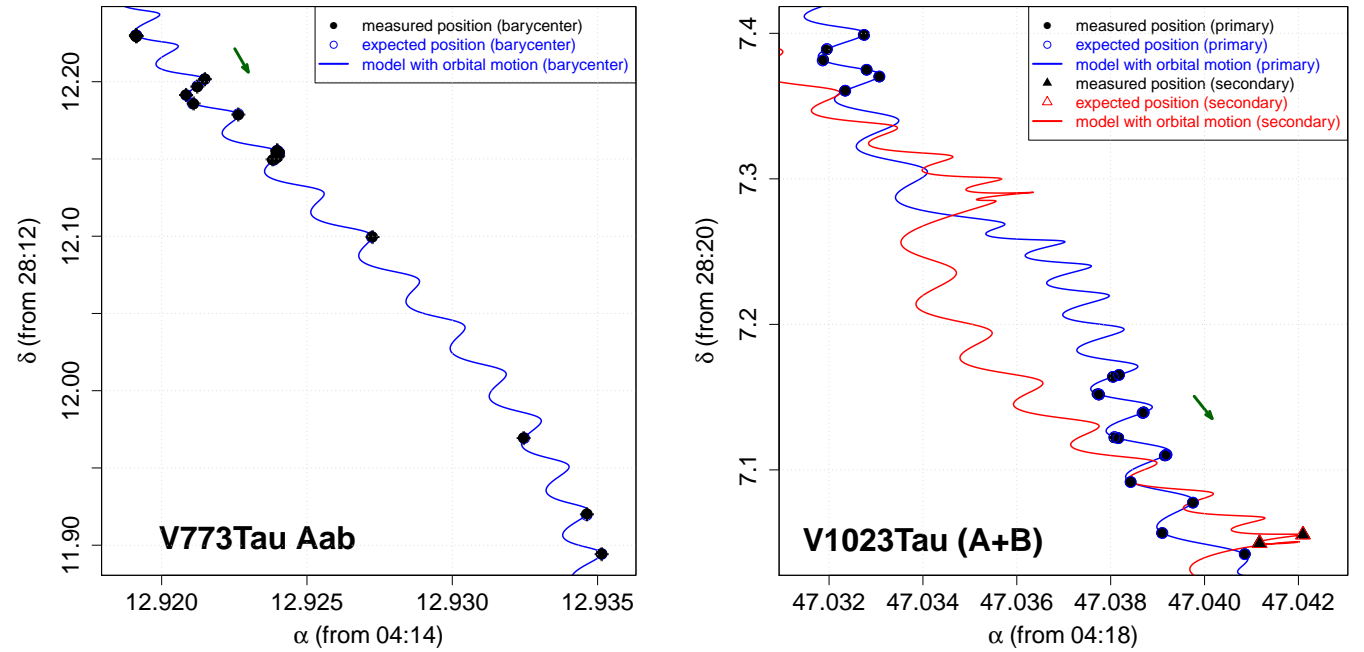


Figure 5. Astrometry fit for binaries and multiple systems in our sample including the orbital motion of the system in the analysis (see Sect. 3.2). The multiple components of each system detected with the VLBA in our observing campaign are shown in different colors. The green arrow shows the direction of the stellar proper motions in the plane of the sky.

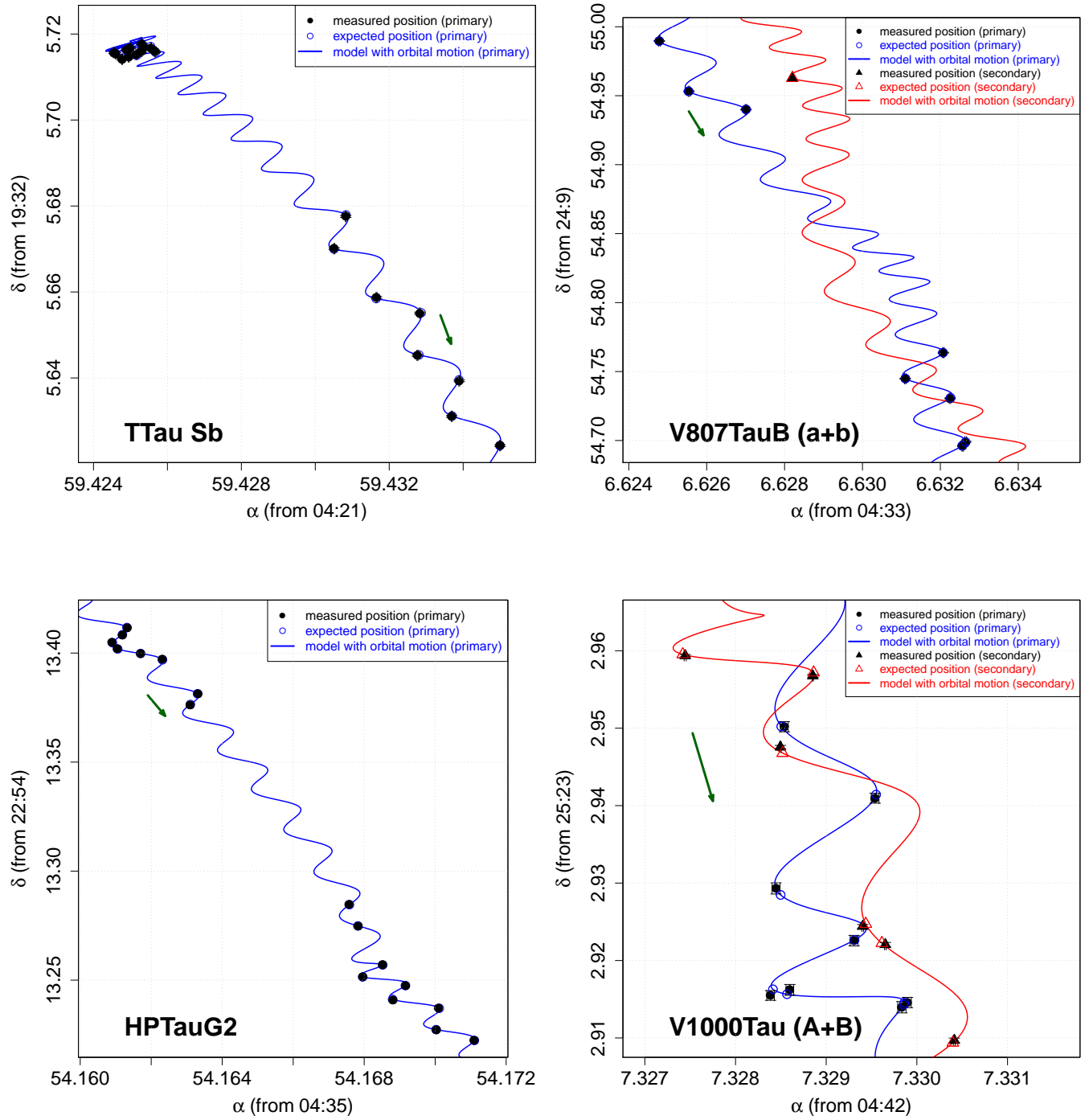


Figure 5. continued.

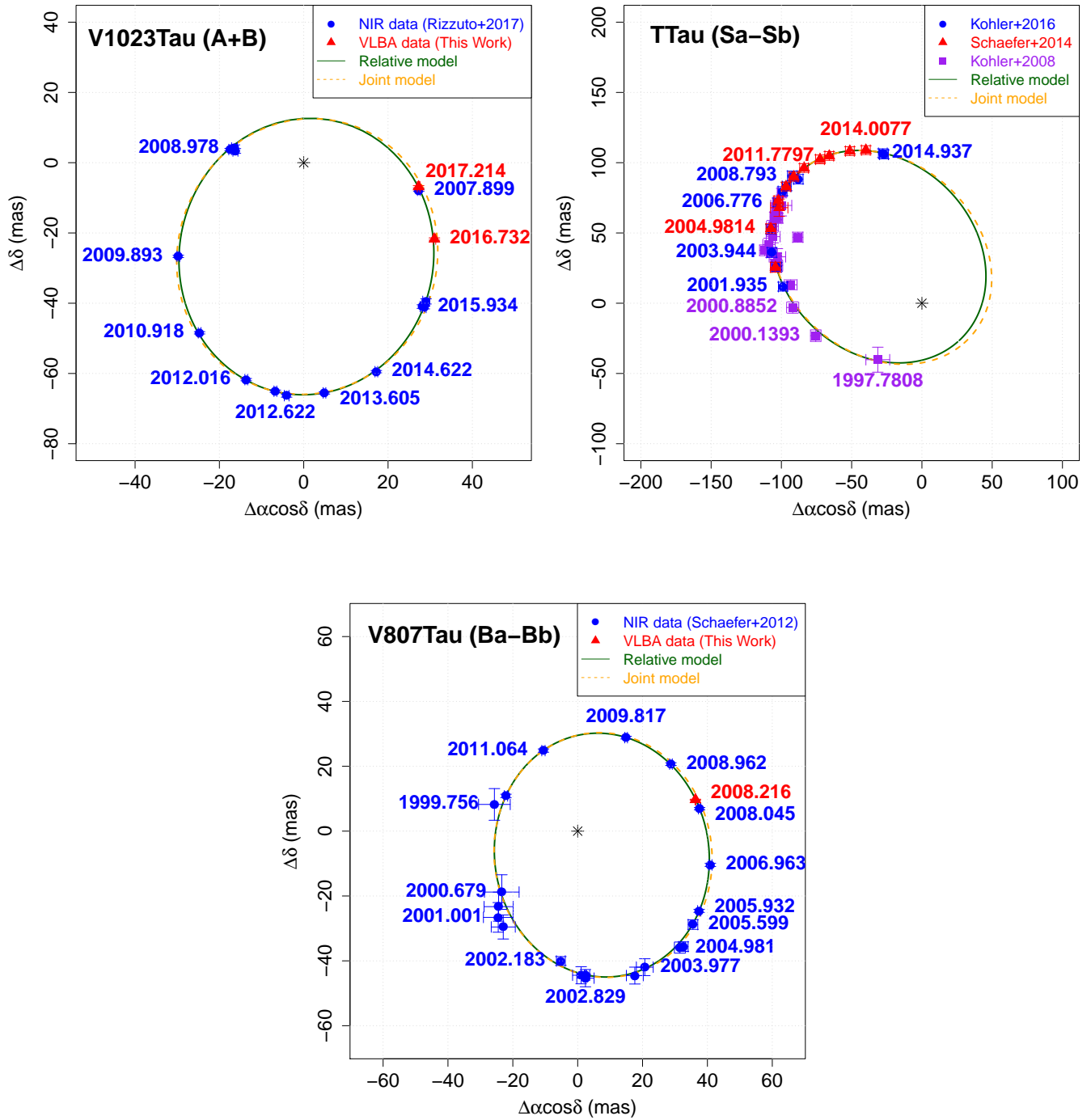


Figure 6. Relative astrometry of the components for three binary systems in our sample with measured relative positions in the literature. The black asterisk indicates the position of the secondary component (relative to the primary).

sured in BM198 before combining them with the other projects. The mean position of J0403+2600 measured in projects BM198 is $\alpha = 04^h03^m05.586049^s$ and $\delta = 26^\circ00'01.50275''$. The mean position of J0403+2600 (relative to J0408+3032) in the other projects is $\alpha = 04^h03^m05.586052^s$ and $\delta = 26^\circ00'01.50137''$. So, we applied a correction of $\Delta\alpha = 0.000003$ s and $\Delta\delta = -0.00138''$ to the measured positions in project BM198. Another important point to mention about projects BM198 is that these observations include data collected with both the VLBA and the Effelsberg antenna. But for consistency with the rest of the data used in this work, we decided to remove the Effelsberg antenna from the data reduction. The same applies to the BM306 project which observed with the High Sensitivity Array (HSA). We removed the external antennae and calibrated the observation using only VLBA data.

The orbital parameters of the short-period binary system V773 Tau Aa-Ab have already been constrained by Torres et al. (2012) based on the past VLBA observations listed in Table 3 supplemented by radial velocity observations from Boden et al. (2007). They derived the dynamical masses of the two components ($m_{Aa} = 1.55 \pm 0.11 M_\odot$ and $m_{Ab} = 1.293 \pm 0.068 M_\odot$) and a trigonometric parallax of $\pi = 7.70 \pm 0.19$ mas computed from the positions of the barycenter of the system including a uniformly accelerated proper motion in the analysis. As explained in their study, the model including a uniform acceleration (see Sect. 3.2) provided a good description to the data, because their observations covered a small fraction of the orbit of the V773 Tau A-B system. However, this not the case when we include the more recent data from the GOBELINS project in this analysis which increases the time base of collected observations to about 13 years. We computed the barycentric positions of the V773 Tau Aa-Ab system for the 3 epochs with simultaneous detections of the two components in our observing campaign and combined them with the re-calibrated barycentric positions reported by Torres et al. (2012). We verified that the model assuming a uniform acceleration indeed provides a poor fit to the data with the extended time base of our observations. We thus performed a full fit to the data including the orbital motion of the V773 Tau A-B in the analysis. Doing so, we derive an orbital period of $P = 20.3 \pm 0.8$ yr that is somewhat shorter than the value of $P = 26.2 \pm 1.1$ yr obtained by Boden et al. (2012) based on relative astrometry and radial velocities. The resulting trigonometric parallax of $\pi = 7.692 \pm 0.085$ mas yields a distance estimate of $d = 130.0^{+1.5}_{-1.4}$ pc for the barycenter of V773 Tau Aa-Ab system that is more ac-

curate and precise than the result of $d = 132.8 \pm 2.3$ pc obtained by Torres et al. (2012).

4.3. V1098 Tau, 2MASS J04182909+2826191, V999 Tau and HD 282630

V1098 Tau, 2MASS J04182909+2826191 and HD 282630 have been detected in only 3 epochs of our observing campaign. On the other hand, V999 Tau has been detected in 5 different projects, but in practice this corresponds to only 3 epochs due to the short time interval between projects BL175IC/BL175I7 and BL175JW/BL175JY. As a result, their trigonometric parallaxes are less precise as compared to the other stars in our sample with more detections. Because of the small number of detections we computed the additional errors on the stellar positions (see Sect. 3.3) from the methodology outlined in Pradel et al. (2006). The resulting errors reach up to 0.8 mas depending on the position of the source in the sky and the angular separation to the main phase calibrator.

4.4. HD 283518

HD 283518 (V410 Tau) was systematically detected in every epoch of our observing campaign. It is known to be a multiple system (see e.g. Harris et al. 2012), but only one component could be detected in our observations. We do not see the signature of the orbital motion in the stellar positions measured in this work indicating that the gravitational effects of the secondary on the primary are negligible. So, we solved for the astrometric parameters of this source using the methodology described in Sect. 3.1 for single stars. We also compared our results with the alternative approach outlined in Sect. 3.2 using a uniform acceleration. Both methods return compatible results (with the same level of accuracy and precision) and the derived acceleration terms in the latter approach are consistent with zero. Thus, the results presented in Table 5 refer to the model without acceleration. The trigonometric parallax that we derive for HD 283518 has a relative error of 0.3% making it the most precise result in our sample.

4.5. V1023 Tau

V1023 Tau (Hubble 4) is another binary system that was resolved in our observations. The primary component of this system is a weak-line T Tauri star of spectral type K7 (Nguyen et al. 2012), and it has been detected in a total of 14 epochs during our observing campaign. On the other hand, the secondary component could be detected in only 2 epochs. In addition, the primary has also been observed between September 2004 and December 2005 for projects BL124 and BL136. These

data have already been analyzed and published by [Torres et al. \(2007\)](#). We combined these observations with the more recent GOBELINS data to fit the measured positions over a timebase of ~ 13 yr which covers one full orbit of the system. Both data sets used the same main phase calibrator so that no correction has to be applied to the measured positions.

First, we performed a full fit of the orbit using only the VLBA observations reported in this paper and in [Torres et al. \(2007\)](#). Then, we combined the VLBA observations of projects BL175J2 and BL175JS where both components were simultaneously detected with the NIR relative astrometry from [Rizzuto et al. \(2018, submitted\)](#) to refine the orbital elements of the binary system. Finally, we combined our VLBA absolute positions with the NIR relative positions to perform a joint fit. Tables 6 and 7 compares our results from the different methods. The distance that we derive here from the full model ($d = 130.1_{-0.5}^{+0.5}$ pc) is somewhat shorter than the value of $d = 132.8 \pm 0.5$ pc obtained by [Torres et al. \(2007\)](#) using VLBA data from projects BL124 and BL136. We argue that the latter result is likely biased by the non-corrected binarity of the source. By combining the VLBA absolute positions with the NIR relative astrometry we find a distance of $d = 129.0_{-1.9}^{+2.0}$ pc that is less precise but fully consistent with our previous result. The weighted mean of both values yields $d = 130.0_{-0.5}^{+0.5}$ pc which is the most precise and accurate distance estimate for this source to date. Our analysis also made it possible to determine, for the first time, the dynamical masses of the individual components of this system ($m_A = 1.234 \pm 0.023 M_\odot$ and $m_B = 0.730 \pm 0.020 M_\odot$). This implies a somewhat smaller mass ratio ($q = 0.592 \pm 0.012$) than the value of $q = 0.73$ previously reported by [Harris et al. \(2012\)](#).

4.6. T Tau

T Tau is a well-known triple system (see e.g. [Duchêne et al. 2002](#)) and the component detected in our observations with the VLBA is T Tau Sb. It has been detected in 8 epochs during our observing campaign for the GOBELINS project. In addition, it was also observed by our team between September 2003 and July 2005 for projects BL118 and BL124 (see Table 3). However, we note that projects BL118 and BL128 observed J0428+1732 as the main phase calibrator, while GOBELINS uses it as a secondary calibrator (the main calibrator is J0412+1856). The mean position of J0428+1732 measured for projects BL118 and BL124 is $\alpha = 04^h28^m35.633679^s$ and $\delta = 17^\circ32'23.58803''$. In the GOBELINS campaign the mean position of J0428+1732 (relative to J0412+1856) is $\alpha = 04^h28^m35.633685^s$ and $\delta = 17^\circ32'23.58840''$. Thus, we applied an offset of

$\Delta\alpha = 0.000006$ s and $\Delta\delta = 0.00037''$ to the measured positions obtained from projects BL118 and BL124.

We fit the measured positions of T Tau Sb based on the full model to solve for the parallax and orbital motion of the binary system. The orbital elements obtained in this work (see Table 6) refer to the T Tau Sa-Sb system. We attempted to include an additional acceleration term due to the T Tau N component of the system, but the resulting acceleration parameter was consistent with zero. The results presented in Table 5 refer to our first solution (without acceleration). The distance that we derive in this paper for T Tau Sb ($d = 148.3_{-2.1}^{+2.1}$ pc) is in good agreement with the result of $d = 147.6 \pm 0.6$ pc published previously by [Loiarn et al. \(2007\)](#) using only data from projects BL118 and BL124. However, we consider our result to be more accurate because it takes into account the binarity/multiplicity of the source. Our solution obtained from the joint fit using the relative astrometry of the T Tau Sa-Sb published in previous studies yields a somewhat more precise distance estimate for this system ($d = 148.7_{-1.0}^{+1.0}$ pc) that confirms our first result. The weighted mean of both results yields a final distance of $d = 148.7_{-0.9}^{+0.9}$ pc.

Other studies have already investigated the orbital motion of the T Tau Sa-Sb system based on relative astrometry and different measurements ([Köhler et al. 2008, 2016](#); [Schaefer et al. 2014](#)). As illustrated in Fig. 6, we combined the relative positions from previous works to provide a more refined solution for the orbital parameters of the system. This analysis does not include VLBA data since our observations can only detect one component of the system. We note that most of the resulting orbital elements obtained in this paper including all measurements are more precise than the results reported in the individual studies. However, the errors on the individual parameters are still larger as compared to other stars in our sample. One reason to explain this result is the small coverage of the orbit which requires further monitoring of the T Tau system.

4.7. V1201 Tau and HD 283641

V1201 Tau and HD 283641 are members of the same hierarchical multiple system where both sources themselves are binary systems (see [Köhler & Leinert 1998](#); [Mason et al. 2001](#)). V1201 Tau and HD 283641 were also identified as wide binaries with a separation of $13.23''$ in a recent study conducted by [Andrews et al. \(2017\)](#) based on data from Gaia-DR1. Indeed, their result is consistent with the mean angular separation of $14.53''$ derived from our observations. The two components of the V1201 Tau system were simultaneously detected in only 2 epochs (projects BL175I1 and BL175KJ). We

measured a flux density of 2.40 ± 0.04 mJy in project BL175I1 (February 28, 2016) for the brightest component (hereafter, V1201TauA) that significantly decreased to 0.15 ± 0.05 mJy in project BL175KJ (September 18, 2017) becoming fainter than the so-defined secondary component V1201 Tau B. We derived a trigonometric parallax only for V1201 Tau B that was detected in 6 epochs. We note from Figure 4 that the fit using a uniform acceleration represents a good description to the data yielding a distance estimate of $d = 157.2 \pm 1.7$ pc. In the case of HD 283641 we detected only one component of the system in our observations. First, we fit the data as described in Sect. 3.1, then we introduced the acceleration. We verified that the inclusion of a uniform acceleration in the model increases the errors on the astrometric parameters and that the derived acceleration terms are consistent with zero. As expected, the distance obtained for HD 283641 ($d = 159.1 \pm 1.8$ pc, without acceleration) is compatible within 1σ of the distance derived for V1201 Tau. Both sources are currently being monitored by our team, and we will deliver a more refined solution (including the orbital motion of the system) when these observations become available.

4.8. XZ Tau

The XZ Tau system is composed of two components (XZ Tau A and XZ Tau B) with angular separation of about $0.3''$ (Harris et al. 2012; Joncour et al. 2017). Carrasco-González et al. (2009) report on the detection of a third component (XZ Tau C) in this system separated by $0.09''$ from XZ Tau A making it a triple system. However, a more recent study conducted by Forgan et al. (2014) did not detect XZ Tau C and cast doubt on the existence of the third component. Only one component of this system could be detected in our observations and we confirm that it corresponds to XZ Tau A. Krist et al. (2008) estimated that the minimum orbital period of the XZ Tau A-B system should be about 99 years which greatly exceeds the time base of our observations. Indeed, we see no evidence of binarity in our data and modeling XZ Tau A as a single star (as described in Sect. 3.1) provides a good fit to the data (see Fig. 4). Finally, it is interesting to note that all components of this system were suggested to be thermal radio sources (see Carrasco-González et al. 2009), but our study shows that XZ Tau A also produces non-thermal emission.

Table 5. Proper motions, parallaxes and distances derived from VLBA observations.

Identifier	$\mu_\alpha \cos \delta$ (mas/yr)	μ_δ (mas/yr)	$a_\alpha \cos \delta$ (mas/yr ²)	a_δ (mas/yr ²)	Parallax (mas)	Distance (pc)
V1096 Tau A	2.089 ± 0.730	-16.167 ± 0.711	11.640 ± 2.945	0.234 ± 3.710	8.055 ± 0.535	$124.1^{+8.8}_{-7.7}$
V1096 Tau B	7.147 ± 2.149	-28.765 ± 2.186	7.924 ± 1.334	$126.2^{+25.5}_{-18.2}$
V773 Tau A	10.253 ± 0.8434	-25.119 ± 0.301	7.692 ± 0.085	$130.0^{+1.5}_{-1.4}$
V1098 Tau	11.148 ± 0.175	-27.327 ± 0.172	8.070 ± 0.310	$123.9^{+5.0}_{-4.6}$
2MASS J04182909+2826191	8.384 ± 0.195	-19.627 ± 0.217	7.583 ± 0.389	$131.9^{+7.1}_{-6.4}$
HD 283518	8.703 ± 0.017	-24.985 ± 0.020	7.751 ± 0.027	$129.0^{+0.5}_{-0.5}$
V1023 Tau	8.371 ± 0.020	-25.490 ± 0.020	7.686 ± 0.032	$130.1^{+0.5}_{-0.5}$
T Tau Sb	6.790 ± 0.432	-11.131 ± 0.444	6.723 ± 0.046	$148.7^{+1.0}_{-1.0}$
V1201 Tau B	10.839 ± 0.050	-13.235 ± 0.058	0.335 ± 0.076	0.147 ± 0.071	6.363 ± 0.069	$157.2^{+1.7}_{-1.7}$
HD 283641	10.913 ± 0.037	-16.772 ± 0.044	6.285 ± 0.070	$159.1^{+1.8}_{-1.8}$
XZ Tau A	10.858 ± 0.027	-16.264 ± 0.060	6.793 ± 0.025	$147.2^{+0.5}_{-0.5}$
V807 Tau B	8.573 ± 0.068	-28.774 ± 0.201	7.899 ± 0.105	$126.6^{+1.7}_{-1.7}$
V1110 Tau	-52.705 ± 0.062	-11.321 ± 0.066	11.881 ± 0.149	$84.2^{+1.1}_{-1.0}$
HP Tau G2	11.248 ± 0.022	-15.686 ± 0.013	6.145 ± 0.029	$162.7^{+0.8}_{-0.8}$
V999 Tau	9.533 ± 0.218	-15.684 ± 0.198	6.972 ± 0.197	$143.4^{+4.2}_{-3.9}$
V1000 Tau	6.010 ± 0.235	-17.720 ± 0.159	7.324 ± 0.132	$136.5^{+2.5}_{-2.4}$
HD 282630	3.897 ± 0.113	-24.210 ± 0.132	7.061 ± 0.125	$141.6^{+2.6}_{-2.5}$
HDE 283572	8.853 ± 0.096	-26.491 ± 0.113	7.722 ± 0.057	$129.5^{+1.0}_{-0.9}$

Table 6. Orbital elements of the binaries and multiple systems in our sample.

System	a_1 (mas)	a_2 (mas)	a (mas)	P (yr)	e	T_p (JD)	Ω ($^\circ$)	ω ($^\circ$)	i ($^\circ$)	M_{Total} (M_\odot)	m_1 (M_\odot)	m_2 (M_\odot)
V773 Tau A-B												
Full model	44.3 ± 5.0	20.301 ± 0.842	0.003 ± 0.012	2459016 ± 554	285.8 ± 0.5	94.3 ± 25.7	72.2 ± 0.9
V1023 Tau A-B												
Full model	17.7 ± 0.3	30.9 ± 0.7	48.6 ± 0.7	9.302 ± 0.045	0.686 ± 0.011	2454692 ± 17	82.5 ± 3.0	84.0 ± 2.5	143.8 ± 1.8	2.918 ± 0.102	1.855 ± 0.067	1.063 ± 0.049
Relative model	41.8 ± 0.1	9.301 ± 0.008	0.680 ± 0.002	2454705 ± 2	64.2 ± 1.8	67.1 ± 1.7	158.4 ± 0.8	1.856 ± 0.005
Joint fit	16.0 ± 0.3	27.0 ± 0.3	43.0 ± 0.4	9.329 ± 0.017	0.682 ± 0.003	2454712 ± 3	66.1 ± 2.3	70.0 ± 2.2	153.8 ± 1.2	1.964 ± 0.033	1.234 ± 0.023	0.730 ± 0.020
T Tau Sa-Sb												
Full model	...	60.4 ± 2.2	...	24.744 ± 0.816	0.548 ± 0.031	2459439 ± 104	90.5 ± 10.8	45.9 ± 14.7	30.1 ± 3.9
Relative model	83.3 ± 1.9	26.946 ± 0.858	0.546 ± 0.031	2459907 ± 240	102.0 ± 39.2	36.0 ± 38.3	13.4 ± 8.1	2.620 ± 0.208
Joint fit	15.7 ± 3.0	70.0 ± 4.4	85.7 ± 5.3	27.933 ± 1.156	0.514 ± 0.041	2460214 ± 333	112.0 ± 28.8	28.7 ± 29.3	22.6 ± 8.9	2.660 ± 0.490	2.172 ± 0.408	0.489 ± 0.134
V807 Tau Ba-Bb												
Full model	17.8 ± 1.4	21.5 ± 2.0	39.3 ± 2.4	12.025 ± 0.397	0.339 ± 0.057	2456013 ± 150	2.7 ± 10.6	70.5 ± 5.7	146.9 ± 4.9	0.849 ± 0.136	0.465 ± 0.078	0.385 ± 0.080
Relative model	38.6 ± 0.2	12.310 ± 0.060	0.293 ± 0.003	2455732 ± 7	1.5 ± 1.2	50.4 ± 1.1	151.2 ± 0.9	0.768 ± 0.022
Joint fit	16.8 ± 0.3	22.0 ± 0.4	38.8 ± 0.5	12.218 ± 0.050	0.299 ± 0.004	2455738 ± 7	3.1 ± 1.9	53.3 ± 1.7	152.0 ± 1.0	0.896 ± 0.015	0.507 ± 0.010	0.388 ± 0.013
HP Tau G2-G3												
Full model	12.6 ± 0.2	11.932 ± 0.102	0.691 ± 0.010	2456794 ± 7	118.4 ± 1.0	263.8 ± 0.8	46.4 ± 0.7
V1000 Tau A-B												
Full model	8.3 ± 0.4	10.1 ± 0.5	18.4 ± 0.6	3.616 ± 0.257	0.428 ± 0.050	2458085 ± 9	264.1 ± 8.2	268.5 ± 3.0	45.6 ± 3.0	1.213 ± 0.181	0.663 ± 0.101	0.550 ± 0.091

4.9. V807 Tau

V807 Tau is a hierarchical triple system and the secondary component was resolved by [Simon et al. \(1995\)](#) into two close companions (V807 Tau Ba/Bb). The secondary has been detected in 5 epochs during the GOBELINS observing campaign. V807 Tau was also observed with the VLBA in the past (from March 2007 to March 2009) by [Schaefer et al. \(2012\)](#) for projects BS171 and BS176. They report on 3 detections of V807 Tau Ba and one detection of V807 Tau Bb. Before combining these data with our own observations we decided to download the files from the NRAO archive and reduce them by applying the same calibration procedure used in this work. Both data sets observed J0426+2327 as the main phase calibrator so that no correction needs to be applied to the positions measured in projects BS171 and BS176. We found that the source detected in the GOBELINS observations corresponds to V807 Tau Ba.

The model including a uniform acceleration produces a poor fit to the measured positions for V807 Tau Ba, because our observations cover almost one full orbit of the Ba-Bb system. We thus performed a full fit including the orbital motion of the close pair in our analysis which indeed represents a better description to the data (see Fig. 5). The distance that we derive from VLBA observations is $d = 126.6 \pm 1.7$ pc. Then, we used the NIR relative positions for the Ba-Bb system obtained by [Schaefer et al. \(2012\)](#) together with the VLBA observation from project BS176A where both components were simultaneously detected to refine the orbital parameters of the system from the relative model (see Fig. 6). By combining the VLBA and NIR data we find a distance of $d = 131.8^{+2.4}_{-2.3}$ pc. The larger discrepancy in the distance estimates delivered by the full model and the joint fit (as compared to the other stars in Table 7) can be explained by the smaller number of data points (i.e., stellar positions) to fit the astrometry. The weighted mean parallax from both methods yields $d = 128.5 \pm 1.4$ pc which is the first distance estimate for V807 Tau B to date.

The dynamical masses of the individual components ($m_{Ba} = 0.507 \pm 0.010 M_{\odot}$ and $m_{Bb} = 0.388 \pm 0.013 M_{\odot}$) that we derive in this paper are more precise than the results obtained by [Schaefer et al. \(2012\)](#). As discussed in their study, they used the average distance of 140 ± 10 pc to the Taurus region to compute the stellar masses. We have re-scaled the individual masses reported in their work to the distance that we derive in this paper which gives $m_{Ba} = 0.471 \pm 0.018 M_{\odot}$ and $m_{Bb} = 0.397 \pm 0.017 M_{\odot}$. However, these numbers are still affected by the systematic error of $0.24 M_{\odot}$ which comes from the ± 10 pc uncertainty in the distance used in their analysis. Both results are still in good agree-

ment, but we argue that the dynamical masses derived in this paper are more accurate due to the improved accuracy and precision of our distance determination.

4.10. V1110 Tau

V1110 Tau has been detected in 4 epochs during our observing campaign. The trigonometric parallax ($\pi = 11.881 \pm 0.149$ mas) and proper motion ($\mu_{\alpha} \cos \delta = -52.705 \pm 0.062$ mas/yr, $\mu_{\delta} = -11.321 \pm 0.066$ mas/yr) that we derive here clearly confirm it as a foreground star not related to the Taurus star-forming clouds. This is also shown in Fig. 2 where V1110 Tau clearly stands out with a position change rate > 50 mas/yr. In addition, Gaia-DR1 also confirms this finding yielding a trigonometric parallax of $\pi = 12.53 \pm 0.61$ mas and proper motion of $\mu_{\alpha} \cos \delta = -54.471 \pm 1.893$ mas/yr, $\mu_{\delta} = -12.194 \pm 1.612$ mas/yr. These values are consistent with but are less precise than our results.

Interestingly, [Martin et al. \(1994\)](#) observed V1110 Tau (Wa Tau 1) and did not detect the Li I line in any of the two components of this binary system. [Wahhaj et al. \(2010\)](#) classified V1110 Tau as a weak-line T Tauri star of spectral type K0 and effective temperature of 5250 K. They used the distance of 145 pc to compute the luminosity of the star ($3.04 L_{\odot}$) and estimate its age (7.3 Myr) based on the [Siess et al. \(2000\)](#) models. We have re-scaled the luminosity of the star to correct for the individual distance ($d = 84.2^{+1.1}_{-1.0}$ pc) that we derived in this paper. This yields a luminosity of $1.03 L_{\odot}$ and age estimate of 24 Myr suggesting that it is much older as indicated in previous studies. More recently, [Xing \(2010\)](#) derived a spectral type of K0 and measured the Li equivalent width of only 39 mÅ. In addition, [Xing & Xing \(2012\)](#) detected H α in absorption and [Rebull et al. \(2010\)](#) found no significant infrared excess for this source based on Spitzer photometry. Altogether, these properties are consistent with V1110 Tau being a young foreground dwarf not related to the Taurus population of YSOs (see also [Briceno et al. 1997](#)).

4.11. HP Tau G2

HP Tau G2 is a weak-line T Tauri star that belongs to a hierarchical triple system with separation of about $10''$ from HP Tau G3 which is a tight binary system (see e.g. [Nguyen et al. 2012](#); [Harris et al. 2012](#)). This source has been detected in a total of 9 epochs in this work, and it was also observed in the past from September 2003 to July 2005 for projects BL118 and BL124 (see Table 3). We corrected the measured positions in these observations before combining them with the more recent GOBELINS data reported in this work. Projects BL118 and BL124 observed J0426+2327 as the

Table 7. Comparison of the astrometry derived for binaries from different methods.

Method	$\mu_\alpha \cos \delta$	μ_δ	Parallax	Distance
	(mas/yr)	(mas/yr)	(mas)	(pc)
V1023 Tau				
Full model	8.371 ± 0.020	-25.490 ± 0.020	7.686 ± 0.032	$130.1^{+0.5}_{-0.5}$
Joint fit	8.393 ± 0.019	-25.489 ± 0.026	7.752 ± 0.116	$129.0^{+2.0}_{-1.9}$
Weighted mean	8.382 ± 0.014	-25.490 ± 0.016	7.691 ± 0.031	$130.0^{+0.5}_{-0.5}$
T Tau Sb				
Full model	4.674 ± 0.310	-10.224 ± 0.212	6.743 ± 0.096	$148.3^{+2.1}_{-2.1}$
Joint fit	4.577 ± 0.272	-11.037 ± 0.250	6.723 ± 0.046	$148.7^{+1.0}_{-1.0}$
Weighted mean	4.619 ± 0.205	-10.564 ± 0.162	6.727 ± 0.041	$148.7^{+0.9}_{-0.9}$
V807 Tau B				
Full model	8.573 ± 0.068	-28.774 ± 0.201	7.899 ± 0.105	$126.6^{+1.7}_{-1.7}$
Joint fit	8.544 ± 0.039	-28.871 ± 0.052	7.588 ± 0.135	$131.8^{+2.4}_{-2.3}$
Weighted mean	8.551 ± 0.034	-28.865 ± 0.050	7.782 ± 0.083	$128.5^{+1.4}_{-1.4}$

main phase calibrator while the GOBELINS observations use it as a secondary calibrator and J0438+2153 as the main calibrator. The mean position of J0426+2327 measured between September 2003 and July 2005 is $\alpha = 04^h 26^m 55.734795^s$, $\delta = 23^\circ 27' 39.63371''$, and the mean position of J0426+2327 (relative to J0438+2153) in the GOBELINS observations is $\alpha = 04^h 26^m 55.734757^s$, $\delta = 23^\circ 27' 39.63403''$. Thus, the corresponding offset to correct the measured positions in projects BL118 and BL124 is $\Delta\alpha = -0.000038$ s and $\Delta\delta = 0.00032''$. After combining the two data sets, we performed a full fit to solve for the parallax, proper motion and orbital motion of the HP Tau G2-G3 system (see Tables 5 and 6). The distance that we derive in this paper ($d = 162.7 \pm 0.8$ pc) is in good agreement with the result of $d = 161.2 \pm 0.9$ pc obtained by Torres et al. (2009) based only on observations collected for projects BL118 and BL124. This confirms that HP Tau G2 is indeed farther than other Taurus stars.

4.12. V1000 Tau

V1000 Tau has been detected in 7 epochs during our observing campaign, and both components were simultaneously detected in 5 epochs. On March 14, 2017 (project BL175JW) we measured the highest flux density for the primary component ($F_\nu = 0.96 \pm 0.05$ mJy). However, both sources appear significantly fainter in the other observations reported in this work with a flux level below 7σ which increases the errors on the individual positions of the sources.

During the calibration process of our observations we noted that two main calibrators have been used for this source during our observing campaign. Projects BL175AE, BL175AO, BL175HD, BL175IC, BL175JW

and BL175KV observed J0438+2153 as main phase calibrator while projects BL175D2, BL175I7, BL175IZ, BL175JY and BL175KS used J0429+2724 in this regard. Thus, we corrected the measured positions in the latter projects before combining the two data sets. J0435+2532 was observed as a secondary calibrator in all projected listed before. The mean position of J0435+2532 (relative to J0438+2153) in the first data set is $\alpha = 04^h 35^m 34.582910^s$, $\delta = 25^\circ 32' 59.69919''$, and the mean position of J0435+2532 (relative to J0429+2724) in the second data set is $\alpha = 04^h 35^m 34.582963^s$, $\delta = 25^\circ 32' 59.69972''$. Thus, we applied an offset of $\Delta\alpha = -0.000053$ s and $\Delta\delta = -0.00052''$ to the measured position of the second data set. We applied the same correction to the positions measured for V999 Tau (see Sect. 4.3) because both sources were observed in the same field and used the same calibrators in all epochs.

We proceeded as follows to calculate the distance to the V1000 Tau system. First, we applied the model with a uniform acceleration to the individual components of the system but it produced a poor fit to the data. We then considered the model including the orbital motion of the system and solved simultaneously for the proper motion, parallax and orbital elements. Doing so, we find a distance of $d = 136.5^{+2.5}_{-2.4}$ pc. This approach also allowed us to derive the individual masses of the two components of this system ($m_A = 0.663 \pm 0.101 M_\odot$ and $m_B = 0.550 \pm 0.091 M_\odot$). To further investigate our result, we compute the barycenter of the V1000 Tau system using the individual masses derived in this paper and perform a fit including the acceleration terms in our equations. This approach yields a distance estimate of $d = 136.4^{+3.4}_{-3.2}$ pc that is in good agreement with our

previous result and confirms our solution despite the low detection threshold.

4.13. *V892 Tau*

V892 Tau is the only source in our sample with a minimum of 3 detections for which we do not provide a trigonometric parallax. Unlike other stars in our sample, V892 Tau appears as a faint source in our observations with a detection level of roughly 6σ in the best case. V892 Tau is a Herbig Ae/Be star with a low-mass companion (Leinert et al. 1997), and at this stage it is not clear whether the positions measured in this work refer to the same component of the system since they provide a poor astrometric fit.

4.14. *HDE 283572*

HDE 283572 was not included in our target list, but it has been observed by Torres et al. (2007) between September 2004 and December 2005. We have recalibrated and re-analyzed these data by applying the same methods used for the GOBELINS observations and described throughout this paper. The new distance estimate of $d = 129.5_{-0.9}^{+1.0}$ pc that we derive here is fully consistent with the previous result of $d = 128.5 \pm 0.6$ pc obtained by Torres et al. (2007).

5. DISCUSSION

5.1. *Comparison with Gaia-DR1*

The first step in our analysis to compare the results obtained in this paper with Gaia-DR1 is to build a list of Taurus stars that have been previously identified in the literature. In a recent study, Joncour et al. (2017) published an updated census with 338 stars (and stellar systems) in this region. We add V1201 Tau, HD 283641 and V1110 Tau to their list which have been investigated in this work and were not included in their compilation.

The Gaia satellite observed 204 stars in our list of known YSOs in the Taurus region but the *Tycho-Gaia Astrometric Solution* (TGAS, Lindegren et al. 2016) catalog from Gaia-DR1 provides trigonometric parallaxes for only 18 stars (and stellar systems). Eight stars are in common with our sample of 18 stars with measured trigonometric parallaxes (see Table 5) including V1110 Tau which is more likely a foreground dwarf (see Sect. 4.10). Figure 7 illustrates the comparison of our results with Gaia-DR1. The rms and mean difference between the trigonometric parallaxes derived in both projects are, respectively, 0.38 mas and -0.15 mas (in the sense, “GOBELINS” minus “TGAS”). These numbers are smaller than the mean error of $\sigma_\pi = 0.46$ mas on the trigonometric parallaxes from Gaia-DR1 in the Taurus region. Thus, our results are in good agreement with

Gaia-DR1, but the trigonometric parallaxes derived in this work are more precise than the ones given in the TGAS catalog. For example, we measured a trigonometric parallax of $\pi = 7.751 \pm 0.027$ mas for HD 283518 that lies exactly onto the equality line (see Fig. 7) and is more precise by almost one order of magnitude than the result of $\pi = 7.78 \pm 0.29$ mas delivered by Gaia-DR1. This confirms the state-of-the-art accuracy and precision that can be obtained from VLBI astrometry, and the good complementarity with the Gaia space mission.

Two points regarding the comparison of our results with Gaia-DR1 are worth mentioning here. First, the trigonometric parallaxes in the TGAS catalog are affected by a systematic error of about 0.30 mas depending, for example, on the position and color of the stars (Lindegren et al. 2016). Thus, we added the value of 0.30 mas quadratically to the formal errors given in the TGAS catalog. The second and potentially more serious problem is that most of our sources in common with Gaia-DR1 are binaries (or multiple systems). In this context, it is important to mention that all sources in the TGAS catalog were modeled as single stars, so that the orbital motion in binaries is neglected. This explains the most discrepant results obtained for some sources in Fig. 7 (e.g. T Tau Sb and V773 Tau A) where this analysis is of ultimate importance and can only be applied with long-term monitoring of the system under investigation. For the reasons mentioned above, we consider the trigonometric parallaxes from the GOBELINS project to be more accurate and precise than the ones given in Gaia-DR1 for the targets in common.

5.2. *Distance and spatial velocity of Taurus stars*

The effective sample of stars that we use in the forthcoming analysis to discuss the distance and kinematics of the Taurus star-forming region consists of 26 stars (or stellar systems). It includes all stars (or stellar systems) listed in Table 5 (excluding V1110 Tau) and the additional 10 sources with trigonometric parallaxes from Gaia-DR1 (see Sect. 5.1). V1110 Tau is not included in this discussion for the reasons presented in Sect. 4.10. We use the proper motions and trigonometric parallaxes derived in this work from VLBI observations, and take the results from the TGAS catalog to complement our sample for stars that were not included in our observing campaign. In the case of V1096 Tau we use the weighted mean parallax and proper motion of the two components given in Sect. 4.1 that provide a better solution for the system than the individual values listed in Table 5. Figure 8 summarizes the trigonometric parallaxes of the stars in our sample, and Figures 9, 10, 11 and 12 illustrate the structure in and around the various

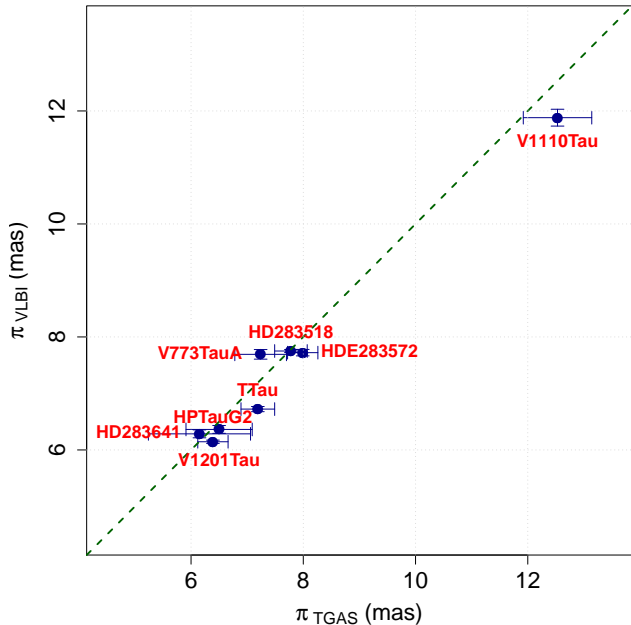


Figure 7. Comparison of the trigonometric parallaxes derived in this paper with the results delivered by the TGAS catalog from Gaia-DR1 for the stars in common. The green dashed line indicates perfect correlation of both data sets.

star-forming clouds investigated in our analysis based on the extinction maps from Dobashi et al. (2005).

We also searched the literature for the radial velocity of the stars in our sample using the data mining tools available in the CDS databases (Wenger et al. 2000). Our search for radial velocities is based on Hartmann et al. (1986), Herbig & Bell (1988), Gontcharov (2006), Kharchenko et al. (2007) and Nguyen et al. (2012). The properties of GOBELINS and Gaia-DR1 stars in our sample are collectively listed in Table 8. Then, we converted the observed trigonometric parallaxes into distances, and used the radial velocities to calculate the three-dimensional Galactic spatial velocities from the procedure described by Johnson & Soderblom (1987). In Table 9 we present the UVW spatial velocity and the peculiar velocity of individual stars in our sample after correcting for the velocity of the Sun with respect to the local standard of rest (LSR). For this correction we use the solar motion obtained by Schönrich et al. (2010). We also present in Table 9 the radial velocities of the stars converted to the LSR which will be used in the forthcoming discussion to compare with the velocity field of the CO molecular gas in this region produced by the Five College Radio Astronomy Observatory (FCRAO). In this case we used the older IAU standard solar motion to convert the radial velocities to the LSR for consis-

tency with the FCRAO maps (see Jackson et al. 2006). In the following we comment on the distance and kinematics of the individual clouds of the Taurus complex. The properties of the various star-forming clouds discussed below are also summarized in Table 10.

5.2.1. Lynds 1495

Lynds 1495 (L1495, Lynds 1962) is the main star-forming site of the Taurus complex and the most important structure to discuss in this work, because it contains about 40% of the stars in our sample. Schmalzl et al. (2010) divided it into five clumps (B 211, B 213, B 216, B 217 and B 218) which form the filament projected on the plane of the sky, and the central part B 10. We note that V1023 Tau, HD 283518 and 2MASS J04182909+2826191 are located in the northern part of B 10 (see Fig. 9). The weighted mean parallax of these sources is $\pi = 7.724 \pm 0.021$ mas which is consistent with a distance estimate of $d = 129.5_{-0.3}^{+0.4}$ pc. On the other hand, V1096 Tau, V1098 Tau and V773 Tau are projected towards the southern part of the B 10 clump with a weighted mean parallax of $\pi = 7.727 \pm 0.081$ mas and distance of $d = 129.4_{-1.3}^{+1.4}$ pc. Thus, we conclude that both substructures are located at the same distance. As discussed in Sect. 4, the trigonometric parallaxes obtained in this paper for V1096 Tau, V1098 Tau and 2MASS J04182909+28261 require further improvement, but based on the current results we find no evidence of significant depth effects within the B 10 clump of the L 1495 cloud. The weighted mean parallax of the six stars mentioned before is $\pi = 7.724 \pm 0.020$ mas. This is consistent with a distance estimate of $d = 129.5_{-0.3}^{+0.3}$ pc which is the most precise and accurate present-day distance determination of L 1495.

Figure 9 reveals 3 stars in our sample (HDE 283572, RY Tau and BP Tau) in the outskirts of L 1495. We note that the trigonometric parallaxes of HDE 283572 ($\pi = 7.722 \pm 0.057$ mas) and BP Tau ($\pi = 7.900 \pm 0.492$ mas) are consistent with the results obtained in this paper for the other stars in the B 10 clump. However, the trigonometric parallax of RY Tau given in the TGAS catalog ($\pi = 5.660 \pm 0.920$ mas) is in obvious disagreement with the other stars suggesting either a problem with the result delivered by Gaia-DR1 (e.g. non-corrected binarity or low precision/accuracy) or that RY Tau is indeed not related to the L 1495 cloud. Moreover, we note that its radial velocity exceeds the mean radial velocity of the other stars in this region by about 9 km/s (see Table 8). The revised weighted mean parallax of L 1495 (including HDE 283572 and BP Tau) is $\pi = 7.724 \pm 0.019$ mas and yields a distance of $d = 129.5_{-0.3}^{+0.3}$ pc confirming our previous result.

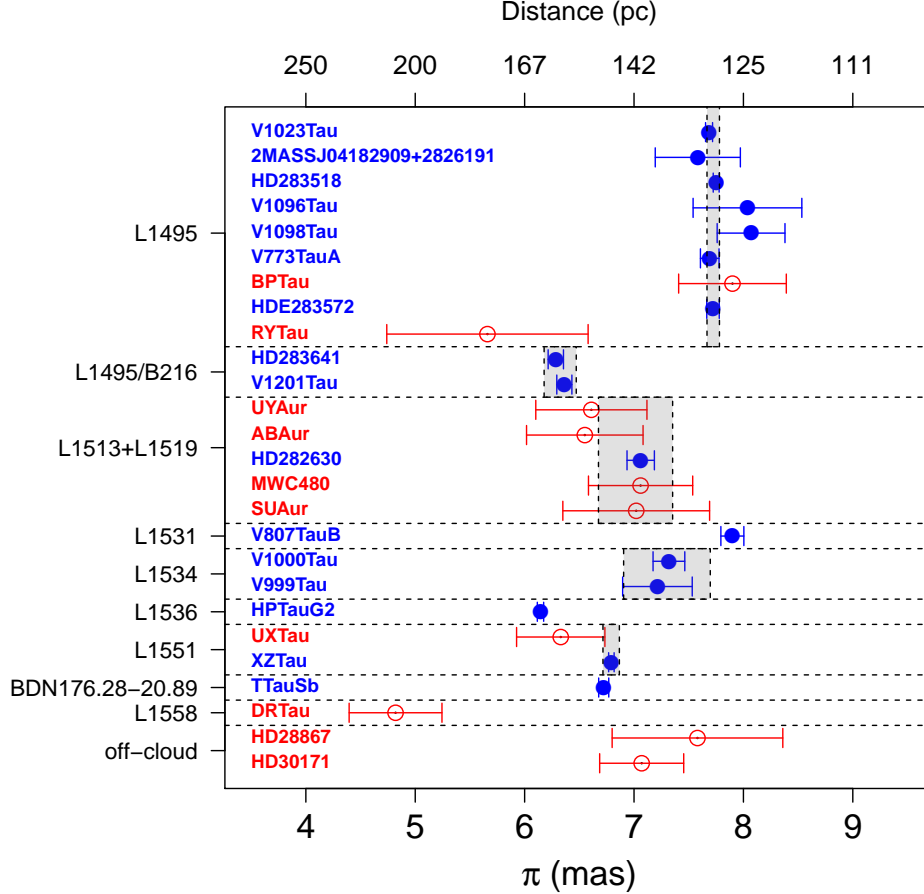


Figure 8. Summary of the trigonometric parallax measurements for Taurus stars. The sources are grouped according to the star-forming cloud to which they belong. Filled and open symbols indicate, respectively, VLBI trigonometric parallaxes obtained in this paper and TGAS results from Gaia-DR1. The gray vertical bars indicate the weighted mean parallax (at the 3σ -level) of the clouds with more than one member in our sample to illustrate the depth effects.

One interesting finding of our analysis is that V1201 Tau and HD 283641, which are projected towards the B 216 clump in the filamentary structure of L 1495, are located at a different distance as compared to the other stars in L 1495. The mean parallax of these two sources is $\pi = 6.325 \pm 0.049$ mas and yields a distance of $d = 158.1_{-1.2}^{+1.2}$ pc. This distance estimate differs by almost 30 pc from the result mentioned before and reveals the existence of important depth effects between the central part of the cloud and the filament. In addition, the spatial velocity that we derive for HD 283641 also suggests that both structures exhibit different kinematic properties (see Table 10).

5.2.2. Lynds 1513 and 1519

UY Aur is projected towards the Lynds 1513 cloud (L1513, Lynds 1962) with a trigonometric parallax of

$\pi = 6.610 \pm 0.508$ mas. This result is in good agreement (at the 1σ level) with the trigonometric parallaxes of AB Aur ($\pi = 6.550 \pm 0.532$ mas) and SU Aur ($\pi = 7.020 \pm 0.671$ mas) which are located in Lynds 1519 (L1519, Lynds 1962). Another two stars (HD 282630 and MWC480) are located in the surroundings of L 1519 (see Fig.10) and their trigonometric parallaxes are also consistent with UY Aur, AB Aur and SU Aur. The trigonometric parallaxes and spatial velocities of these sources are all consistent between themselves within the admittedly large errors. The weighted mean parallax is $\pi = 7.014 \pm 0.113$ mas and yields a distance of $d = 142.6_{-2.3}^{+2.3}$ pc that we consider at this stage to be representative of both L 1513 and L 1519.

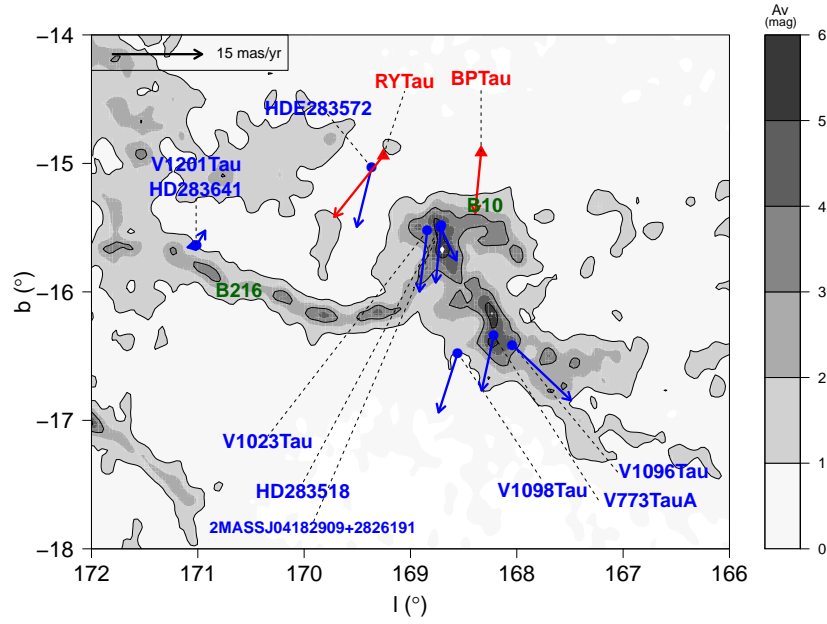


Figure 9. Structure of the L 1495 cloud ($d = 129.5^{+0.3}_{-0.3}$ pc) overlaid on the extinction map from Dobashi et al. (2005). Blue circles and red triangles denote, respectively, the stars with VLBI and TGAS trigonometric parallax. The vectors indicate the stellar proper motions from Table 8 converted to the Galactic reference system and corrected for the Solar motion (Schönrich et al. 2010) using the formalism described by Abad & Vieira (2005)

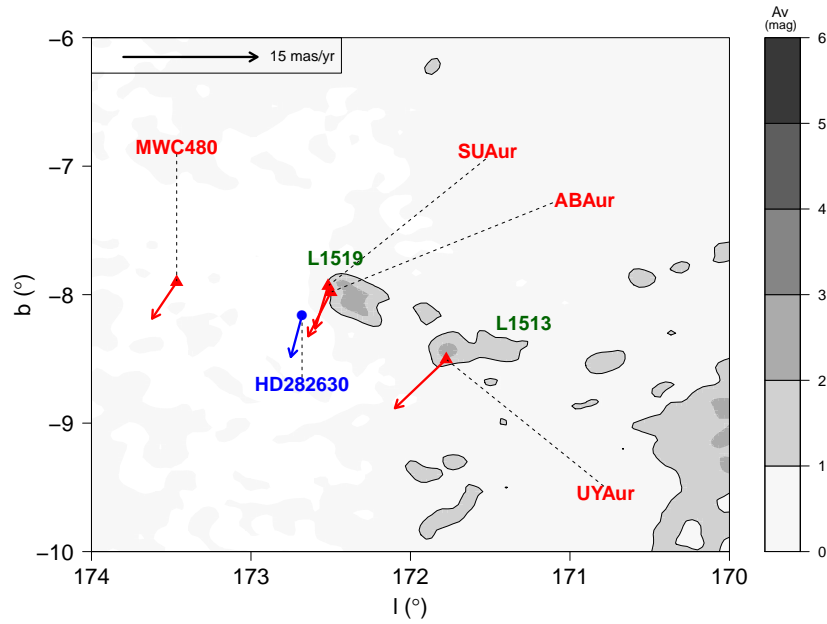


Figure 10. Structure of the L 1513 ($d = 151^{+13}_{-11}$ pc) and L 1519 ($d = 142.1^{+2.4}_{-2.3}$ pc) clouds overlaid on the extinction map from Dobashi et al. (2005). Blue circles and red triangles denote, respectively, the stars with VLBI and TGAS trigonometric parallax. The vectors indicate the stellar proper motions from Table 8 converted to the Galactic reference system and corrected for the Solar motion (Schönrich et al. 2010) using the formalism described by Abad & Vieira (2005)

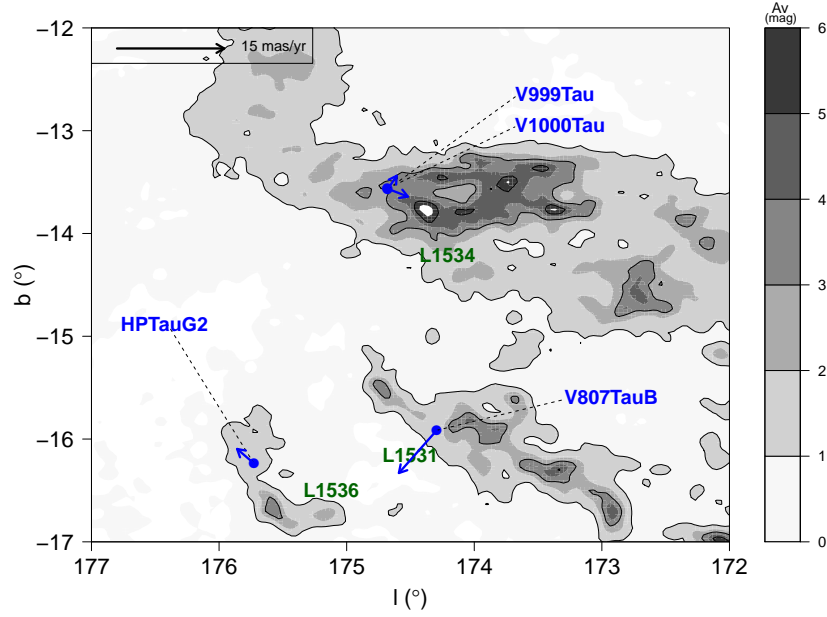


Figure 11. Structure of the L 1531 ($d = 126.6^{+1.7}_{-1.7}$ pc), L 1534 ($d = 138.6^{+2.1}_{-2.1}$ pc) and L 1536 ($d = 162.7^{+0.8}_{-0.8}$ pc) clouds overlaid on the extinction map from Dobashi et al. (2005). Blue circles and red triangles denote, respectively, the stars with VLBI and TGAS trigonometric parallax. The vectors indicate the stellar proper motions from Table 8 converted to the Galactic reference system and corrected for the Solar motion (Schönrich et al. 2010) using the formalism described by Abad & Vieira (2005)

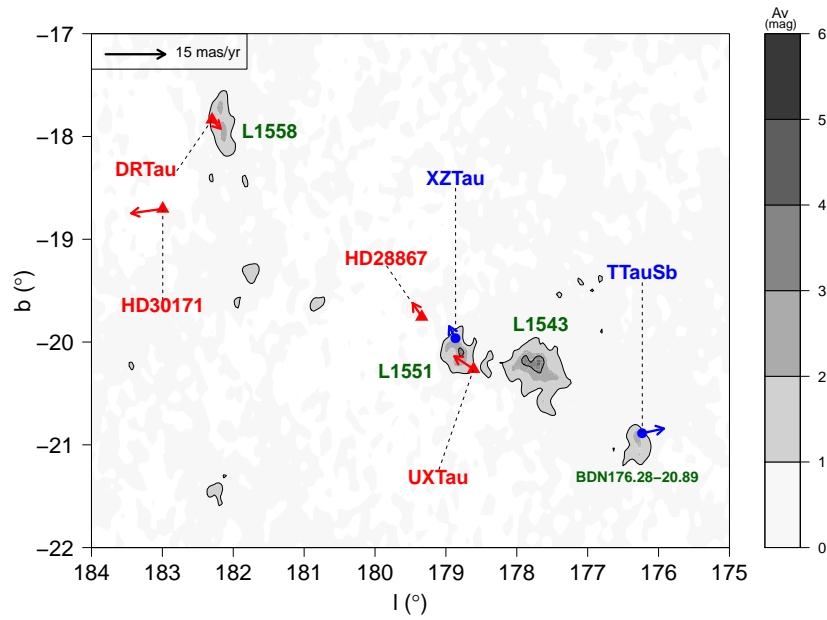


Figure 12. Structure of the L 1551 ($d = 147.3^{+0.5}_{-0.5}$ pc) and L 1558 ($d = 208^{+20}_{-17}$ pc) clouds overlaid on the extinction map from Dobashi et al. (2005). Blue circles and red triangles denote, respectively, the stars with VLBI and TGAS trigonometric parallax. The vectors indicate the stellar proper motions from Table 8 converted to the Galactic reference system and corrected for the Solar motion (Schönrich et al. 2010) using the formalism described by Abad & Vieira (2005)

Table 8. Proper motions, trigonometric parallaxes, distances and radial velocities of the GOBELINS-Gaia sample in Taurus.

Star	2MASS Identifier	$\mu_\alpha \cos \delta$ (mas/yr)	μ_δ (mas/yr)	π (mas)	d (pc)	Ref.	V_r (km/s)	Ref.
V1096 Tau	J04132722+2816247	2.612 ± 0.691	-17.372 ± 0.676	8.037 ± 0.497	$124.4^{+8.2}_{-7.2}$	ThisWork	12.00 ± 5.00	1
V773 Tau A	J04141291+2812124	10.253 ± 0.843	-25.119 ± 0.301	7.692 ± 0.085	$130.0^{+1.5}_{-1.4}$	ThisWork	16.00 ± 2.50	2
HD 283518	J04183110+2827162	8.703 ± 0.017	-24.985 ± 0.020	7.751 ± 0.027	$129.0^{+0.5}_{-0.4}$	ThisWork	19.90 ± 0.30	3
V1023 Tau	J04184703+2820073	8.371 ± 0.020	-25.490 ± 0.020	7.686 ± 0.032	$130.1^{+0.5}_{-0.5}$	ThisWork	15.00 ± 1.70	4
BP Tau	J04191583+2906269	8.683 ± 0.355	-25.846 ± 0.239	7.900 ± 0.492	$126.6^{+8.4}_{-7.4}$	Gaia-DR1	15.24 ± 0.04	3
RY Tau	J04215740+2826355	9.100 ± 0.140	-25.859 ± 0.091	5.660 ± 0.920	$176.7^{+34.3}_{-24.7}$	Gaia-DR1	24.30 ± 1.90	2
HDE 283572	J04215884+2818066	8.853 ± 0.096	-26.491 ± 0.113	7.722 ± 0.057	$129.5^{+1.0}_{-0.9}$	ThisWork	14.22 ± 0.08	3
T Tau Sb	J04215943+1932063	6.790 ± 0.432	-11.131 ± 0.444	6.723 ± 0.046	$148.7^{+1.0}_{-1.0}$	ThisWork	19.23 ± 0.02	3
HD 283641	J04244904+2643104	10.913 ± 0.037	-16.772 ± 0.044	6.285 ± 0.070	$159.1^{+1.8}_{-1.8}$	ThisWork	16.23 ± 0.04	3
UX Tau	J04300399+1813493	12.641 ± 0.435	-17.552 ± 0.257	6.330 ± 0.404	$158.0^{+0.8}_{-0.5}$	Gaia-DR1	15.45 ± 0.02	3
XZ Tau	J04314007+1813571	10.858 ± 0.027	-16.264 ± 0.060	6.793 ± 0.025	$147.2^{+0.5}_{-0.5}$	ThisWork	18.30 ± 0.04	3
V807 Tau B	J04330664+2409549	8.573 ± 0.068	-28.774 ± 0.201	7.899 ± 0.105	$126.6^{+1.7}_{-1.7}$	ThisWork	16.85 ± 0.03	3
HD 28867	J04333297+1801004	12.017 ± 0.047	-18.635 ± 0.030	7.580 ± 0.780	$131.9^{+15.1}_{-12.3}$	Gaia-DR1	-14.70 ± 7.40	5
HP Tau G2	J04355415+2254134	11.248 ± 0.022	-15.686 ± 0.013	6.145 ± 0.029	$162.7^{+0.8}_{-0.8}$	ThisWork	16.60 ± 1.00	3
V999 Tau	J04420548+2522562	9.533 ± 0.218	-15.684 ± 0.198	6.972 ± 0.197	$143.4^{+4.2}_{-3.9}$	ThisWork	14.70 ± 2.00	1
HD 30171	J04455129+1555496	9.824 ± 1.675	-24.288 ± 0.994	7.070 ± 0.384	$141.4^{+8.1}_{-7.3}$	Gaia-DR1	21.13 ± 0.17	3
DR Tau	J04470620+1658428	1.372 ± 2.747	-11.225 ± 1.785	4.820 ± 0.424	$207.5^{+20.0}_{-16.8}$	Gaia-DR1	21.10 ± 0.04	3
UY Aur	J04514737+3047134	6.099 ± 2.824	-27.027 ± 1.840	6.610 ± 0.508	$151.3^{+12.6}_{-10.8}$	Gaia-DR1	13.92 ± 0.07	3
HD 282630	J04553695+3017553	3.897 ± 0.113	-24.210 ± 0.132	7.061 ± 0.125	$141.6^{+5.6}_{-2.9}$	ThisWork	13.58 ± 0.01	3
AB Aur	J04554582+3033043	3.889 ± 0.056	-24.050 ± 0.039	6.550 ± 0.533	$152.7^{+13.5}_{-11.1}$	Gaia-DR1	8.90 ± 0.90	2
SU Aur	J04555938+3034015	3.857 ± 0.126	-24.367 ± 0.088	7.020 ± 0.671	$142.5^{+12.4}_{-12.4}$	Gaia-DR1	14.26 ± 0.05	3
V1098 Tau	J04144797+2752346	11.148 ± 0.175	-27.327 ± 0.172	8.070 ± 0.310	$123.9^{+5.0}_{-4.6}$	ThisWork
2MASS J04182909+2826191	J04182909+2826191	8.384 ± 0.195	-19.627 ± 0.217	7.583 ± 0.389	$131.9^{+7.1}_{-6.4}$	ThisWork
V1201 Tau	J04244815+2643161	10.839 ± 0.050	-13.235 ± 0.058	6.363 ± 0.069	$157.2^{+1.7}_{-1.7}$	ThisWork
V1000 Tau	J04420732+2523032	6.010 ± 0.235	-17.720 ± 0.159	7.324 ± 0.132	$136.5^{+2.5}_{-2.4}$	ThisWork
MWC480	J04584626+2950370	4.790 ± 0.081	-25.044 ± 0.049	7.060 ± 0.476	$141.6^{+10.2}_{-9.0}$	Gaia-DR1

NOTE—References for radial velocities: (1) Herbig & Bell (1988); (2) Gontcharov (2006); (3) Nguyen et al. (2012); (4) Hartmann et al. (1986); (5) Kharchenko et al. (2007).

Table 9. Spatial velocity for Taurus stars with measured trigonometric parallaxes and radial velocities.

Star	2MASS Identifier	U (km/s)	V (km/s)	W (km/s)	V_{space} (km/s)	u (km/s)	v (km/s)	w (km/s)	V_{pec} (km/s)	V_{r}^{LSR} (km/s)
(1)	(2)	(3)	(4)	(5)	(6)	(7)	(8)	(9)	(10)	(11)
V1096Tau	J04132722+2816247	-11.4 ^{+4.9} _{-4.9}	-6.3 ^{+2.0} _{-2.0}	-9.1 ^{+2.4} _{-2.4}	15.9 ^{+3.9} _{-3.9}	-0.3 ^{+5.0} _{-5.0}	6.0 ^{+2.0} _{-2.2}	-1.8 ^{+2.4} _{-2.5}	6.2 ^{+2.2} _{-2.2}	6.29 ± 5.00
V773TauA	J04141291+2812124	-16.5 ^{+2.6} _{-2.6}	-12.5 ^{+1.1} _{-1.1}	-10.3 ^{+1.3} _{-1.3}	23.1 ^{+2.0} _{-2.0}	-5.4 ^{+2.7} _{-2.7}	-0.3 ^{+1.2} _{-1.2}	-3.1 ^{+1.4} _{-1.4}	6.2 ^{+2.4} _{-2.4}	10.27 ± 2.50
HD283518	J04183110+2827162	-20.0 ^{+0.3} _{-0.3}	-11.2 ^{+0.1} _{-0.1}	-11.5 ^{+0.1} _{-0.1}	25.0 ^{+0.2} _{-0.2}	-8.9 ^{+0.8} _{-0.8}	1.1 ^{+0.5} _{-0.5}	-4.3 ^{+0.4} _{-0.4}	9.9 ^{+0.7} _{-0.7}	14.13 ± 0.30
V1023Tau	J04184703+2820073	-15.3 ^{+1.6} _{-1.6}	-12.4 ^{+0.4} _{-0.4}	-10.6 ^{+0.5} _{-0.5}	22.3 ^{+1.2} _{-1.2}	-4.2 ^{+1.8} _{-1.8}	-0.1 ^{+0.6} _{-0.6}	-3.4 ^{+0.6} _{-0.6}	5.4 ^{+1.4} _{-1.4}	9.20 ± 1.70
BP Tau	J04191583+2906269	-15.7 ^{+0.2} _{-0.2}	-12.0 ^{+1.1} _{-1.1}	-10.4 ^{+1.1} _{-1.1}	22.4 ^{+0.8} _{-0.8}	-4.6 ^{+0.7} _{-0.7}	0.2 ^{+1.2} _{-1.2}	-3.2 ^{+1.2} _{-1.2}	5.6 ^{+0.9} _{-0.9}	9.57 ± 0.04
RY Tau	J04215740+2826355	-24.7 ^{+2.3} _{-2.4}	-16.9 ^{+3.4} _{-3.4}	-14.8 ^{+3.7} _{-3.7}	33.4 ^{+2.9} _{-2.9}	-13.6 ^{+2.4} _{-2.4}	-4.7 ^{+3.4} _{-3.4}	-7.6 ^{+3.7} _{-3.7}	16.3 ^{+2.8} _{-3.2}	18.46 ± 1.90
HDE283572	J04215884+2818066	-14.6 ^{+0.1} _{-0.1}	-13.3 ^{+0.2} _{-0.2}	-10.4 ^{+0.2} _{-0.2}	22.3 ^{+0.2} _{-0.2}	-3.5 ^{+0.7} _{-0.7}	-1.0 ^{+0.5} _{-0.5}	-3.1 ^{+0.4} _{-0.4}	4.8 ^{+0.6} _{-0.6}	8.36 ± 0.08
TTauSb	J04215943+1932063	-18.0 ^{+0.2} _{-0.2}	-8.0 ^{+0.5} _{-0.5}	-8.1 ^{+0.5} _{-0.5}	21.3 ^{+0.3} _{-0.3}	-6.9 ^{+0.7} _{-0.7}	4.2 ^{+0.7} _{-0.7}	-0.8 ^{+0.6} _{-0.6}	8.2 ^{+0.7} _{-0.7}	11.83 ± 0.02
HD283641	J04244904+2643104	-17.1 ^{+0.1} _{-0.1}	-12.5 ^{+0.2} _{-0.2}	-6.5 ^{+0.2} _{-0.2}	22.2 ^{+0.1} _{-0.1}	-6.0 ^{+0.6} _{-0.6}	-0.2 ^{+0.5} _{-0.5}	0.8 ^{+0.4} _{-0.4}	6.1 ^{+0.7} _{-0.7}	10.02 ± 0.04
UX Tau	J04300399+1813493	-14.5 ^{+0.5} _{-0.5}	-15.9 ^{+1.5} _{-1.5}	-6.1 ^{+1.3} _{-1.3}	22.4 ^{+1.2} _{-1.2}	-3.4 ^{+0.8} _{-0.8}	-3.7 ^{+1.4} _{-1.3}	1.1 ^{+1.3} _{-1.3}	5.1 ^{+1.3} _{-1.3}	7.68 ± 0.02
XZ Tau	J04314007+1813571	-17.0 ^{+0.1} _{-0.1}	-13.4 ^{+0.1} _{-0.1}	-7.3 ^{+0.1} _{-0.1}	22.8 ^{+0.1} _{-0.1}	-5.9 ^{+0.7} _{-0.7}	-1.1 ^{+0.5} _{-0.5}	0.0 ^{+0.4} _{-0.4}	6.0 ^{+0.7} _{-0.7}	10.50 ± 0.04
V807TauB	J04330664+2409549	-15.8 ^{+0.1} _{-0.1}	-15.1 ^{+0.3} _{-0.3}	-11.4 ^{+0.3} _{-0.3}	24.7 ^{+0.3} _{-0.3}	-4.7 ^{+0.8} _{-0.8}	-2.9 ^{+0.6} _{-0.6}	-4.2 ^{+0.5} _{-0.5}	6.9 ^{+0.6} _{-0.6}	10.04 ± 0.03
HD28867	J04333297+1801004	14.3 ^{+7.5} _{-7.4}	-13.9 ^{+1.7} _{-1.7}	3.5 ^{+3.7} _{-3.8}	20.2 ^{+5.4} _{-5.4}	25.4 ^{+7.5} _{-7.5}	-1.6 ^{+1.4} _{-1.4}	10.7 ^{+3.8} _{-3.8}	27.6 ^{+7.0} _{-7.0}	-22.57 ± 7.40
HP TauG2	J04355415+2254134	-16.7 ^{+1.0} _{-1.0}	-13.8 ^{+0.2} _{-0.2}	-5.5 ^{+0.4} _{-0.4}	22.3 ^{+0.7} _{-0.7}	-5.6 ^{+1.2} _{-1.2}	-1.5 ^{+0.5} _{-0.5}	1.8 ^{+0.5} _{-0.5}	6.1 ^{+1.1} _{-1.1}	9.52 ± 1.00
V999Tau	J04420548+2522562	-15.0 ^{+2.0} _{-2.1}	-11.1 ^{+0.7} _{-0.7}	-5.0 ^{+1.0} _{-1.0}	19.3 ^{+1.7} _{-1.7}	-3.9 ^{+2.2} _{-2.2}	1.1 ^{+0.8} _{-0.8}	2.3 ^{+1.0} _{-1.0}	4.6 ^{+1.9} _{-1.9}	7.96 ± 2.00
HD30171	J04455129+1555496	-17.7 ^{+0.8} _{-0.8}	-18.1 ^{+2.0} _{-2.0}	-10.8 ^{+2.1} _{-2.1}	27.5 ^{+1.7} _{-1.7}	-6.6 ^{+1.1} _{-1.1}	-5.8 ^{+2.1} _{-2.1}	-3.5 ^{+2.1} _{-2.1}	9.5 ^{+1.7} _{-1.8}	12.71 ± 0.17
DR Tau	J04470620+1658428	-18.0 ^{+1.3} _{-1.2}	-10.5 ^{+3.7} _{-4.3}	-11.5 ^{+3.8} _{-3.9}	23.9 ^{+2.6} _{-2.8}	-6.9 ^{+1.4} _{-1.4}	1.7 ^{+3.7} _{-4.3}	-4.3 ^{+3.8} _{-3.9}	8.3 ^{+2.4} _{-2.5}	12.83 ± 0.04
UY Aur	J04514737+3047134	-14.9 ^{+0.5} _{-0.6}	-16.0 ^{+3.4} _{-3.9}	-10.5 ^{+3.6} _{-3.6}	24.3 ^{+2.7} _{-3.1}	-3.8 ^{+0.9} _{-0.9}	-3.7 ^{+3.4} _{-4.0}	-3.3 ^{+3.6} _{-3.6}	6.3 ^{+2.8} _{-3.1}	8.05 ± 0.07
HD282630	J04553695+3017553	-14.1 ^{+0.1} _{-0.1}	-12.8 ^{+0.4} _{-0.4}	-9.7 ^{+0.3} _{-0.3}	21.3 ^{+0.3} _{-0.3}	-3.0 ^{+0.7} _{-0.7}	-0.6 ^{+0.6} _{-0.6}	-2.4 ^{+0.5} _{-0.5}	3.9 ^{+0.6} _{-0.7}	7.57 ± 0.01
ABAur	J04554582+3033043	-9.6 ^{+1.0} _{-1.0}	-14.4 ^{+1.5} _{-1.5}	-9.6 ^{+1.3} _{-1.3}	19.7 ^{+1.2} _{-1.2}	1.5 ^{+1.2} _{-1.2}	-2.1 ^{+1.4} _{-1.4}	-2.3 ^{+1.2} _{-1.2}	3.5 ^{+1.3} _{-1.3}	2.94 ± 0.90
SU Aur	J04555938+3034015	-14.8 ^{+0.1} _{-0.1}	-12.8 ^{+1.7} _{-1.7}	-9.8 ^{+1.3} _{-1.3}	21.9 ^{+1.0} _{-1.1}	-3.7 ^{+0.7} _{-0.8}	-0.6 ^{+1.7} _{-1.7}	-2.6 ^{+1.3} _{-1.4}	4.6 ^{+0.6} _{-1.0}	8.30 ± 0.05

NOTE—Columns (3)-(6) provide the stellar spatial velocity not corrected for the Solar motion. The peculiar velocity of the stars after correcting for the velocity of the Sun with respect to the LSR are given in columns (7)-(10). The radial velocity of the stars (see Table 8) converted to the LSR are given in column (11).

5.2.3. *Lynds 1531, 1534 and 1536*

V999 Tau and V1000 Tau are projected towards Lynds 1534 (L1534, Lynds 1962). The weighted mean parallax of these two sources is $\pi = 7.215 \pm 0.110$ mas. This yields a distance estimate of $d = 138.6_{-2.1}^{+2.1}$ pc. Our results also reveal that the nearby (in the plane of the sky) star-forming clumps Lynds 1531 (L 1531) and Lynds 1536 (L 1536) are located at different distances. The distance that we derive in this work for L 1531 and L 1536 is based solely on the trigonometric parallaxes of V807 Tau B and HP Tau G2, and represents one first distance determination to these clouds that will be refined when more data for the remaining cloud members becomes available. We find a distance of $d = 126.6_{-1.7}^{+1.7}$ pc and $d = 162.7_{-0.8}^{+0.8}$ pc, respectively, for L 1531 and L 1536. This reveals a difference of about 36 pc between these two clouds along the line of sight.

Based on the VLBI trigonometric parallaxes derived in this paper we find that V807 Tau B is the closest star ($d = 126.6 \pm 1.7$ pc) in Taurus. The nominal distances obtained for V1096 Tau and V1098 Tau in L1495 indicate that they are somewhat closer than V807 Tau B, but the larger errors given in our solution due to the non-corrected binarity of V1096 Tau and the small number of detections for V1098 Tau make our results for these sources rather uncertain. On the other hand, we confirm HP Tau G2 as the remotest star ($d = 162.7 \pm 0.8$ pc) in the complex. Despite the different distances, we note that V807 Tau B and HP Tau G2 move with the same speed. However, their velocity vectors differ significantly as the w -component of HP Tau G2 points to a different direction than most stars in our sample (see Table 9).

5.2.4. *Lynds 1551 and L1558*

XZ Tau is projected towards Lynds 1551 (L1551, Lynds 1962) with a trigonometric parallax of $\pi = 6.793 \pm 0.025$ mas while UX Tau located on the border of L 1551 (see Fig. 12) has a trigonometric parallax of $\pi = 6.330 \pm 0.404$ mas. The weighted mean of these values yields $\pi = 6.791 \pm 0.025$ mas, and a distance estimate of $d = 147.3_{-0.5}^{+0.5}$ pc. We note that this result is in good agreement with the distance of $d = 148.7_{-0.9}^{+0.9}$ pc obtained in this work for T Tau Sb which is projected towards the BDN 176.28-20.89 cloud (see Dobashi et al. 2005). We thus conclude that L 1551 and BDN 176.28-20.89 are located at the same distance. Interestingly, this result also constrains the distance to the recently imaged HL Tau star (ALMA Partnership et al. 2015) which is also projected towards L 1551 and located $< 0.5'$ from XZ Tau.

On the other hand, we note that DR Tau, which is projected towards Lynds 1558 (L 1558, Lynds 1962) has

a trigonometric parallax of $\pi = 4.820 \pm 0.424$ mas in the TGAS catalog. If we assume that the result delivered by Gaia-DR1 for this star is accurate enough, this will put DR Tau (and L 1558) in the background of the Taurus star-forming complex at a distance of $d = 208_{-17}^{+20}$ pc. More study is clearly warranted in this regard, and the upcoming (and more precise) trigonometric parallaxes from Gaia-DR2 will allow us to confirm this scenario.

In addition to the stars mentioned in this section, we note that HD 28867 and HD 30171 are located in the vicinity of L 1551 and L 1558. HD 28867 has a radial velocity of $V_r = -14.70 \pm 7.40$ km/s which is in obvious disagreement with the observed radial velocity of other group members (see Table 8). On the other hand, HD 30171 has a trigonometric parallax and spatial velocity that are more consistent with the properties of the L 1551 cloud (see Tables 8 and 9) despite the closer proximity in the plane of the sky with L 1558 (see also Fig. 12). In a recent study, Kraus et al. (2017) performed a global reassessment of the membership status of known YSOs in Taurus, and suggested the existence of a distributed older population of stars. HD 28867 was not included in their study and HD 30171 was classified as a YSO candidate member confirming that its membership status is rather uncertain. For these reasons, we have assigned HD 28867 and HD 30171 to an “off-cloud” population that will require further investigation with Gaia-DR2.

5.2.5. *Taurus (all stars)*

In Table 10 we list the mean distance and spatial velocity derived for all stars in our sample (V1110 Tau, HD 28867, HD 30171 and RY Tau are excluded from this analysis for the reasons discussed before). The mean distance of $d = 141.8 \pm 0.2$ pc that we derive from our analysis is still consistent with the canonical distance estimate of $d = 140 \pm 10$ pc (Kenyon et al. 1994) which is commonly used in the literature for the Taurus region. However, the resulting distance is only representative of a few clouds in the Taurus complex, and it does not reveal the important depth effects that exist in this region as demonstrated in our study. Interestingly, we conclude from Table 10 that the B 216 clump in the filamentary structure of L 1495 is moving at $(\Delta U, \Delta V, \Delta W) = (-1.7, -0.8, 4.9) \pm (0.1, 0.2, 0.2)$ km/s with respect to the central part of the cloud, which implies a relative bulk motion of about 5.2 ± 0.2 km/s between both structures. It is also interesting to note that L 1551, which is the most southern cloud in our sample, is moving at $(\Delta U, \Delta V, \Delta W) = (-1.6, -1.7, 4.2) \pm (0.1, 0.1, 0.1)$ km/s with respect to L 1495 and has a relative motion of 4.8 ± 0.1 km/s. On the other hand, we see from Table 10

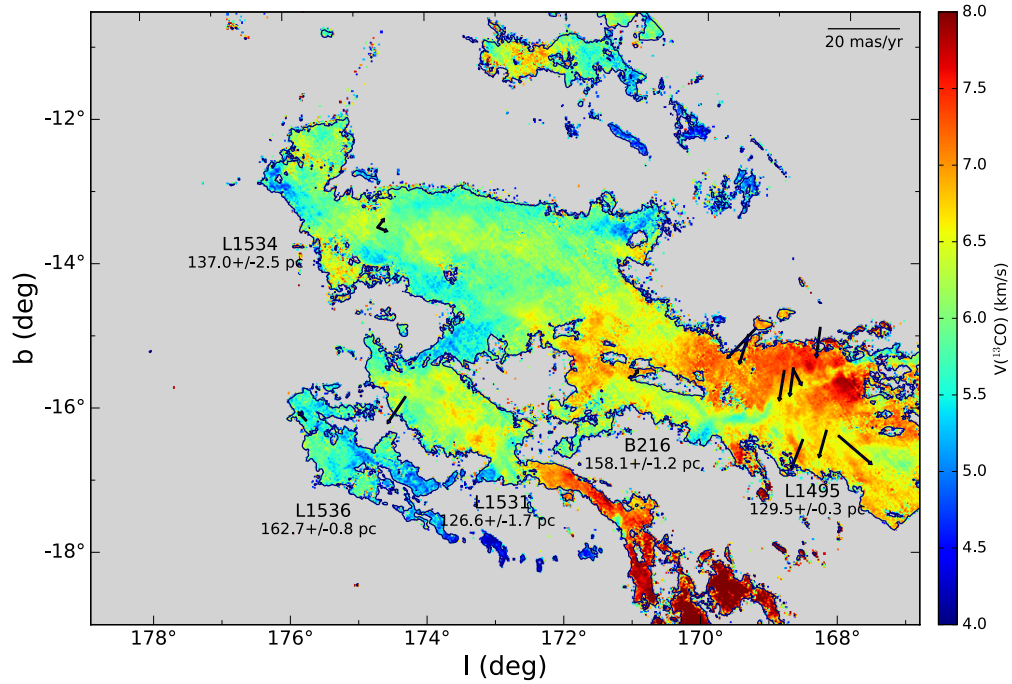


Figure 13. Location of the stars in our sample overlaid on the ^{13}CO map from Goldsmith et al. (2008). The vectors represent the stellar proper motions corrected for the Solar motion (Schönrich et al. 2010) using the formalism described by Abad & Vieira (2005). The most prominent star-forming clouds in the central portion of the complex and their distances are indicated in this diagram.

Table 10. Distance and spatial velocity of the various clouds in Taurus.

Cloud	N_1	N_2	π	d	U	V	W	V_{space}
			(mas)	(pc)	(km/s)	(km/s)	(km/s)	(km/s)
L 1495	8	6	7.724 ± 0.019	$129.5^{+0.3}_{-0.3}$	-15.4 ± 0.1	-11.7 ± 0.1	-11.1 ± 0.1	23.4 ± 0.1
L 1495 (B 216)	2	1	6.325 ± 0.049	$158.1^{+1.2}_{-1.2}$	-17.1 ± 0.1	-12.5 ± 0.2	-6.5 ± 0.2	22.2 ± 0.1
L 1513	1	1	6.610 ± 0.508	151^{+13}_{-11}	-14.9 ± 0.6	-16.0 ± 3.7	-10.5 ± 3.6	24.3 ± 2.9
L 1519	4	3	7.035 ± 0.116	$142.1^{+2.4}_{-2.3}$	-14.1 ± 0.1	-12.9 ± 0.4	-9.7 ± 0.3	21.3 ± 0.3
L 1531	1	1	7.899 ± 0.105	$126.6^{+1.7}_{-1.7}$	-15.8 ± 0.1	-15.1 ± 0.3	-11.4 ± 0.3	24.7 ± 0.3
L 1534	2	1	7.215 ± 0.110	$138.6^{+2.1}_{-2.1}$	-15.0 ± 2.0	-11.1 ± 0.7	-5.0 ± 1.0	19.3 ± 1.7
L 1536	1	1	6.145 ± 0.029	$162.7^{+0.8}_{-0.8}$	-16.7 ± 1.0	-13.8 ± 0.2	-5.5 ± 0.4	22.3 ± 0.7
L 1551	2	2	6.791 ± 0.025	$147.3^{+0.5}_{-0.5}$	-17.0 ± 0.1	-13.4 ± 0.1	-7.2 ± 0.1	22.8 ± 0.1
L 1558	1	1	4.820 ± 0.424	208^{+20}_{-17}	-18.0 ± 1.2	-10.5 ± 4.0	-11.5 ± 3.8	23.9 ± 2.7
Taurus (all stars)	23	18	7.054 ± 0.012	$141.8^{+0.2}_{-0.2}$	-15.2 ± 0.1	-12.8 ± 0.1	-8.7 ± 0.1	22.8 ± 0.1

NOTE—We provide for each subgroup the number of stars with known trigonometric parallax (N_1) and radial velocity (N_2), the weighted mean parallax with the corresponding distance, and the weighted mean spatial velocity.

that the spatial velocity for L 1519 is fully consistent within 1 km/s of the mean spatial velocity computed for all stars in our sample.

We find that the dispersion of the spatial velocities among the various clouds is $(\sigma_U, \sigma_V, \sigma_W) = (2.4, 2.5, 2.1)$ km/s. For comparison, the velocity dispersion derived from the proper motions converted to tangential velocities in right ascension and declination are 2.4 km/s and 3.1 km/s, respectively. This implies that the one-dimensional velocity dispersion in Taurus is somewhat higher than the value of 1 km/s adopted by [Luhman et al. \(2009\)](#), and smaller than the value of 6 km/s estimated by [Bertout & Genova \(2006\)](#). This value is also similar to the one-dimensional velocity dispersion obtained by [Dzib et al. \(2017\)](#) and [Kounkel et al. \(2017\)](#) for YSOs in the Orion Nebula Cluster.

One interesting question that arises from our study is whether the stars and the molecular gas in this region exhibit the same kinematic properties. In this context, [Goldsmith et al. \(2008\)](#) performed a large-scale survey of the ^{12}CO and ^{13}CO molecular gas in Taurus which we use here to further discuss our results. Figure 13 summarizes the distance of the various clouds in the central portion of the Taurus complex that we derive in this paper overlaid on the ^{13}CO velocity field produced in that survey. We extracted the ^{12}CO and ^{13}CO spectra at the position of the stars in our sample in a velocity interval from 3 to 13 km/s, computed the centroid velocity of the molecular gas in each case and estimated their errors from the r.m.s. of the individual spectra. We note that for some stars in our sample there was no apparent signal in one of the two spectra extracted from the ^{12}CO and ^{13}CO maps. So, we decided to restrict our analysis to the stars with measured centroid velocities from both spectra and took the weighted mean of the computed values as our final estimate for the velocity of the gas at the position of a given star. It is important to mention, that this analysis is restricted to only 9 stars in our sample with measured radial velocities in the literature (see Table 8) that are included in the region surveyed by [Goldsmith et al. \(2008\)](#) and fulfill this condition.

In Figure 14 we compare (i) the velocity of the molecular gas with the radial velocity of the stars (both are given with respect to the LSR), and (ii) the distance of the stars with the velocity of the associated gaseous clouds. First, we note that the velocity of the molecular gas (measured at the position of our sources) and the spectroscopic radial velocity of the stars are mostly consistent confirming that the stars are indeed associated with the underlying gaseous clouds. It is important to mention that most stars used in this analysis are binaries which explains both the existence of discrepant values

(e.g. HD 283518) and the large errors on the radial velocities given in the literature (e.g. V1096 Tau). Second, we note that the velocity of the gas ranges from 6.5 to 7.5 km/s for most sources projected towards the central part of the L 1495 cloud ($d = 129.5_{-0.3}^{+0.3}$ pc), and it varies from 6.0 to 6.5 km/s at the position of the remotest stars in this sample: V999 Tau ($d = 143.4_{-3.9}^{+4.2}$ pc), HD 283641 ($d = 159.1_{-1.8}^{+1.8}$ pc) and HP Tau G2 ($d = 162.7_{-0.8}^{+0.8}$ pc). Although a perfect correlation between the distance of the stars and the velocity of the gas is not straightforward from Fig. 14 (see e.g. V773Tau A and V807 Tau B), we found evidences that the observed velocity of the molecular gas at the position of our targets decreases with the increasing distance of the star. This finding and the trigonometric parallaxes derived in this paper support our conclusion that the different structures of the Taurus complex are located at different distances. We will continue to investigate this issue using the upcoming parallaxes from Gaia-DR2 and a more significant number of stars to provide an accurate picture of the gas and stellar kinematics in this region.

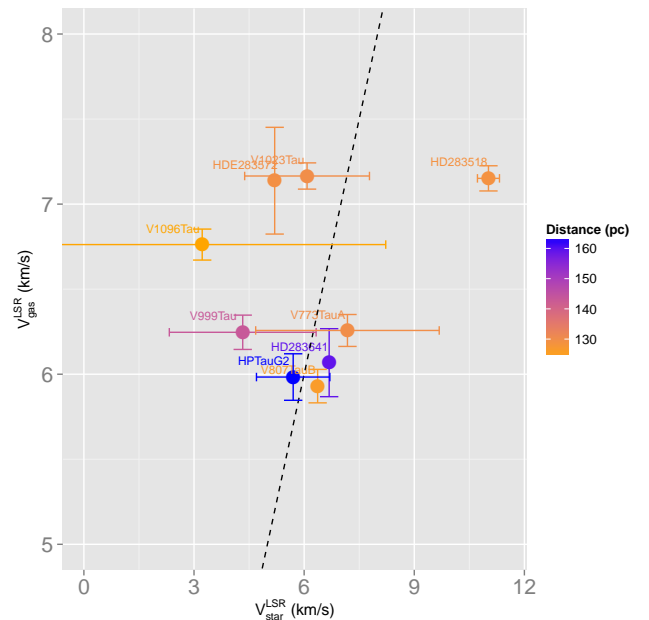


Figure 14. Comparison of the stellar radial velocity with the velocity of the ^{12}CO and ^{13}CO molecular gas measured at the position of each star. The colors indicate the distance of each star obtained in this study from VLBI astrometry. The dashed line indicates perfect correlation between the velocity of the gas and the radial velocity of the stars.

Finally, we note that the angular size of the Taurus complex in the plane of sky is about 12° in both Galactic longitude and Galactic latitude (see e.g. Fig. 1) which roughly corresponds to 30 pc using the mean distance given in Table 10. From the closest (L 1495) and remotest (L 1536) molecular cloud with measured VLBI trigonometric parallaxes in this study (this excludes L 1558) we estimate the depth of 33 pc. Thus, we conclude that the distance range in the plane of the sky and in the line of sight are equivalent.

6. CONCLUSIONS

In this study we reported on multi-epoch VLBI radio observations taken as part of the GOBELINS project in the Taurus star-forming region. We detected 26 YSOs with the VLBA, and presented the astrometry of 18 stars (or stellar systems) in our sample. The absolute positions measured in this work were modeled to derive the trigonometric parallaxes and proper motions of both single stars and binaries to a few percent of accuracy. By combining our observations with data from previous studies in the literature we were able to solve simultaneously for the astrometry and orbital motion of the sources in binary systems over an extended time base, and provide a more accurate solution for the trigonometric parallax. Thus, our results are more accurate than the trigonometric parallaxes from Gaia-DR1 for both single stars and binaries where the orbital motion of such systems was not taken into account. The VLBI trigonometric parallaxes presented in this paper are also more precise than the results from Gaia-DR1 by almost one order of magnitude. Our analysis also made it possible to determine the dynamical masses of the individual components in four systems (V1023 Tau, T Tau S, V807 Tau B and V1000 Tau).

We converted the trigonometric parallaxes derived in this study into stellar distances and investigated the three-dimensional structure of the Taurus complex. We confirm the existence of significant depth effects and concluded that the various star-forming clouds of the complex are located at different distances. We found a mean distance of 129.5 ± 0.3 pc to the central part of the dark cloud L 1495, and report on the distance of 158.1 ± 1.2 pc towards the B 216 clump in the filamentary structure of this cloud. Based on our VLBI observations we conclude that V807 Tau B, which is projected towards L 1531, is the closest star in our sample located at 126.6 ± 1.7 pc. On the other hand, HP Tau G2 projected towards the nearby (in the plane of the sky) L 1536 cloud is the farthest star in the complex located at 162.7 ± 0.8 pc. Altogether, this implies a depth of about 36 pc based solely on the distances derived from

VLBI trigonometric parallaxes. In particular, we note that one of the clouds for which we derive a distance (Lynds 1551) contains the young star HL Tau that has recently been subject of many studies upon the ALMA imaging of its protoplanetary disk. We argue that the distance derived here ($d = 147.3 \pm 0.5$ pc) should be used for any future study of that specific source.

Finally, we combined the stellar distances obtained in this paper with published radial velocities to compute the spatial velocities of Taurus stars. We verified that the one-dimensional velocity dispersion among the various clouds in the complex amounts to 2-3 km/s. Moreover, we showed that the velocity of the molecular gas structures is somewhat smaller for the remotest stars in our sample ($d \simeq 160$ pc) as compared the closest stars projected towards L 1495 ($d \simeq 130$ pc).

The distances produced by the GOBELINS project in Taurus represent one important step to map the three-dimensional structure of the complex with unprecedented accuracy and precision. In addition, they also provide us with an independent consistency check of the upcoming trigonometric parallaxes from Gaia-DR2 for the targets in common. We anticipate that we will soon be able to deliver more results for other targets in our sample (including binaries and multiple systems) that are currently being monitored by our team and we will use Gaia-DR2 trigonometric parallaxes to provide a more complete picture of the Taurus region.

P.A.B.G. acknowledges financial support from the São Paulo Research Foundation (FAPESP) through grants 2013/04934-8 and 2015/14696-2. L.L. acknowledges the financial support of DGAPA, UNAM (project IN112417), and CONACyT, Mexico. G.-N.O.L acknowledges support from the Alexander von Humboldt Foundation in the form of a Humboldt Fellowship. M.K. acknowledges support provided by the NSF through grant AST-1449476, and from the Research Corporation via a Time Domain Astrophysics Scialog award (#24217).

Facilities: VLBA (NRAO) - The National Radio Astronomy Observatory is operated by Associated Universities, Inc., under cooperative agreement with the National Science Foundation. The Long Baseline Observatory is a facility of the National Science Foundation operated under cooperative agreement by Associated Universities, Inc. DiFX correlator - This work made use of the Swinburne University of Technology software correlator, developed as part of the Australian Major National Research Facilities Programme and op-

erated under licence. This work has made use of the computing facilities of the Laboratory of Astroinformatics (IAG/USP, NAT/Unicisul), whose purchase was

made possible by the Brazilian agency FAPESP (grant 2009/54006-4) and the INCT-A.

Software: AIPS (Greisen 2003), emcee (Foreman-Mackey et al. 2013), astropy (Astropy Collaboration et al. 2013), novas (Barron et al. 2011).

REFERENCES

- Abad, C., & Vieira, K. 2005, *A&A*, 442, 745, doi: [10.1051/0004-6361:20035609](https://doi.org/10.1051/0004-6361:20035609)
- ALMA Partnership, Brogan, C. L., Pérez, L. M., et al. 2015, *ApJL*, 808, L3, doi: [10.1088/2041-8205/808/1/L3](https://doi.org/10.1088/2041-8205/808/1/L3)
- Andrews, J. J., Chanamé, J., & Agüeros, M. A. 2017, *MNRAS*, 472, 675, doi: [10.1093/mnras/stx2000](https://doi.org/10.1093/mnras/stx2000)
- Astropy Collaboration, Robitaille, T. P., Tollerud, E. J., et al. 2013, *A&A*, 558, A33, doi: [10.1051/0004-6361/201322068](https://doi.org/10.1051/0004-6361/201322068)
- Barron, E. G., Kaplan, G. H., Bangert, J., et al. 2011, in *Bulletin of the American Astronomical Society*, Vol. 43, American Astronomical Society Meeting Abstracts #217, 344.14
- Bertout, C., & Genova, F. 2006, *A&A*, 460, 499, doi: [10.1051/0004-6361:20065842](https://doi.org/10.1051/0004-6361:20065842)
- Bertout, C., Robichon, N., & Arenou, F. 1999, *A&A*, 352, 574
- Boden, A. F., Torres, G., Duchêne, G., et al. 2012, *ApJ*, 747, 17, doi: [10.1088/0004-637X/747/1/17](https://doi.org/10.1088/0004-637X/747/1/17)
- Boden, A. F., Torres, G., Sargent, A. I., et al. 2007, *ApJ*, 670, 1214, doi: [10.1086/521296](https://doi.org/10.1086/521296)
- Briceno, C., Hartmann, L. W., Stauffer, J. R., et al. 1997, *AJ*, 113, 740, doi: [10.1086/118293](https://doi.org/10.1086/118293)
- Cambrésy, L. 1999, *A&A*, 345, 965
- Carrasco-González, C., Rodríguez, L. F., Anglada, G., & Curiel, S. 2009, *ApJL*, 693, L86, doi: [10.1088/0004-637X/693/2/L86](https://doi.org/10.1088/0004-637X/693/2/L86)
- Dame, T. M., Hartmann, D., & Thaddeus, P. 2001, *ApJ*, 547, 792, doi: [10.1086/318388](https://doi.org/10.1086/318388)
- Deller, A. T., Brisken, W. F., Phillips, C. J., et al. 2011, *PASP*, 123, 275, doi: [10.1086/658907](https://doi.org/10.1086/658907)
- Dobashi, K., Uehara, H., Kandori, R., et al. 2005, *PASJ*, 57, S1, doi: [10.1093/pasj/57.sp1.S1](https://doi.org/10.1093/pasj/57.sp1.S1)
- Duchêne, G. 1999, *A&A*, 341, 547
- Duchêne, G., Ghez, A. M., & McCabe, C. 2002, *ApJ*, 568, 771, doi: [10.1086/338987](https://doi.org/10.1086/338987)
- Duchêne, G., Ghez, A. M., McCabe, C., & Weinberger, A. J. 2003, *ApJ*, 592, 288, doi: [10.1086/375624](https://doi.org/10.1086/375624)
- Dzib, S. A., Loinard, L., Rodríguez, L. F., et al. 2015, *ApJ*, 801, 91, doi: [10.1088/0004-637X/801/2/91](https://doi.org/10.1088/0004-637X/801/2/91)
- . 2017, *ApJ*, 834, 139, doi: [10.3847/1538-4357/834/2/139](https://doi.org/10.3847/1538-4357/834/2/139)
- Elias, J. H. 1978, *ApJ*, 224, 857, doi: [10.1086/156436](https://doi.org/10.1086/156436)
- ESA. 1997, *VizieR Online Data Catalog*, 1239
- Forbrich, J., Dupuy, T. J., Reid, M. J., et al. 2016, *ApJ*, 827, 22, doi: [10.3847/0004-637X/827/1/22](https://doi.org/10.3847/0004-637X/827/1/22)
- Foreman-Mackey, D., Hogg, D. W., Lang, D., & Goodman, J. 2013, *PASP*, 125, 306, doi: [10.1086/670067](https://doi.org/10.1086/670067)
- Forgan, D., Ivison, R. J., Sibthorpe, B., Greaves, J. S., & Ibar, E. 2014, *MNRAS*, 439, 4057, doi: [10.1093/mnras/stu271](https://doi.org/10.1093/mnras/stu271)
- Gaia Collaboration, Brown, A. G. A., Vallenari, A., et al. 2016, *A&A*, 595, A2, doi: [10.1051/0004-6361/201629512](https://doi.org/10.1051/0004-6361/201629512)
- Goldsmith, P. F., Heyer, M., Narayanan, G., et al. 2008, *ApJ*, 680, 428, doi: [10.1086/587166](https://doi.org/10.1086/587166)
- Gomez, M., Hartmann, L., Kenyon, S. J., & Hewett, R. 1993, *AJ*, 105, 1927, doi: [10.1086/116567](https://doi.org/10.1086/116567)
- Gontcharov, G. A. 2006, *Astronomy Letters*, 32, 759, doi: [10.1134/S1063773706110065](https://doi.org/10.1134/S1063773706110065)
- Goodman, J., & Weare, J. 2010, *Communications in Applied Mathematics and Computational Science*, 5, 65, doi: [10.2140/camcos.2010.5.65](https://doi.org/10.2140/camcos.2010.5.65)
- Gottlieb, D. M., & Upson, II, W. L. 1969, *ApJ*, 157, 611, doi: [10.1086/150101](https://doi.org/10.1086/150101)
- Greenstein, J. L., & Shapley, H. 1937, *Annals of Harvard College Observatory*, 105, 359
- Greisen, E. W. 2003, *Information Handling in Astronomy - Historical Vistas*, 285, 109, doi: [10.1007/0-306-48080-8.7](https://doi.org/10.1007/0-306-48080-8.7)
- Harris, R. J., Andrews, S. M., Wilner, D. J., & Kraus, A. L. 2012, *ApJ*, 751, 115, doi: [10.1088/0004-637X/751/2/115](https://doi.org/10.1088/0004-637X/751/2/115)
- Hartmann, L. 2002, *ApJ*, 578, 914, doi: [10.1086/342657](https://doi.org/10.1086/342657)
- Hartmann, L., Hewett, R., Stahler, S., & Mathieu, R. D. 1986, *ApJ*, 309, 275, doi: [10.1086/164599](https://doi.org/10.1086/164599)
- Herbig, G. H., & Bell, K. R. 1988, *Third Catalog of Emission-Line Stars of the Orion Population : 3 : 1988*
- Jackson, J. M., Rathborne, J. M., Shah, R. Y., et al. 2006, *ApJS*, 163, 145, doi: [10.1086/500091](https://doi.org/10.1086/500091)
- Johnson, D. R. H., & Soderblom, D. R. 1987, *AJ*, 93, 864, doi: [10.1086/114370](https://doi.org/10.1086/114370)
- Joncour, I., Duchêne, G., & Moraux, E. 2017, *A&A*, 599, A14, doi: [10.1051/0004-6361/201629398](https://doi.org/10.1051/0004-6361/201629398)
- Joy, A. H. 1945, *ApJ*, 102, 168, doi: [10.1086/144749](https://doi.org/10.1086/144749)
- Kenyon, S. J., Dobrzycka, D., & Hartmann, L. 1994, *AJ*, 108, 1872, doi: [10.1086/117200](https://doi.org/10.1086/117200)

- Kenyon, S. J., Gómez, M., & Whitney, B. A. 2008, *Low Mass Star Formation in the Taurus-Auriga Clouds*, ed. B. Reipurth, 405
- Kharchenko, N. V., Scholz, R.-D., Piskunov, A. E., Röser, S., & Schilbach, E. 2007, *Astronomische Nachrichten*, 328, 889, doi: [10.1002/asna.200710776](https://doi.org/10.1002/asna.200710776)
- Köhler, R., Kasper, M., Herbst, T. M., Ratzka, T., & Bertrang, G. H.-M. 2016, *A&A*, 587, A35, doi: [10.1051/0004-6361/201527125](https://doi.org/10.1051/0004-6361/201527125)
- Köhler, R., & Leinert, C. 1998, *A&A*, 331, 977
- Köhler, R., Ratzka, T., Herbst, T. M., & Kasper, M. 2008, *A&A*, 482, 929, doi: [10.1051/0004-6361:20079269](https://doi.org/10.1051/0004-6361:20079269)
- Kounkel, M., Hartmann, L., Loinard, L., et al. 2017, *ApJ*, 834, 142, doi: [10.3847/1538-4357/834/2/142](https://doi.org/10.3847/1538-4357/834/2/142)
- Kraus, A. L., Herczeg, G. J., Rizzuto, A. C., et al. 2017, *ApJ*, 838, 150, doi: [10.3847/1538-4357/aa62a0](https://doi.org/10.3847/1538-4357/aa62a0)
- Krist, J. E., Stapelfeldt, K. R., Hester, J. J., et al. 2008, *AJ*, 136, 1980, doi: [10.1088/0004-6256/136/5/1980](https://doi.org/10.1088/0004-6256/136/5/1980)
- Leinert, C., Richichi, A., & Haas, M. 1997, *A&A*, 318, 472
- Lestrade, J.-F., Preston, R. A., Jones, D. L., et al. 1999, *A&A*, 344, 1014
- Lindgren, L., Lammers, U., Bastian, U., et al. 2016, *A&A*, 595, A4, doi: [10.1051/0004-6361/201628714](https://doi.org/10.1051/0004-6361/201628714)
- Loinard, L., Mioduszewski, A. J., Torres, R. M., et al. 2011, in *Revista Mexicana de Astronomía y Astrofísica*, vol. 27, Vol. 40, *Revista Mexicana de Astronomía y Astrofísica Conference Series*, 205–210
- Loinard, L., Torres, R. M., Mioduszewski, A. J., et al. 2007, *ApJ*, 671, 546, doi: [10.1086/522493](https://doi.org/10.1086/522493)
- Luhman, K. L., Mamajek, E. E., Allen, P. R., & Cruz, K. L. 2009, *ApJ*, 703, 399, doi: [10.1088/0004-637X/703/1/399](https://doi.org/10.1088/0004-637X/703/1/399)
- Lynds, B. T. 1962, *ApJS*, 7, 1, doi: [10.1086/190072](https://doi.org/10.1086/190072)
- Martin, E. L., Rebolo, R., Magazzu, A., & Pavlenko, Y. V. 1994, *A&A*, 282, 503
- Mason, B. D., Wycoff, G. L., Hartkopf, W. I., Douglass, G. G., & Worley, C. E. 2001, *AJ*, 122, 3466, doi: [10.1086/323920](https://doi.org/10.1086/323920)
- McCuskey, S. W. 1939, *ApJ*, 89, 568, doi: [10.1086/144082](https://doi.org/10.1086/144082)
- Meistas, E., & Straizys, V. 1981, *AcA*, 31, 85
- Melis, C., Reid, M. J., Mioduszewski, A. J., Stauffer, J. R., & Bower, G. C. 2014, *Science*, 345, 1029, doi: [10.1126/science.1256101](https://doi.org/10.1126/science.1256101)
- Menten, K. M., Reid, M. J., Forbrich, J., & Brunthaler, A. 2007, *A&A*, 474, 515, doi: [10.1051/0004-6361:20078247](https://doi.org/10.1051/0004-6361:20078247)
- Nguyen, D. C., Brandeker, A., van Kerkwijk, M. H., & Jayawardhana, R. 2012, *ApJ*, 745, 119, doi: [10.1088/0004-637X/745/2/119](https://doi.org/10.1088/0004-637X/745/2/119)
- Ortiz-León, G. N., Loinard, L., Kounkel, M. A., et al. 2017a, *ApJ*, 834, 141, doi: [10.3847/1538-4357/834/2/141](https://doi.org/10.3847/1538-4357/834/2/141)
- Ortiz-León, G. N., Dzib, S. A., Kounkel, M. A., et al. 2017b, *ApJ*, 834, 143, doi: [10.3847/1538-4357/834/2/143](https://doi.org/10.3847/1538-4357/834/2/143)
- Panopoulou, G. V., Tassis, K., Goldsmith, P. F., & Heyer, M. H. 2014, *MNRAS*, 444, 2507, doi: [10.1093/mnras/stu1601](https://doi.org/10.1093/mnras/stu1601)
- Pradel, N., Charlot, P., & Lestrade, J.-F. 2006, *A&A*, 452, 1099, doi: [10.1051/0004-6361:20053021](https://doi.org/10.1051/0004-6361:20053021)
- Racine, R. 1968, *AJ*, 73, 233, doi: [10.1086/110624](https://doi.org/10.1086/110624)
- Rebull, L. M., Padgett, D. L., McCabe, C.-E., et al. 2010, *ApJS*, 186, 259, doi: [10.1088/0067-0049/186/2/259](https://doi.org/10.1088/0067-0049/186/2/259)
- Schaefer, G. H., Prato, L., Simon, M., & Patience, J. 2014, *AJ*, 147, 157, doi: [10.1088/0004-6256/147/6/157](https://doi.org/10.1088/0004-6256/147/6/157)
- Schaefer, G. H., Prato, L., Simon, M., & Zavala, R. T. 2012, *ApJ*, 756, 120, doi: [10.1088/0004-637X/756/2/120](https://doi.org/10.1088/0004-637X/756/2/120)
- Schmalzl, M., Kainulainen, J., Quanz, S. P., et al. 2010, *ApJ*, 725, 1327, doi: [10.1088/0004-637X/725/1/1327](https://doi.org/10.1088/0004-637X/725/1/1327)
- Schneider, S., & Elmegreen, B. G. 1979, *ApJS*, 41, 87, doi: [10.1086/190609](https://doi.org/10.1086/190609)
- Schönrich, R., Binney, J., & Dehnen, W. 2010, *MNRAS*, 403, 1829, doi: [10.1111/j.1365-2966.2010.16253.x](https://doi.org/10.1111/j.1365-2966.2010.16253.x)
- Seidelmann, P. K. 1992, *Explanatory Supplement to the Astronomical Almanac. A revision to the Explanatory Supplement to the Astronomical Ephemeris and the American Ephemeris and Nautical Almanac.*
- Siess, L., Dufour, E., & Forestini, M. 2000, *A&A*, 358, 593
- Simon, M., Ghez, A. M., Leinert, C., et al. 1995, *ApJ*, 443, 625, doi: [10.1086/175554](https://doi.org/10.1086/175554)
- Straizys, V., & Meistas, E. 1980, *AcA*, 30, 541
- Torres, R. M., Loinard, L., Mioduszewski, A. J., et al. 2012, *ApJ*, 747, 18, doi: [10.1088/0004-637X/747/1/18](https://doi.org/10.1088/0004-637X/747/1/18)
- Torres, R. M., Loinard, L., Mioduszewski, A. J., & Rodríguez, L. F. 2007, *ApJ*, 671, 1813, doi: [10.1086/522924](https://doi.org/10.1086/522924)
- . 2009, *ApJ*, 698, 242, doi: [10.1088/0004-637X/698/1/242](https://doi.org/10.1088/0004-637X/698/1/242)
- Ungerechts, H., & Thaddeus, P. 1987, *ApJS*, 63, 645, doi: [10.1086/191176](https://doi.org/10.1086/191176)
- van de Kamp, P. 1967, *Principles of Astrometry.* (W. H. Freeman and Company)
- Wahhaj, Z., Cieza, L., Koerner, D. W., et al. 2010, *ApJ*, 724, 835, doi: [10.1088/0004-637X/724/2/835](https://doi.org/10.1088/0004-637X/724/2/835)
- Wenger, M., Ochsenbein, F., Egret, D., et al. 2000, *A&AS*, 143, 9, doi: [10.1051/aas:2000332](https://doi.org/10.1051/aas:2000332)
- Woitak, J. 2003, *A&A*, 406, 685, doi: [10.1051/0004-6361:20030805](https://doi.org/10.1051/0004-6361:20030805)
- Xing, L. F. 2010, *ApJ*, 723, 1542, doi: [10.1088/0004-637X/723/2/1542](https://doi.org/10.1088/0004-637X/723/2/1542)
- Xing, L.-F., & Xing, Q.-F. 2012, *A&A*, 537, A91, doi: [10.1051/0004-6361/201117133](https://doi.org/10.1051/0004-6361/201117133)